Mathematical modelling of glycolysis in differentiated mouse adipocytes 3T3-L1

by

William de Villiers

Thesis presented in partial fulfilment of the requirements for the degree of Master of Science (Biochemistry) in the Faculty of Science at Stellenbosch University

Supervisor: Prof. J.L. Snoep

Co-supervisor: Dr. T. Kouril
Dr. D. van Niekerk
Dr. J.B. van Dyk

March 2021

Declaration

By submitting this thesis electronically, I declare that the entirety of the work contained therein is my own, original work, that I am the sole author thereof (save to the extent explicitly otherwise stated), that reproduction and publication thereof by Stellenbosch University will not infringe any third party rights and that I have not previously in its entirety or in part submitted it for obtaining any qualification.

Date: 2020/12/01 .....

Abstract

Mathematical modelling of glycolysis in differentiated mouse adipocytes 3T3-L1

W. de Villiers

Department of Biochemistry,
University of Stellenbosch,
Private Bag X1, Matieland 7602, South Africa.

Thesis: MSc(Biochemistry)

December 2020

Diabetes mellitus is a metabolic disease characterised by high blood sugar levels, primarily caused by insulin resistance and the resulting inability of the body to process glucose. Any tissue or cell that utilizes glucose is a target of diabetes research. Obesity is closely related to the development of diabetes due to the swelling of adipocytes caused by triacylglycerol formation. As glucose and its breakdown by glycolysis are directly responsible for supplying triacylglycerol formation, the focus of this work was on glycolysis in 3T3-L1 adipocytes. A bottom-up modelling approach was used in which all enzymes within glycolysis and the initial lipogenic enzyme G3PDH were characterised in order to create a kinetic model for glycolysis in 3T3-L1 adipocytes. Non-diabetic adipocyte cell extracts were utilized due to the need for a reference state model. Validation was performed using an HPLC analysis of glycolytic intermediates and co-factors. The validation was partially successful with glucose consumption and several glycolytic intermediate dynamics well described. Lactate production was underestimated in the model due to the high G3PDH activity within cell extracts which caused a significant fraction of the glucose to be converted via the glycerol branch, which was not seen to the same degree in the HPLC analysis. Being the first model of its kind to be constructed for adipocytes, this work has laid the groundwork for further modelling of adipocyte glucose metabolism to better understand the diabetic condition in adipose tissue.

Opsomming

Diabetes mellitus is 'n metaboliese siekte wat gekenmerk word deur hoë bloedsuikervlakke, hoofsaaklik veroorsaak deur insulienweerstandigheid en die gevolglike onvermoë van die liggaam om glukose te verwerk. Enige weefsel of sel wat glukose gebruik, is 'n teiken vir navorsing oor diabetes. Vetsug hou nou verband met die ontwikkeling van diabetes as gevolg van die swelling van adiposiete wat veroorsaak word deur die vorming van triasielgliserol. Aangesien glukose en die afbreek daarvan deur glikolise direk verantwoordelik is vir die verskaffing van triasielgliserolvorming, was die fokus van hierdie werk op glikolise in 3T3-L1-adiposiete. 'n Benaderingsmodel benadering is gebruik waarin alle ensieme binne glikolise en die aanvanklike lipogene ensiem G3PDH gekarakteriseer is om 'n kinetiese model vir glikolise in 3T3-L1 adiposiete te skep. Nie-diabetiese adiposiet selekstrakte is gebruik as gevolg van die behoefte aan 'n verwysingstoestandmodel. Validasie is uitgevoer met behulp van 'n HPLC-analise van glikolitiese tussenprodukte en medefaktore. Die validering was gedeeltelik suksesvol met glukoseverbruik en verskeie glikolitiese intermediêre dinamika wat goed beskryf is. Laktaatproduksie is in die model onderskat as gevolg van die hoë G3PDH-aktiwiteit in selekstrakte, wat veroorsaak het dat 'n beduidende fraksie van die glukose via die gliserolvertakking omgeskakel is, wat nie in dieselfde mate in die HPLC-analise gesien is nie. Aangesien dit die eerste model in sy soort is wat vir adiposiete vervaardig is, het dit die basis gelê vir verdere modellering van metabolisme van adiposiete glukose om die diabetiese toestand in vetweefsel beter te verstaan.

Contents

Declaration i

Abstract ii

Opsomming iii

Contents iv

1 General Introduction 1

2 Literature Review 4
- 2.1 Introduction . . . 4
- 2.2 Glycolysis . . . 6
- 2.3 Triacylglycerol synthesis . . . 12
- 2.4 Systems Biology . . . 15
- 2.5 Modelling of glycolysis in adipocytes . . . 16

3 Methods and Materials 18
- 3.1 Culturing of 3T3-L1 adipocytes . . . 18
- 3.2 Culture Harvesting and Lysate Preparation . . . 18
- 3.3 Enzyme Characterisation . . . 19
- 3.4 Fitting rate equations . . . 23
- 3.5 Computational Modelling . . . 23
- 3.6 Glycolytic Intermediate and Co-Factor HPLC Determinations . 23

4 Results 25
- 4.1 Kinetic characterization . . . 25
- 4.2 Model construction . . . 45
- 4.3 Model validation . . . 52

5 Discussion and Conclusions 63

List of References 67

Appendix 81

Model simulations 81
HPLC chromatograms 88

Chapter 1

General Introduction

Diabetes mellitus is a metabolic disease, often dubbed a "lifestyle" disease. Diabetes has already reached global epidemic proportions, not being limited to countries synonymous with obesity, the primary cause of diabetes. As of 2017, diabetes affected 425 million adults worldwide which is projected to increase to 629 million adults by 2045.[1] Type II diabetes accounts for over 90% of all diabetes cases.[2,3] It is for this reason that this project focuses on type II diabetes. Primarily, type II diabetes is closely related to obesity, as well as poor lifestyle choices and genetics.[4] The primary method to lower the occurrence of type II diabetes would be with diet education and lifestyle changes. However, this is not likely to be successful in reality due to a combination of globally available cheap high-carbohydrate foods, the high cost of healthy living, and the lack of emphasis placed on health in society. Understanding the molecular mechanisms of diabetes and treating the disease can assist us in solving this global epidemic.

Type II diabetes is characterised by high blood glucose levels and an inability to process glucose properly due to an increase in insulin resistance.[11] Myocytes and adipocytes that make up muscle and adipose tissue respectively, are responsible for the bulk of glucose consumption.[96] To understand diabetes would be to understand the three mechanisms that control glucose consumption in both myocytes and adipocytes: insulin signalling, glucose uptake, and glycolysis. This project focuses on glycolysis in adipocytes.

Adipose tissue plays a critical role in whole-body glucose and energy homeostasis although consuming less than 10% of the total glucose taken up by an individual.[5] In adipocytes, glycolysis is responsible for energy production as well as producing the intermediates used in triacylglycerol synthesis.[14] Adipocyte glucose uptake is primarily achieved through GLUT4, an insulin dependent glucose transporter.[13] A reduction in insulin sensitivity results in a reduction of GLUT4 translocation to the cell membrane. This in turn lowers glucose availability for glycolysis and impairs the functioning of the adipose tissue.

Adipose tissue is not only affected by the insulin resistance caused by diabetes and plays a role in the development of diabetes through the production of excess triacylglycerols. These fat molecules cause the swelling of adipocytes and the subsequent leaking of triacylglycerols into the blood stream which aids in the development of diabetes due to the effect triacylglycerols have on other tissues such as muscle.[97] The swelling of adipocytes also allows for macrophage infiltration, leading to cytokine production.[98] These cytokines enter the blood stream and aid in the development of diabetes by affecting a variety of tissues. As the production of triacylglycerol is directly controlled by glycolysis, it would seem evident that glycolysis plays a larger part in the development of diabetes than has been previously assumed.

Kinetic modelling proves a useful tool for characterising and describing metabolic processes such as glycolysis. Systemic behaviour can be described as well as the control that each enzyme in glycolysis has over properties of the system as a whole. Currently, there exist many detailed models of muscle metabolism, with the most extensive model including components from glycolysis, the citric acid cycle, glycogen synthesis and utilisation, lipogenesis, and lipolysis.[99] In terms of glycolysis, the most extensive mammalian glycolytic model that currently exists is also for muscle metabolism.[105] However, the same extensive models do not exist for adipose tissue metabolism. Currently, the majority of models include components for glucose consumption and lactate production while being heavily focused on triacylglycerol synthesis pathways. The most extensive adipose tissue glycolytic model created is a whole-body model that includes compartments for human brain, muscle, and adipose tissue.[100] This model attempts to model the human body's response to glucose. However, in terms of overlap with this project, the model does not characterise the entire glycolytic pathway in adipose tissue and is only able to correctly simulate physiological trends of experimental data.

For the purpose of constructing a model for glycolysis in adipocytes for the eventual treatment of diabetes mellitus, it would be ideal to construct a diabetic whole-cell model for human adipocytes but a few considerations need to be taken. First, there exists a lack of kinetic models that characterise the entirety of normal glycolysis in whole-cell adipocytes or adipocyte cell extracts let alone those describing diabetic states. Second, the availability of mouse adipocytes (3T3-L1 adipocytes) for laboratory experimentation is far greater than human adipocytes. For the amount of data needed to construct a glycolytic model and for the scope of the project, adipocyte availability plays a crucial role. It is for these reasons that the construction and subsequent validation of a kinetic model for glycolysis in 3T3-L1 cell free extracts was chosen to form the foundation of the metabolic modelling of adipocytes and further, diabetic adipocytes. This is the basis for the research question of this project: Can glycolysis in 3T3-L1 adipocytes be described on the basis of individual

glycolytic enzyme kinetics? The aims and objectives desiged to address this question are as follows:

1. Culturing of mature 3T3-L1 adipocytes
    a) Differentiation protocol optimisation of pre-adipocytes into mature adipocytes
    b) Harvesting and lysate preparation protocol optimisation
2. Determination of glycolytic enzyme kinetic parameters
    a) Perform enzyme-linked assays for each glycolytic enzyme
    b) Acquire kinetic parameters for each enzyme by performing non-linear model fits on enzyme assay data sets
3. Model construction and validation
    a) Using derived rates equations and kinetic parameters, create an ODE-based model for glycolysis in 3T3-L1 adipocyte cell extracts
    b) Perform HPLC analysis on cell extracts to acquire time course data for glycolytic intermediates and co-factors upon the injection of glucose
    c) Perform model validation by comparing simulation results to HPLC data

This thesis is broken down into five chapters with this chapter serving to provide motivation for the research question and the steps taken to address it. Chapter two serves to address all relevant literature for the molecular description of diabetes mellitus, the link between adipocytes and diabetes, the different types of adipose tissue, glycolysis, triacylglycerol synthesis, and the existing models for adipose tissue metabolism. Chapter three describes methods and materials used to achieve each aim and objective. Chapter four covers the results and discussion that address the research question. Chapter five is a general discussion and conclusion of the project's importance with regard to the fight against diabetes mellitus.

Chapter 2

Literature Review

2.1 Introduction

Diabetes was first described three and a half millennia ago.[9] In 400-500 AD diabetes was separated into type 1 and type 2 diabetes. Type 2 diabetes at this time was already prevalent mostly in overweight individuals.[9] In the 1700s, diabetes mellitus was first mentioned to separate it from diabetes insipidus, a condition characterized by excessive urination. It was only in 1921, when insulin was discovered, that an effective treatment was developed for diabetes mellitus.[9] With such a long history, it is of great concern that year on year, the prevalence of diabetes mellitus is increasing. Globally, there were 30 million diabetes cases in 1985, 135 million in 1995, 217 million in 2005, and 425 million in 2017.[1,10] This increase would be more dramatic if it were not for readily available information on diet, exercise, and general healthy living. To more effectively treat diabetes mellitus, the inner processes of tissues affected by diabetes need to be better understood.

Diabetes mellitus is characterized by high blood glucose and insulin resistance.[11] Insulin resistance refers to insulin receptors losing sensitivity to insulin. This in turn inhibits the insulin signalling pathway. The cascade that begins with insulin binding to the insulin receptor ends with the translocation of GLUT4, a glucose transporter, to the membrane of the tissue in which the insulin signalling pathway is present.[12] As GLUT4 is the only glucose transporter affected by insulin in this manner, it is a focus in the research into diabetes mellitus. GLUT4 is primarily found in adipose tissue, skeletal muscle, and cardiac muscle.[13] The insulin signalling cascade as well as glucose uptake by GLUT4 are of great importance in understanding the mechanics by which diabetes mellitus elicits its effects. Glucose that enters the cell via GLUT4 is utilized by the cytosolic process, glycolysis. Just like the two processes of signalling and transport, the intrinsic mechanisms of glycolysis could point to a multitude of solutions to diabetes. This is even more evident when it comes to adipose tissue as the metabolism of glucose via glycolysis in adipocytes leads to lipogenesis,

the biosynthesis of triacylglycerols, that are stored within adipocytes.[14] When glucose is in excess, triacylglycerol synthesis is an always active process.[15] This leads to the accumulation of triacylglycerols within adipocytes. It is this accumulation that plays a critical role in the development of diabetes, affecting adipose tissue and many other tissues.

The accumulation of triacylglycerols leads to the leaking of free fatty acids from adipose tissue into surrounding tissues and the bloodstream.[104] Free fatty acids are able to interfere with other tissue functioning. This is mainly seen in muscle as free fatty acids severely interfere with several kinases important to the insulin signalling pathway as well as insulin receptor substrates. This directly increases insulin sensitivity of muscle. Free fatty acids also activate nuclear factor-kappa B in muscle, leading to the release of proinflammatory cytokines.[104] In addition, excessive triacylglycerol synthesis leads to an increase in adipocytokine release by adipocytes.[102] Of these adipocytokines, tumour necrosis factor alpha, interleukin 6, and monocyte chemoattractant protein-1 promote macrophage infiltration into adipose tissue. Macrophage content of obese adipose tissue can be as high as 50% while in lean adipose tissue it is 5%.[102] This disruption in macrophage content leads to further production of tumour necrosis factor alpha and interleukin 6 as well as other proinflammatory cytokines such as interleukin 1 beta resulting in a state of chronic low-grade inflammation.[102] This inflammation is a body-wide effect that displays the danger of adipose tissue dysfunction. Adipose tissue not only affects other tissues in its dysfunction but in its healthy functioning as well. Adipose tissue serves as an endocrine organ not only when dysfunctional. Key adipokines are produced by adipose tissue that have far reaching effects on other tissue. The link between muscle and adipose tissue is the most noticeable. Leptin, an adipokine synonymous with weight control, simulates muscle fatty acid oxidation.[103] This is achieved through the activation of AMP-activated protein kinase. Adiponectin is another adipokine that elicits the same effect in muscle as leptin.[103]

Depending on the function and morphology, adipose tissue can be categorized into white, brown or beige.[16] White adipose tissue (WAT) is responsible for the synthesis and storage of triacylglycerols.[14] Brown adipose tissue (BAT), through the synthesis and subsequent degradation of triacylglycerols, is responsible for the efficient production and distribution of heat.[17] Beige adipose tissue is found within pockets of WAT and serves the same purpose as BAT. WAT can be converted into beige adipose tissue via the process of browning.[16] As the functions suggest, it is specifically the accumulation of triacylglycerols in WAT that is involved in the development of diabetes.[18]

2.2 Glycolysis

Glycolysis is a cytosolic process responsible for the breakdown of glucose into pyruvate, producing a net gain of two ATP, two NADH, and two pyruvate molecules for each molecule of glucose consumed. Nearly all living organisms carry out glycolysis but certain tissues take up more glucose than others, leading to tissues such as muscle playing a seemingly more important role in glucose homeostasis.[101] Glycolysis, while supplying energy to the cell, is critical in supplying branch pathways with metabolites such as glucose-6-phosphate for the pentose phosphate pathway as well as glycogen synthesis in muscle. Pyruvate, the end product of glycolysis, is utilized in the citric acid cycle.[19] Lactate, produced from pyruvate by lactate dehydrogenase, is utilized in many other tissues as fuel.[20] Arguably the most important branch pathway for adipose tissue is the glycerol pathway in which dihydroxyacetone phosphate (DHAP) is converted into glycerol 3-phosphate (G3P) to be used in triacylglycerol synthesis.[14] An overview of the glycolytic pathway is shown in Fig 2.1.

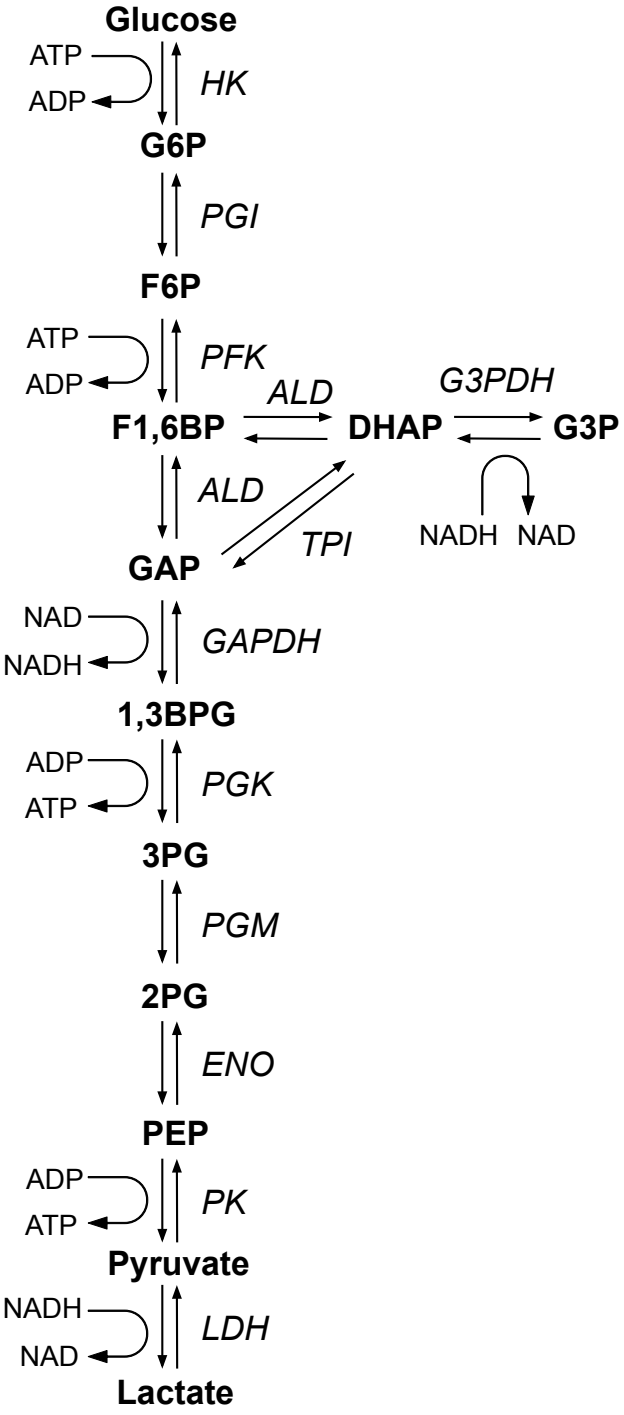

Figure 2.1: The classic glycolytic pathway within 3T3-L1 adipocytes. Metabolites are in bold with enzymes in italics. The acronyms are as follows: hexokinase (HK), phosphoglucoisomerase (PGI), phosphofructokinase (PFK), aldolase (ALD), triosephosphate isomerase (TPI), glycerol 3-phosphate dehydrogenase (G3PDH), glyceraldehyde 3- Phosphate Dehydrogenase (GAPDH),

phosphoglycerate kinase (PGK), phosphoglycerate mutase (PGM) , enolase (ENO), pyruvate kinase (PK), lactate dehydrogenase (LDH), adenosine triphosphate (ATP), adenosine diphosphate (ADP), adenosine monophosphate (AMP), nicotinamide adenine dinucleotide (NAD), and nicotinamide adenine dinucleotide hydride (NADH).

What follows is a review of the literature on each glycolytic enzyme. An overview is provided followed by any pertinent information on the enzymes in adipose tissue. The effects of obesity and insulin on each glycolytic enzyme are highlighted as this makes up the bulk of glycolytic enzyme data in adipose tissue.

2.2.1 Hexokinase

Hexokinase (HK), the first enzyme of glycolysis, catalyses the conversion of glucose and ATP to glucose 6-phosphate (G6P) and ADP. There are four HK isoforms with hexokinase 2 (HK2) being highly expressed in adipose tissue.[21] During differentiation of adipocytes, HK2 expression levels are increased sevenfold followed by a decrease in expression thereafter, showing a clear correlation between triacylglycerol formation and hexokinase expression.[22] Glucose concentration and HK2 expression levels are inversely proportional with high glucose concentrations (30 mM) causing a threefold decrease in HK2 expression levels.[23] HK2 expression levels are also affected by changes in temperature. In mouse inguinal brown adipose tissue and inguinal white adipose tissue, HK2 gene expression in cold conditions (4°C) sees a twofold increase.[21]

2.2.2 Phosphoglucoisomerase

Phosphoglucoisomerase (PGI) catalyses the reversible conversion of G6P to fructose 6-phosphate (F6P). PGI is found both in the cytoplasm and outside the cell. In the cytoplasm PGI is involved in glycolysis, gluconeogenesis and the pentose phosphate pathway.[24] In kidneys, heart, brain and muscle, PGI mimics the function of neuroleukin, a neurotrophic factor found outside the cell, due to PGI and neuroleukin being almost identical.[25,26] When elevated, serum PGI serves as a biomarker for many types of cancer[27] as tumour cells secrete PGI. This has led to research into PGI as a drug target.[28]

2.2.3 Phosphofructokinase

There are two classes of phosphofructokinase (PFK), PFK1 and PFK2. PFK1 catalyses the conversion of F6P and ATP to fructose 1,6-bisphosphate (F1,6BP) and ADP. PFK2 catalyses the conversion of F6P and ATP to fructose 2,6-bisphosphate (F2,6BP) and ADP. PFK1 is a tetramer with each subunit having

a muscle (M), liver (L), or platelet (P) form.[29] The composition of the enzyme produces many isozymes such as M4 exclusively found in muscle tissue, and L4 exclusively found in liver tissue. Erythrocytes have several isozymes comprised of M and L subunits as well as L4 and M4. Platelets and fibroblast PFK1 isozymes primarily have P subunits while brain tissue has a combination of P, L, and M subunits.[29] Adipose tissue has been found to have L and P subunits.[22]

In adipose tissue, PFK1 expression levels, similarly to HK, are affected by temperature. During cold exposure (4°C), expression levels of PFK1 L and P subunits are upregulated threefold in brown adipose tissue with the former also being upregulated twofold in white adipose tissue.[22] PFK1 in adipose tissue has been shown to be inhibited by ATP and activated by F2,6BP.[30] The phosphorylation of PFK1 in white and brown adipose tissue by cyclic AMP-dependent protein kinase has been found to activate the enzyme. This is achieved by decreasing the inhibitory effect of ATP and lowering the affinity of PFK1 for F2,6BP.[30]

2.2.4 Aldolase

Aldolase catalyses the reversible cleavage of F1,6BP to DHAP and glyceraldehyde 3-phosphate (GAP). There are three aldolase isozymes.[31] Aldolase A is predominately expressed in embryos and muscle but is ubiquitously expressed in most tissues.[31,32] It serves to catalyse the above reversible reaction. Other functions of aldolase A include, but are not limited to, regulation of cell proliferation[33] and modulation of cell morphology.[34] Aldolase B is predominantly expressed in the liver.[31] It is able to catalyse the same reaction of aldolase A but can also catalyse the conversion of fructose 1-phosphate (F1P) to glyceraldehyde (GA) and DHAP.[35] Aldolase B is the only aldolase isozyme that does not show a preference between F1P and F1,6BP while aldolase A and C more readily metabolise F1,6BP.[35] Aldolase C is predominately expressed in the brain. Its primary function is that of aldolase A while also being involved in the functioning of the central nervous system.[36]

In adipose tissue, aldolase A mRNA expression and protein levels are upregulated by high insulin concentrations (100 nM) but are unaffected by high glucose concentrations (25 mM).[37] Aldolase B is mRNA expression and protein levels are downregulated by high insulin concentrations as well as high glucose concentrations.[37] In mice, aldolase B mRNA expression levels are upregulated in obese specimens compared to lean mice and even further upregulation is seen for diabetic mice.[38] Obesity and diabetes do not significantly affect mRNA expression levels of aldolase A.[38]

2.2.5 Triosephosphate isomerase

Triosephosphate isomerase (TPI) catalyses the reversible conversion of DHAP to GAP. The reaction heavily favours DHAP formation in a 20:1 ratio.[39] In most cells this is avoided by the constant consumption of GAP by lower glycolysis, resulting in the majority of carbon flowing through glycolysis towards pyruvate formation. From this, the typical ratio of two lactate molecules produced for each glucose molecule consumed can be seen. In adipose tissue this has been shown to not be the case with the ratio being closer to 1:1 for glucose:lactate due to the upregulation of glycerol 3-phosphate formation from DHAP.[23] TPI has many moonlighting functions. It serves as a marker in several cancers[40] and may function as both a virulence factor[41] and an allergen.[42] TPI has also been found to play a role in neurodegenerative diseases such as Alzheimer's disease.[43]

2.2.6 Glyceraldehyde 3-Phosphate Dehydrogenase

Glyceraldehyde 3-Phosphate Dehydrogenase (GAPDH) catalyses the conversion of GAP and NAD^+ to 1,3-bisphosphoglycerate (1,3BPG) and NADH. Five GAPDH isoforms exist.[44] It is hypothesised that four of these isoforms are a result of post-translational modification of cytosolic GAPDH.[45] More specifically, these isoforms arise through nuclear translocation. Once localised to the nucleus they perform several functions including apoptosis, tRNA transport, and DNA replication and repair.[45] Cytosolic GAPDH is one of the least active enzymes within glycolysis.[46] In adipose tissue, the activity of GAPDH in catalysing the above reaction is upregulated by obesity.[47]

2.2.7 Phosphoglycerate kinase

Phosphoglycerate kinase (PGK) catalyses the conversion of 1,3BPG and ADP to 3-phosphoglyceric acid (3PG) and ATP. In humans, two isoforms of PGK exist. PGK1 is found in all somatic cells[48] while PGK2 is found in sperm cells only.[49] Other than glycolysis, PGK1 is involved in DNA replication and repair.[50] PGK2 is involved in fertility and sperm mobility.[51] In adipose tissue, it was found that obesity in human subjects downregulates the activity of PGK.[52]

2.2.8 Phosphoglycerate mutase

Phosphoglycerate mutase (PGM) catalyses the conversion of 3PG to 2-phosphoglyceric acid (2PG). There are two classes of PGM: the cofactor-independent iPGM, found in all plants and the cofactor-dependent dPGM found in all vertebrates.[53] dPGM is a dimer and exists as one of three isozymes, resulting from each of its subunits having either a brain-type (b-type) or muscle-type

(m-type) form. All tissues contain the three isozymes but the distribution in specific muscle tissues is different. A PGM enzyme with two m-type subunits (mm) is primarily found in smooth muscle. An m-type and a b-type combination (mb) is found primarily in skeletal and cardiac muscle. A two b-type PGM (bb) is primarily found in all other tissues.[54] This is evident as bb PGM is the predominant isozyme in white mouse adipose tissue.[55] In obese (ob/ob) mice, m-type subunits are expressed in subcutaneous adipose tissue but not in visceral adipose tissue.[56] In human patients with cardiovascular disease, chronic insulin treatment increases the post-translational modifications of PGM in mesenchymal cells in epicardial adipose tissue.[57]

2.2.9 Enolase

Enolase catalyses the conversion of 2PG to phosphoenolpyruvic acid (PEP). Enolase is a dimer and exists as one of five isozymes, resulting from each of its subunits having an α, β, or γ form. All possible homodimer combinations are predominantly expressed in humans.[58] $\alpha\alpha$ enolase is primarily expressed in adipose, kidney, spleen, brain and liver tissue. $\beta\beta$ enolase is almost exclusively expressed in muscle tissue. $\gamma\gamma$ enolase is primarily expressed in neural tissue[58] as well as having higher levels in adipose tissue as compared with other peripheral tissues.[59] Of the non-prominent isozymes, $\alpha\beta$ enolase is expressed in muscle.[60] $\alpha\gamma$ enolase only exists as an intermediate in neural tissue when an $\alpha\alpha$ enolase switches to a $\gamma\gamma$ enolase during neural tissue development in primate and rats.[61] Evidence of the existence of $\beta\gamma$ enolase has yet to be found.[62]

In human adipose tissue, $\alpha\alpha$ enolase is expressed more in omental fat than in subcutaneous fat with obesity within omental fat not playing a role in $\alpha\alpha$ enolase expression.[63] In rat white adipose tissue, female specimens have been shown to have higher expression levels of $\beta\beta$ enolase as compared with males.[64] This is true for obese and non-obese specimens. Obesity in male rats upregulates white adipose tissue $\beta\beta$ enolase while female white adipose tissue $\beta\beta$ enolase expression is unaffected by obesity.[64]

2.2.10 Pyruvate kinase

Pyruvate kinase (PK) catalyses the conversion of PEP and ADP to pyruvate and ATP. In vertebrates, four isozymes of PK exist: L, R, M1, and M2.[65] L is primarily expressed in the liver. R is primarily expressed in erythrocytes. M1 is primarily expressed in brain and muscle. M2 is primarily expressed in most other tissues including adipose tissue.[65] M1 PK only exists in a tetramer form while M2 PK is able to exist as either a dimer or tetramer. The dimer form has a low affinity for PEP while the tetramer form has a high affinity for PEP.[66] M2 is the only PK isozyme that is allosterically regulated by F1,6BP.[67] In several cancer cell lines, a high insulin concentration (100 nM) has been found

to upregulate the expression of M2 PK twofold. High insulin concentrations inhibit activity of M2 PK in the same cell lines.[68]

In 3T3-L1 adipocytes, a M2 PK deficiency leads to improved differentiation of pre-adipocytes. The same deficiency in white adipose tissue has also been found to increase uncoupling Protein 1 (UCP1) expression and mitochondria biogenesis suggesting a link to adipose tissue browning.[69] In rat epididymal adipose tissue, treatment with glucose (4.5 mM) or insulin (0.056 nM) does not affect M2 PK activity while a combination of the two enhances M2 PK activity. A combination of glucose, insulin, and glutamine (4.4 mM) increase M2 PK activity threefold.[70]

2.2.11 Lactate dehydrogenase

Lactate dehydrogenase (LDH) catalyses the conversion of pyruvate and NADH to lactate and NAD^+. LDH is a tetramer and exists as one of five isozymes, resulting from each of its subunits having an H or M form.[71] LDH1 (4H) is primarily found in the heart and brain tissue as well as in erythrocytes. LDH2 (3H1M) is primarily found in serum. LDH3 (2H2M) is primarily found in lung tissue. LDH4 (1H3M) is primarily found in the pancreas, kidney, and placenta. LDH5 (4M) is primarily found in straited muscle tissue and liver tissue.[71]

In rat epididymal adipose tissue, all five isozymes are expressed.[72] Rats on a fasting diet show an increase in LDH1 and LDH2 activity while a decrease is seen in LDH3, LDH4, and LDH5 activity. The same outcome is found in diabetic rats.[72] Exposure to insulin (2 units/ml) for two days, increases the percentage of LDH5 as a total of LDH content within the epididymal adipose tissue of diabetic rats while decreasing that of LDH 1-4. Insulin does not have a significant effect on LDH isozyme composition in non-diabetic rats.[72]

2.3 Triacylglycerol synthesis

Triacylglycerol synthesis within adipocytes requires two metabolites: G3P and fatty acids. The origin of these metabolites for use in triacylglycerol synthesis varies depending on the availability of glucose and lipoproteins. During periods of glucose abundance, G3P is produced by glycerol 3-phosphate dehydrogenase (G3PDH) using DHAP as substrate. During periods of fasting or starvation, G3P is sourced from the degradation of triacylglycerols, a process known as lipolysis.[73] This process utilizes adipose triglyceride lipase (ATGL) to convert triacylglycerols to 1,2-diacylglycerol or 2,3-diacylglycerol while freeing a fatty acid molecule.[74] Hormone-sensitive lipase (HSL) converts these two metabolites to 2-monoacylglycerol while freeing up a fatty acid molecule.[75] Monoacylglycerol lipase (MGL) converts this metabolite to glycerol while freeing up a fatty acid molecule.[76] Finally, glycerol is converted into G3P by glycerol kinase

(GK).[77]

Fatty acids, as is seen above, can be generated from lipolysis as the degradation of triacylglycerols frees three fatty acid molecules. For the purposes of lipogenesis, fatty acids have two sources: the citric acid cycle and lipoproteins.[78] As shown in Fig 2.2, the former source begins with the conversion of pyruvate to acetyl coenzyme A (acetyl-CoA) by three enzymes that form the pyruvate dehydrogenase complex (PDC).[79] Through the oxidation of acetyl-CoA, the citric acid cycle is able to convert oxaloacetate to citrate using citrate synthase (CS).[80] The citric acid cycle through eight reactions is able to produce two carbon dioxide molecules, one GTP/ATP, and reduced forms of NADH and FADH2 as well as regenerating oxaloacetate.[19] However, when fatty acids need to be synthesised, citrate can be transported out of the mitochondria by the citrate transporter.[81] It is then converted to acetyl-CoA by citrate lyase (CL). Acetyl-CoA is converted to malonyl-CoA by acetyl-CoA carboxylase (ACC). Finally, the multi-enzyme complex, fatty acid synthase (FAS) converts malonyl-CoA to the 16-carbon fatty acid, palmitic acid.[82] This fatty acid can undergo several modifications to form longer fatty acids.[83] For the synthesis of fatty acids shorter than a 16-carbon chain, the multi-reaction process that produces palmitic acid is terminated early.[84] The other source of fatty acids, lipoproteins, are found outside of the adipocyte cell in very low-density lipoproteins, formed in the liver, and chylomicrons, formed in the endoplasmic reticulum.[85] These lipoproteins contain triacylglycerols which can be hydrolysed by lipoprotein lipase to two fatty acids and one monoacylglycerol molecule.[85] The fatty acids can be transported into the cell by a membrane-associated fatty acid-binding protein such as albumin.[86,87]

With both G3P and fatty acid synthesised, triacylglycerols are synthesised by a four-step process. First, G3P and one fatty acid molecule are converted into lysophosphatidic acid by glycerol-3-phosphate acyltransferase (GPAT).[88] Second, lysophosphatidic acid and one fatty acid molecule are converted into phosphatidic acid by acylglycerophosphate acyltransferase (AGPAT).[88] Third, phosphatidic acid is converted into 1,2-diacylglycerol by phosphatidate phosphatase (PAP).[89] Fourth and inverse from the first step of lipolysis, 1,2-diacylglycerol and one fatty acid molecule are converted into triacylglycerols by diglyceride acyltransferase (DGAT).[90]

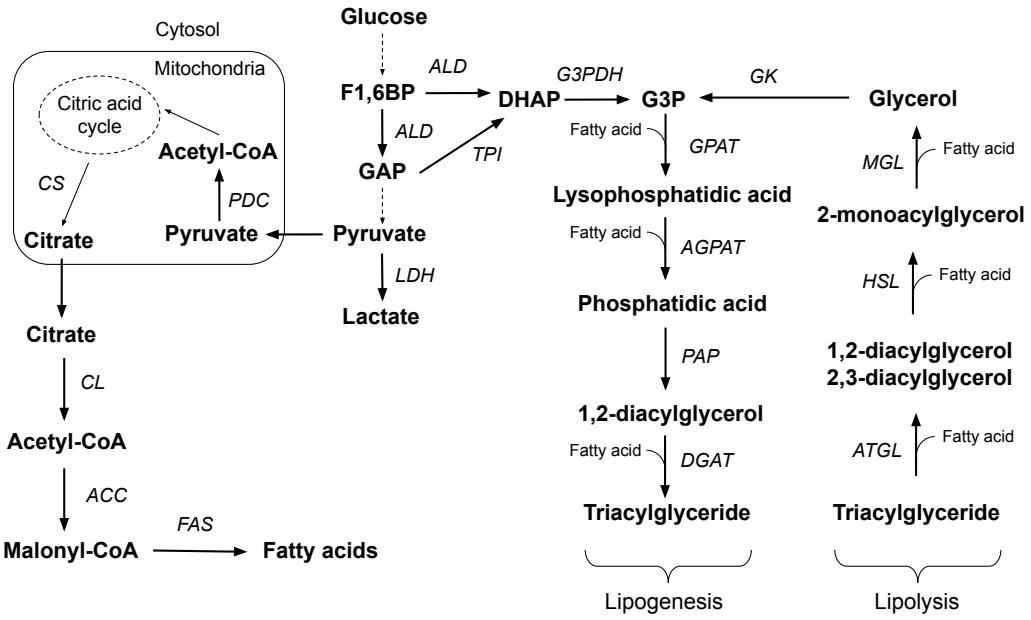

Figure 2.2: Lipogenesis, lipolysis, and fatty acid synthesis in adipose tissue. Metabolites are in bold with enzymes in italics. Dashed arrows represent clusters of enzymes. The acronyms are as follows: aldolase (ALD), triosephosphate isomerase (TPI), glycerol 3-phosphate dehydrogenase (G3PDH), glycerol-3-phosphate acyltransferase (GPAT), acylglycerophosphate acyltransferase (AGPAT), phosphatidate phosphatase (PAP), diglyceride acyltransferase (DGAT), glycerol kinase (GK), monoacylglycerol lipase (MGL), hormone-sensitive lipase (HSL), adipose triglyceride lipase (ATGL), lactate dehydrogenase (LDH), pyruvate dehydrogenase complex (PDC), citrate synthase (CS), citrate lyase (CL), acetyl-CoA carboxylase (ACC), fatty acid synthase (FAS).

2.3.1 Glycerol-3-phosphate dehydrogenase

Glycerol 3-phosphate dehydrogenase (G3PDH) catalyses the conversion of DHAP and NADH to G3P and NAD^+. G3PDH has two isoforms, G3PDH-C found in the cytoplasm and G3PDH-M found in the mitochondria. The former catalyses the above reaction and thus is utilised in glycolysis and lipogenesis[91] while the latter catalyses the conversion of G3P to DHAP. G3PDH-M is also involved in the electron transport chain.[92] Before the isozymes were discovered, G3PDH was isolated and characterised in human white adipose tissue.[93] The kinetic parameters obtained represent G3PDH-C as the study was focused on linking glycolysis to triacylglycerol synthesis. It has also been found that in human subcutaneous adipose tissue, G3PDH-C mRNA expression levels and G3PDH-C activity is increased in obese individuals.[94,95] This increase in G3PDH-C expression levels is proportional to an increase in fatty acid translocase mRNA expression levels.[95]

2.4 Systems Biology

Biological processes no matter how complex, always form part of greater systems. These systems range from simple transport of molecules around the body to complex signalling pathways responsible for a multitude of functions. The cell is a system just as any tissue is a system. Systems biology can be described as the approach to studying the functioning of systems through the use of mathematical modelling. Models are used to describe systemic behaviour based on the individual components that comprise them.

Metabolic studies have progressed greatly since the advent of systems biology. There are two approaches within systems biology to construct metabolic models: top-down and bottom-up. Top-down modelling involves fitting models to system data such as metabolite profiles and are generally applied to larger systems, or to systems for which it is hard to characterise the individual components.[153] Bottom-up modelling is the opposite, using individual components to describe the system. This approach is mechanistic in nature.[153] A clear example of bottom-up modelling is using the characterisation of individual enzymes to describe a system or pathway such as glycolysis which can be further used to understand carbon metabolism within the cell.

Metabolism is an ideal field of study using systems biology as much basic information is already known; e.g. which reactions consume and produce which metabolites as well as the stoichiometry of the reactions. If it is known which reactions are catalysed by which enzymes, it is simple to set up ordinary differential equations (ODEs) on the basis of enzyme kinetics. Substrate is consumed and product is produced as a function of the rate of the enzyme that catalyses the reaction. There are several prime examples of bottom-up modelling of glycolysis in *Saccharomyces cerevisiae*[133], *Plasmodium falciparum*[143], and *Trypanosoma brucei*.[146]

In adipocytes, in addition to glycolysis, lipid metabolism plays an important role. Lipid metabolism is another ideal system to be studied with mathematical modelling. Although not as comprehensive as the glycolytic models mentioned previously, examples of models for yeast lipid metabolism[147,148] as well as triglyceride and free fatty acid metabolism in human white adipocytes[149] have been created. Models for lipid metabolism disfunction have been created as well. Three of these comprehensive models address lipid degradation and disorders associated with it. These models describe the effect of substrate overload on mitochondrial fatty-acid beta-oxidation (mFAO) caused by substrate competition in mouse hepatocytes. The first describes the first ever created dynamic model for fatty acid β-oxidation.[151] This model includes the basis of substrate competition within mouse hepatocytes. The second describes the effect of substrate competition on substrate overload leading to a decline in flux.[150] The third investigated further into the mechanism of substrate overload

and how it leads to a decline in flux.[152] mFAO disorders lead to life-threatening metabolic conditions, and elucidating the biochemical mechanisms underlying the disease is a good example of how powerful mathematical modelling of biological systems is.

2.5 Modelling of glycolysis in adipocytes

To date, almost all kinetic models of adipose tissue metabolism investigate glucose consumption, lactate production, and the triacylglycerol synthesis pathway while giving little attention to the intermediary reactions of glycolysis. Because of this, there is a lack of kinetic characterisation of glycolytic enzymes in adipose tissue.

There exists a model for glycogenolysis in skeletal muscle that characterises all glycolytic enzymes with the exception of hexokinase as the carbon source, in this model, is glycogen.[105] Despite exclusively using parameters from literature - sourced from rabbit, mouse, pig, chicken, rat, and human - this model is the closest to a complete glycolytic model for any mammalian tissue. Other more extensive metabolic models seem to ignore the majority of glycolytic enzymes as glucose consumption and lactate production are the most important effects of glycolysis. This can be seen in the most extensive metabolic model for muscle metabolism containing components for glycolysis, the citric acid cycle, glycogen synthesis and utilisation, lipogenesis, and lipolysis.[99] In this model, glycolysis is separated into several metabolic reaction flux expressions: glucose conversion to G6P, a lumping of all four reactions that convert G6P to GAP and DHAP, GAP conversion to 1,3BPG, a lumping of all four reactions that convert 1,3BPG to pyruvate, and finally the conversion of pyruvate to lactate. However, for the scope and size of the model, this level of characterisation of glycolytic enzymes is all that is needed.

While models of muscle metabolism tend to focus on glycolysis in part, adipose tissue metabolic models tend to focus on lipogenesis and lipolysis. These models mostly include components for glycolysis as just a source of glycerol-3-phosphate from glucose and aceytl-CoA from pyruvate.[106] There is a whole-body model, containing components for human brain, muscle, and adipose tissue, that attempted to characterise the human body's response to glucose.[100] The adipose tissue part of this model, like most others, was focused on lipogenesis and lipolysis but also characterised adipose tissue glycolysis in part. Kinetic parameters for glycolytic enzymes were obtained from literature or optimised from clinical data. Model time course simulations of glucose, G6P, F6P, pyruvate, lactate, and G3P as well as ATP and ADP were generated as well as other non-glycolytic metabolites. While not simulating all metabolites of glycolysis, this model is quite extensive compared to most adipose tissue models in terms of glycolysis. The trends observed were then validated with literature

data and it was concluded that the simulated trends sufficiently match those of the validation data set with hyperglycaemic conditions resulting in triacylglycerol synthesis and hypoglycaemic conditions resulting in triacylglycerol break down. While relatively extensive, this model is still far off from the level of detail needed to address the research question of this project. An adipose tissue metabolic model similar in detail to the model for glycogenolysis in skeletal muscle[105] is needed with each glycolytic enzyme characterised in detail.

Chapter 3

Methods and Materials

3.1 Culturing of 3T3-L1 adipocytes

3T3-L1 pre-adipocytes (obtained from Tygerberg medical campus, South Africa) were incubated with 5% carbon dioxide at 37°C in 90% v/v 4.5 g/L Dulbecco's Modified Eagle Medium (DMEM) supplemented to 0.44 mM glucose (excluding glucose already present in DMEM) and 10% v/v newborn calf serum (NBCS). This medium was refreshed every two days until 100% confluence was achieved. After reaching confluence, the pre-adipocytes were incubated for an additional two days.

The confluent pre-adipocytes were differentiated into adipocytes in three stages. Firstly, the culture was incubated for three days at 5% carbon dioxide at 37°C in 90% v/v 4.5 g/L DMEM supplemented to 0.44 mM glucose (excluding glucose already present in DMEM), 10% v/v fetal bovine serum (FBS), 0.5 mM IBMX, 1μM dexamethasone and 10 mg/l insulin. Secondly, the culture was incubated for two days in the same conditions and in the same media as the first stage but dexamethasone and IBMX were not included in the media. Thirdly, the culture was incubated for five days in the same conditions and the same media as the second stage but insulin was not included in the media. The media in stage three was refreshed on the third day of the five-day period.

3.2 Culture Harvesting and Lysate Preparation

Before harvesting, cell cultures were serum starved in 4.5 g/L DMEM for 15 hours. Cells were then washed twice with 1X PBS to remove excess media followed by the scraping of cells from the flask or dish and suspension in assay buffer (0.1M Tris pH 7.0, 15mM NaCl, 0.14M KCl, 0.5mM $CaCl_2$, and 5 mM Phosphate). If the cells are stored, the suspension was supplemented to 0.25 mM PMSF. To lyse the harvested adipocytes, 1% v/v Triton X-100 was used.

The cells were placed on ice for 30 minutes and vortexed every 10 minutes for approximately 10 seconds. Equal parts hexane and lysate were mixed thoroughly with a vortex. The mixture is centrifuged at 20817 rcf at 4°C for 15 minutes. The aqueous layer containing all the glycolytic enzymes was then removed and stored on ice.

3.3 Enzyme Characterisation

Characterisation of glycolytic enzymes was performed using NAD^+/ NADH/ $NADP^+$ linked enzymes assays. These assays, adapted from Teusink et al.[133], provide a specific activity for each enzymes as well as affinities for substrates and products. The assays were carried out in 96-well plates (*Greiner bio-one F-Bottom* microtiter plate) at 37°C and measured at 340 nm on a spectrophotometer (*BioTek PowerWave* 340 *BMG Labtech SPECTROstar*^{Nano} spectrophotometer). In all assays, the NAD^+/ NADH/ $NADP^+$ concentration was 0.8 mM with all linking enzymes at 5 U/ml. The concentration of magnesium was always kept at double that of ATP or ADP to ensure ATP was primarily in its active form. All glycolytic enzymes were characterised in either the forward or reverse direction with the exception of PGI and LDH being characterised in both. Which direction the enzyme was characterized in was dependent on the feasibility of obtaining data sets for the direction as is the case for reactions that have heaviliy favoured directions. G3PDH and AK, while not forming part of glycolysis, were also characterised.

From the coupled assays, rates were obtained that represented the change in absorbance as a function of time. In order to convert this to μmol.min^{-1}.mg^{-1} which is utilised in the model two elements needed to be established: the protein concertation of the lysate used and the pathlength of the sample in the well. Protein concentration was determined by means of a Bradford reaction which establishes the relationship between absorbance and total protein concentration using the Beer-Lambert law. For the pathlength, an NADH calibration curve was created which established the relationship between absorbance and concentration of substrate within the well. From the NADH calibration curve, the extinction coefficient of NADH and pathlength was determined for the wells used in the assay.

3.3.1 Biological variance of enzyme characterisations

Each enzyme was characterised with a varying number of cell lysates depending on the number of data sets required. Each cell lysate was prepared from a unique culture flask that has 3T3-L1 adipocytes grown, differentiated and harvested in isolation from other cultures. In this way each lysate was unique with a different protein concentration. In total, 17 cell lysates were used in the

characterisation of all enzymes included in the model. The following are how many lysates were used for each enzyme: hexokinase (2), phosphoglucoisomerase (2), phosphofructokinase (2), aldolase (1), triosephosphate isomerase (1), glycerol 3-phosphate dehydrogenase (1), glyceraldehyde 3-phosphate Dehydrogenase (1), phosphoglycerate kinase (3), enolase (1), pyruvate kinase (2), lactate dehydrogenase (2), adenylate kinase (2). Three lysates were used to test multiple enzymes in part: one for hexokinase and PGI, one for PGK and PK, and one for enolase and PK.

3.3.2 Hexokinase

Hexokinase was characterised in the forward direction. The reaction was linked to $NADP^+$ reduction by G6PDH. Three data sets were obtained: varying glucose as substrate (0-6 mM) at 4 mM ATP, varying ATP as substrate (0-20 mM) at 10 mM glucose, and varying AMP as inhibitor (0-20 mM) at 10 mM glucose and 4 mM ATP. The first two data sets utilized the same lysate with the third data set utilizing its own lysate.

3.3.3 Phosphoglucoisomerase

Phosphoglucoisomerase was characterised in both the forward and reverse direction. The forward reaction was linked to $NADH^+$ oxidation by G3PDH utilizing PFK and ALD as linking enzymes and ATP at 4 mM. The reverse reaction was linked to $NADP^+$ reduction by G6PDH. One data set was obtained for the forward reaction: varying G6P as substrate (0-20 mM) at 0 mM F6P. One data set was obtained for the reverse reaction: varying F6P as substrate (0-3.5 mM) at 0 mM G6P. Both data sets utilized different lysates.

3.3.4 Phosphofructokinase

Phosphofructokinase was characterised in the forward direction. The reaction was linked to $NADH^+$ oxidation by G3PDH utilizing ALD as a linking enzyme. Two data sets were obtained: varying F6P as substrate (0-3.5 mM) at 1.25 mM ATP, and varying ATP as substrate (0-4 mM) at 1.75 mM F6P. Both data sets were obtained with the same lysate but this experiment was repeated with an additional lysate. This still resulted in two data sets as the repeat experiment was treated as a biological repeat.

3.3.5 Aldolase

Aldolase was characterised in the forward direction. The reaction was linked to $NADH^+$ oxidation by G3PDH. One data set was obtained: varying F1,6BP as substrate (0-8.5 mM).

3.3.6 Triosephosphate isomerase

Triosephosphate isomerase was characterised in the forward direction. The reaction was linked to $NADH^+$ oxidation by G3PDH. One data set was obtained: varying GAP as substrate (0-10 mM).

3.3.7 Glyceraldehyde 3-phosphate dehydrogenase

Glyceraldehyde 3-phosphate dehydrogenase was characterised in the reverse direction. Two data sets were obtained: varying 1,3BPG as substrate (0-0.010582 mM) at 0.8 mM NADH, and varying NADH as substrate (0-0.8 mM) at 0.010582 mM F6P. As 1,3BPG could not be added directly to the reaction mixture, 3PG (0-20 mM) was converted to 1,3BPG using PGK and ATP within the reaction mixture. The concentration of 1,3BPG was calculated from the equilibrium constant of PGK (3200[133])

3.3.8 Phosphoglycerate kinase

Phosphoglycerate kinase was characterised in the reverse direction. The reaction was linked to $NADH^+$ oxidation by GAPDH. Three data sets were obtained: varying 3PG as substrate (0-20 mM) at 4 mM ATP, varying ATP as substrate (0-60 mM) at 20 mM 3PG, and varying ADP as inhibitor (0-20 mM) at 20 mM glucose and 4 mM ATP. The first two data sets utilized the same lysate with the third data set utilizing its own lysate.

3.3.9 Phosphoglycerate mutase

Three attempts were made to characterise phosphoglycerate mutase in the forward direction. The reaction was linked to $NADH^+$ oxidation by LDH utilizing enolase and PK as linking enzymes. Three data sets were obtained: all varied 3PG as substrate (0-20 mM, 0-80 mM, and 0-200 mM) at 4 mM

ADP. None of the data sets were feasible. This is because the activity of PGM was so low (or non-existent) that no distinguishable change in absorbance at 340 nm could be detected. Three different lysates were used in these attempts.

3.3.10 Enolase

Enolase was characterised in the forward direction. The reaction was linked to $NADH^+$ oxidation by LDH utilizing PK as a linking enzyme. One data set was obtained: varying 2PG as substrate (0-10 mM).

3.3.11 Pyruvate kinase

Pyruvate kinase was characterised in the forward direction. The reaction was linked to $NADH^+$ oxidation by LDH. Three data sets were obtained: varying PEP as substrate (0-12.5 mM) at 4 mM ADP, varying ADP as substrate (0-6 mM) at 2.5 mM PEP, and varying ATP as inhibitor (0-50 mM) at 10 mM PEP and 6 mM ADP. The first two data sets utilized the same lysate with the third data set utilizing its own lysate.

3.3.12 Lactate dehydrogenase

Lactate dehydrogenase was characterised in both the forward and reverse direction. Two data sets were obtained for the forward reaction: varying pyruvate as substrate (0-10 mM) at 0.8 mM NADH, and varying NADH as substrate (0-0.8 mM) at 10 mM pyruvate. Two data sets was obtained for the reverse reaction: varying lactate as substrate (0-250 mM) at 0.8 mM NAD^+, and varying NAD^+ as substrate (0-13 mM) at 250 mM lactate. The first two data sets utilized the same lysate with the third and fourth data set utilizing the same lysate.

3.3.13 Glycerol 3-phosphate dehydrogenase

Glycerol 3-phosphate dehydrogenase was characterised in the forward direction. Two data sets were obtained: varying DHAP as substrate (0-10 mM) at 0.8 mM NADH, and varying DHAP as substrate (0-10 mM) at 0.4 mM NADH.

3.3.14 Adenylate kinase

Adenylate kinase was characterised in both the forward and reverse direction. The forward reaction was linked to $NADP^+$ reduction by G6PDH utilizing HK as a linking enzyme. The reverse reaction was linked to $NADH^+$ oxidation by LDH utilizing PK as a linking enzyme. One data set was obtained for the forward reaction: varying ADP as substrate (0-12 mM) at 0 mM ATP and 0 mM AMP. Two data sets were obtained for the reverse reaction: varying ATP as substrate (0-4 mM) at 0 mM ADP and 5 mM AMP, and varying AMP as substrate (0-5 mM) at 0 mM ADP and 4 mM ATP. The first data set utilized its own lysate with the second and third data sets utilizing the same lysate.

3.4 Fitting rate equations

Twelve data arrays were created out of the combined data sets for each of the 12 enzymes characterised. Corresponding rate equations were fitted to the data arrays using the NonlinearModelFit function in *Wolfram Mathematica 11.2*®. The NonlinearModelFit provides best fit estimates for maximal activities and Michaelis constants depending on what was included in the rate equation for each enzyme.

3.5 Computational Modelling

The kinetic model, constructed in *Wolfram Mathematica 11.2*®, consists of variables, initial values for variables, rate equations, kinetic parameters, and ODEs that describe the rate of change in the variables (i.e. metabolites). The ODEs were integrated using the NDSolve function. It is from the output of this function that model time course plots are generated that can be overlaid with experimental data for model validation. The ODEs utilized in model construction were fully reversible and were used for all enzymes regardless of whether they were characterised in a single direction or both. Equilibrium constants and kinetic parameters were used from literature to achieve the reversibility of the rate equations.

3.6 Glycolytic Intermediate and Co-Factor HPLC Determinations

Co-factors and intermediates were quantified using ion-pairing reverse phase HPLC. The column used was a Phenomenex Luna (5μm) C-18 reverse phase column. Separation was achieved using a 40 mM ion-pairing agent, tetrabutyl

ammonium salt (TBA), dissolved in water at a pH of 7.4 (+-0.4). The mobile phase used was 95% TBA solution + 5% acetonitrile with a gradient which is at its highest point at 70% TBA Solution + 30% acetonitrile. A UV-vis detector was used to detect co-factors at 254 nm. Intermediates in radiolabelled samples were detected with a radio-labelled detector (LabLogic Beta-Ram model 5) detecting the 14C-radio isotope. Protein concentration was determined by means of a Bradford reaction.

Chapter 4

Results

4.1 Kinetic characterization

With the end goal of constructing and validating a kinetic model for glycolysis in 3T3-L1 adipocyte cell-free extracts, a bottom-up approach is used in which each glycolytic enzyme is characterised and kinetic behaviour described using a kinetic rate equation. From the characterisation of each enzyme, parameterised rate equations are obtained which are combined in an ODE model. This model is validated in its ability to predict system data sets.

4.1.1 Hexokinase

Hexokinase catalyses the conversion of glucose and ATP to G6P and ADP. 3T3-L1 adipocyte hexokinase was characterised in the forward direction using glucose and ATP as substrate (Fig 4.1). The inhibitory effect of AMP on the forward reaction was included in the characterization (Fig 4.1). The data was fitted using an irreversible Michaelis-Menten equation (Eq. 4.1) which describes the kinetics sufficiently well. The fitted parameters values are displayed in Table 4.1.

$$vHK = \frac{V_{f_{HK}} \cdot \frac{ATP}{K_{ATP}} \cdot \frac{glc}{K_{glc}}}{(1 + \frac{ATP}{K_{ATP}}) \cdot (1 + \frac{glc}{K_{glc}}) \cdot (1 + \frac{AMP}{K_{i_{AMP}}})} \tag{4.1}$$

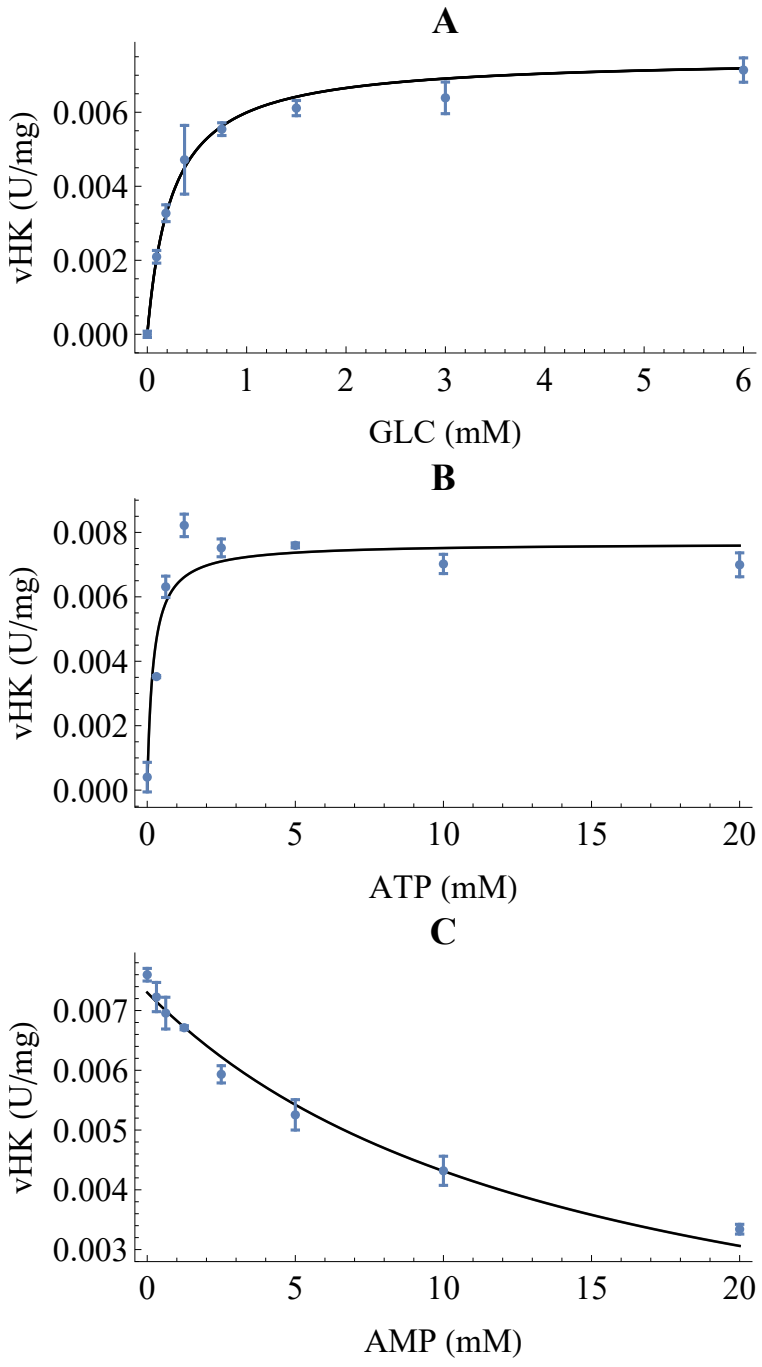

Figure 4.1: Characterization of 3T3-L1 adipocyte hexokinase. HK converts glucose and ATP to G6P and ADP. HK saturation curves using glucose (A) and ATP (B) are shown as well as the inhibition of the forward reaction by AMP (C). The points represent experimental data while the fitted lines represent the result of fitting equation 4.1 to the entire dataset. This fitting provides the parameter values presented in Table 4.1. The error bars represent standard deviation with each data point measured in three technical repeats.

Table 4.1: Kinetic parameters for 3T3-L1 adipocyte hexokinase. Kinetic data for the forward reaction of hexokinase was fitted using equation 4.1. The fitted parameters (± standard error) include maximal specific activity for the forward reaction as well as binding constants of hexokinase for ATP and glucose.

Parameter	Fitted Value	Literature Value	Reference
$V_{f_{HK}}$ (μmol.min^{-1}.mg^{-1})	0.0079 ± 0.00025	-	-
K_{glc} (mM)	0.25 ± 0.045	0.3	107
K_{ATP} (mM)	0.20 ± 0.54	0.7	107
$K_{i_{AMP}}$ (mM)	14 ± 2.8	2.5	108

4.1.2 Phosphoglucoisomerase

Phosphoglucoisomerase catalyses the conversion of G6P to F6P. 3T3-L1 adipocyte PGI was characterised in the forward and reverse direction using G6P and F6P as substrate, respectively (Fig 4.2). The data was fitted using a reversible Michaelis-Menten equation (Eq. 4.2) which describes the data well. The fitted parameters values are displayed in Table 4.2.

$$vPGI = \frac{V_{f_{PGI}} \cdot \frac{g6p}{K_{g6p}} - V_{r_{PGI}} \cdot \frac{f6p}{K_{f6p}}}{1 + \frac{g6p}{K_{g6p}} + \frac{f6p}{K_{f6p}}} \tag{4.2}$$

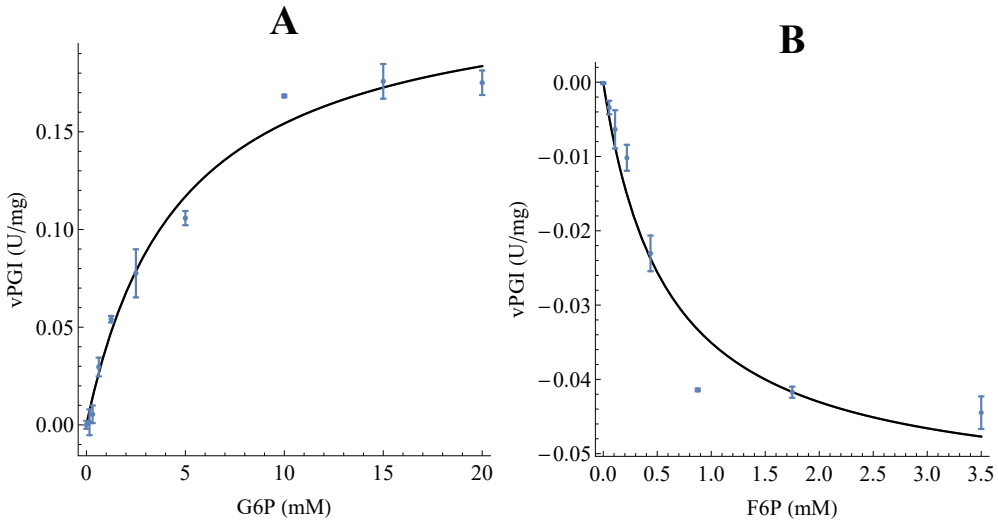

Figure 4.2: Characterization of 3T3-L1 adipocyte PGI. PGI converts G6P to

F6P. PGI saturation curves using G6P (A) for the forward reaction and F6P (B) for the reverse reaction are shown. The points represent experimental data while the fitted lines represent the result of fitting equation 4.2 to the entire dataset. This fitting provides the parameter values presented in Table 4.2. The error bars represent standard deviation with each data point measured in three technical repeats.

Using the Haldane equation (Eq. 4.3), an equilibrium constant for PGI was calculated to be 0.52. This is higher than reported literature value of 0.33[138] but the literature value falls within the error range of the experimentally determined parameter values.

$$Keq = \frac{V_f \cdot K_{product}}{V_r \cdot K_{substrate}} \tag{4.3}$$

Table 4.2: Kinetic parameters for 3T3-L1 adipocyte PGI. Kinetic data for the forward and reverse reaction of PGI was fitted using equation 4.2. The fitted parameters (± standard error) include maximal specific activity for the forward and reverse reaction as well as binding constants of PGI for G6P and F6P.

Parameter	Fitted Value	Literature Value	Reference
$V_{f_{PGI}}$ (μmol.min^{-1}.mg^{-1})	0.23 ± 0.011	-	-
$V_{r_{PGI}}$ (μmol.min^{-1}.mg^{-1})	0.056 ± 0.0098	-	-
K_{g6p} (mM)	4.7 ± 0.63	0.48	109
K_{f6p} (mM)	0.59 ± 0.30	0.031	110

4.1.3 Phosphofructokinase

Phosphofructokinase catalyses the conversion of F6P and ATP to F1,6BP and ADP. 3T3-L1 adipocyte PFK was characterised in the forward direction using F6P and ATP as substrate (Fig 4.3). The data was fitted using an irreversible Michaelis-Menten equation (Eq. 4.4) which describes the kinetics relatively well. It was observed for PFK that there was a modest substrate inhibition for ATP. This was included in the rate equation assuming binding of ATP at an allosteric site with the same binding constant as for its binding at the active site. Without this constraint on the binding constant the parameter was not identifiable, so the binding constants were forced to be identical. The fitted parameters values are displayed in Table 4.3.

$$vPFK = \frac{V_{f_{PFK}} \cdot \frac{ATP}{K_{ATP}} \cdot \frac{f6p}{K_{f6p}}}{(1 + \frac{ATP^2}{K_{ATP}{}^2}) \cdot (1 + \frac{f6p}{K_{f6p}})} \tag{4.4}$$

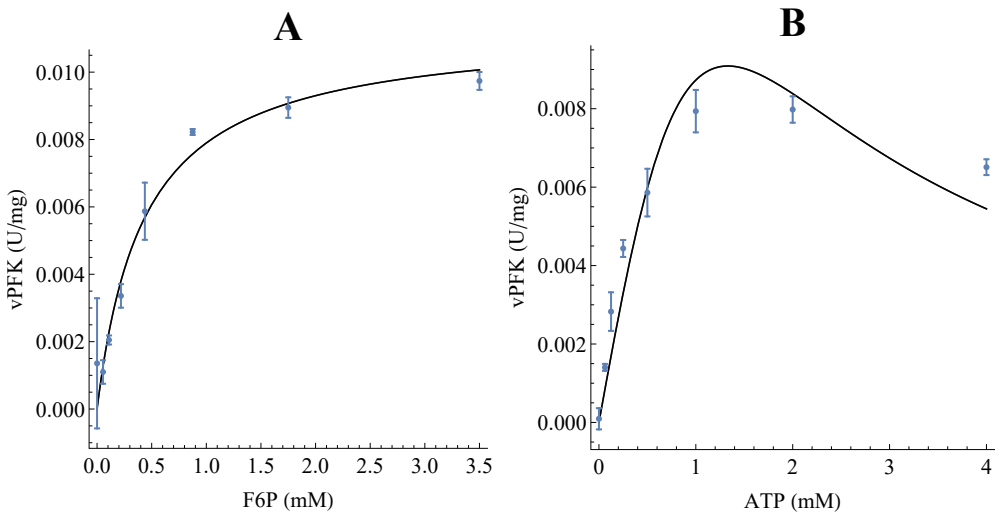

Figure 4.3: Characterization of 3T3-L1 adipocyte PFK. PFK converts F6P and ATP to F1,6BP and ADP. PFK saturation curves using F6P (A) and ATP (B) are shown. The points represent experimental data while the fitted lines represent the result of fitting equation 4.4 to the entire dataset. This fitting provides the parameter values presented in Table 4.3. The error bars represent standard deviation with each data point measured in two biological repeats.

Table 4.3: Kinetic parameters for 3T3-L1 adipocyte PFK. Kinetic data for the forward reaction of PFK was fitted using equation 4.4. The fitted parameters (± standard error) include maximal specific activity for the forward reaction as well as binding constants of PFK for ATP and F6P.

Parameter	Fitted Value	Literature Value	Reference
$V_{f_{PFK}}$ (μmol.min^{-1}.mg^{-1})	0.023 ± 0.0015	-	-
K_{f6p} (mM)	0.43 ± 0.11	0.18	111
K_{ATP} (mM)	1.3 ± 0.12	0.08	111

4.1.4 Aldolase

Aldolase catalyses the conversion of F1,6BP to DHAP and GAP. 3T3-L1 adipocyte aldolase was characterised in the forward direction using F1,6BP as substrate (Fig 4.4). The data was fitted using an irreversible Michaelis-Menten equation (Eq. 4.5) which describes the kinetics well. The fitted parameters

values are displayed in Table 4.4. Although aldolase does catalyse a reversible reaction, due to limitations in the coupled enzyme assays it was not possible to perform reversible kinetics for this characterisation. However, a reversible rate equation (Eq. 4.17) is used for model construction using an equilibium constant and binding constants from literature (see Table 4.13 and 4.14).

$$vALD = \frac{V_{f_{ALD}} \cdot \frac{f16bp}{K_{f16bp}}}{1 + \frac{f16bp}{K_{f16bp}}} \tag{4.5}$$

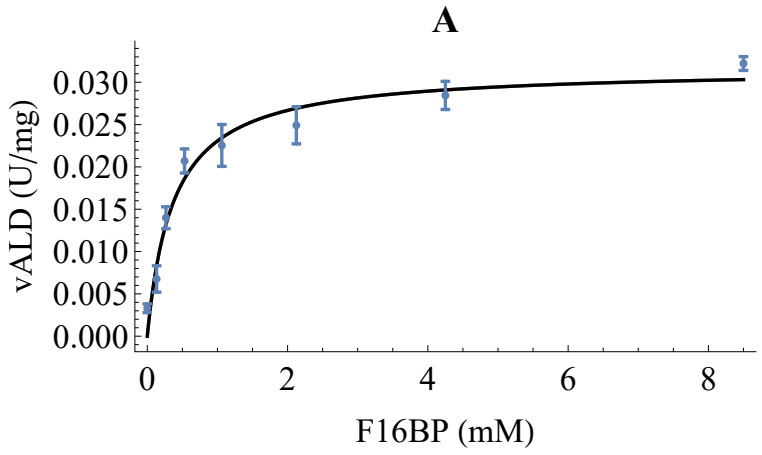

Figure 4.4: Characterization of 3T3-L1 adipocyte aldolase. Aldolase converts F1,6BP to DHAP and GAP. An aldolase saturation curve using F1,6BP (A) is shown. The points represent experimental data while the fitted lines represent the result of fitting equation 4.5 to the entire dataset. This fitting provides the parameter values presented in Table 4.4. The error bars represent standard deviation with each data point measured in three technical repeats.

Table 4.4: Kinetic parameters for 3T3-L1 adipocyte aldolase. Kinetic data for the forward reaction of aldolase was fitted using equation 4.5. The fitted parameters (± standard error) include maximal specific activity for the forward reaction as well as binding constants of aldolase for F1,6BP.

Parameter	Fitted Value	Literature Value	Reference
$V_{f_{ALD}}$ (μmol.min^{-1}.mg^{-1})	0.032 ± 0.0017	-	-
K_{f16bp} (mM)	0.37 ± 0.080	0.05	105

4.1.5 Triosephosphate isomerase

Triosephosphate isomerase catalyses the conversion of DHAP to GAP. 3T3-L1 adipocyte TPI was characterised in the reverse direction using GAP as substrate (Fig 4.5). GAP exhibits an inhibitory effect at concentrations greater than 2.5 mM. The data was fitted using an irreversible Michaelis-Menten equation (Eq. 4.6) which describes the kinetics relatively well, although the fitting requires more data sets. This can be seen in the high standard errors on kinetic parameters displayed in Table 4.5. Although TPI does catalyse a reversible reaction, due to limitations in the coupled enzyme assays it was not possible to perform reversible kinetics for this characterisation. However, a reversible rate equation (Eq. 4.18) is used for model construction using an equilibium constant and binding constants from literature (see Table 4.13 and 4.14).

$$vTPI = -\frac{V_{r_{TPI}} \cdot \frac{gap}{K_{gap}}}{(1 + \frac{gap}{K_{gap}})} \tag{4.6}$$

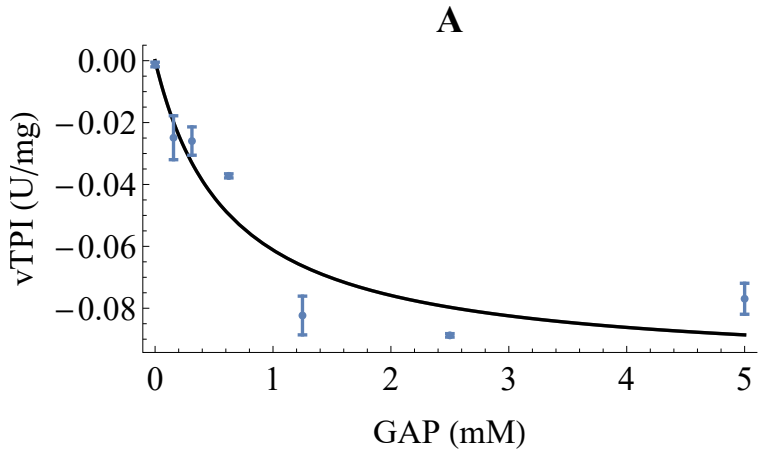

Figure 4.5: Characterization of 3T3-L1 adipocyte TPI. TPI converts DHAP to GAP. A TPI saturation curve using GAP (A) is shown. The points represent experimental data while the fitted lines represent the result of fitting equation 4.6 to the entire dataset. This fitting provides the parameter values presented in Table 4.5. The error bars represent standard deviation with each data point measured in three technical repeats.

Table 4.5: Kinetic parameters for 3T3-L1 adipocyte TPI. Kinetic data for the forward reaction of TPI was fitted using equation 4.6. The fitted parameters (± standard error) include maximal specific activity for the forward reaction as well as binding constants of TPI for GAP.

Parameter	Fitted Value	Literature Value	Reference
$V_{r_{TPI}}$ (μmol.min^{-1}.mg^{-1})	0.10 ± 0.014	-	-
K_{gap} (mM)	0.63 ± 0.29	0.47	112

4.1.6 Glyceraldehyde 3-Phosphate Dehydrogenase

Glyceraldehyde 3-Phosphate Dehydrogenase catalyses the conversion of GAP and NAD^+ to 1,3BPG and NADH. 3T3-L1 adipocyte GAPDH was characterised in the reverse direction using 1,3BPG and NADH as substrates (Fig 4.6). 3PG was added to the assay with PGK to produce 1,3BPG. The concentration of 1,3BPG was calculated from the equilibrium constant of PGK (3200[133]). The data was fitted using an irreversible Michaelis-Menten equation (Eq. 4.7) which describes the kinetics very well. The NADH saturation curve has intrinsic experimental limitations due to NADH being the chromogenic substrate in the assay. Half of the NADH concentrations used in the saturation curve were too low to produce a change in absorbance at 340 nm upon conversion to NAD^+. This can be solved by repeating the assay varying 1,3BPG with varying concentrations of NADH. The fitted parameters values are displayed in Table 4.6. Although GAPDH does catalyse a reversible reaction, due to limitations in the coupled enzyme assays it was not possible to perform reversible kinetics for this characterisation. However, a reversible rate equation (Eq. 4.19) is used for model construction using an equilibium constant and binding constants from literature (see Table 4.13 and 4.14).

$$vGAPDH = -\frac{V_{r_{GAPDH}} \cdot \frac{bpg}{K_{1,3bpg}} \cdot \frac{nadh}{K_{NADH}}}{(1 + \frac{bpg}{K_{1,3bpg}}) \cdot (1 + \frac{nadh}{K_{NADH}})} \tag{4.7}$$

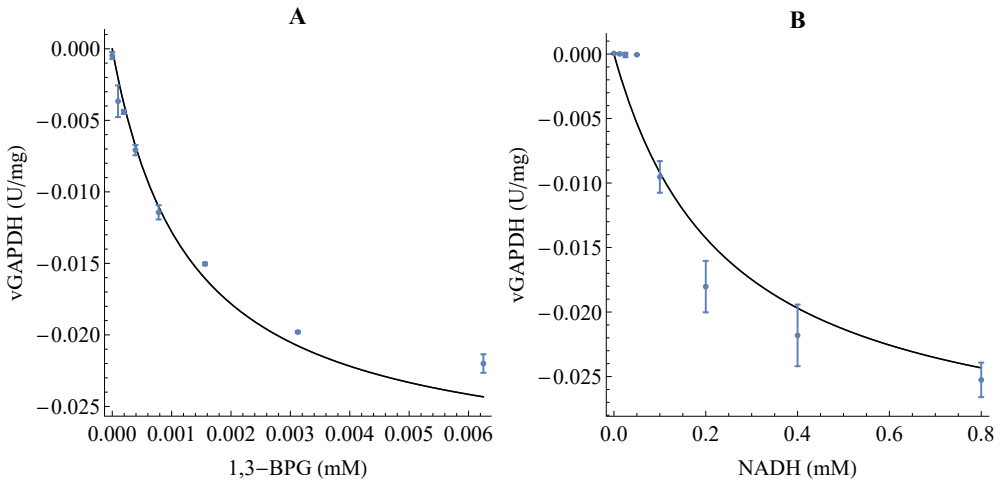

Figure 4.6: Characterization of 3T3-L1 adipocyte GAPDH. GAPDH converts GAP and NAD^+ to 1,3BPG and NADH. GAPDH saturation curves using 1,3BPG (A) and NADH (B) are shown. The points represent experimental data while the fitted lines represent the result of fitting equation 4.7 to the entire dataset. This fitting provides the parameter values presented in Table 4.6. The error bars represent standard deviation with each data point measured in three technical repeats.

Table 4.6: Kinetic parameters for 3T3-L1 adipocyte GAPDH. Kinetic data for the reverse reaction of GAPDH was fitted using equation 4.7. The fitted parameters (± standard error) include maximal specific activity for the reverse reaction as well as binding constants of GAPDH for 1,3BPG and NADH.

Parameter	Fitted Value	Literature Value	Reference
$V_{r_{GAPDH}}$ (μmol.min^{-1}.mg^{-1})	0.038 ± 0.0058	-	-
$K_{1,3bpg}$ (mM)	0.0013 ± 0.00068	0.0008	113
K_{NADH} (mM)	0.25 ± 0.083	0.0033	113

4.1.7 Phosphoglycerate kinase

Phosphoglycerate kinase catalyses the conversion of 1,3BPG and ADP to 3PG and ATP. 3T3-L1 adipocyte PGK was characterised in the reverse direction using 3PG and ATP as substrates (Fig 4.7). The inhibitory effect of ADP, as a competitive inhibitor, on the reverse reaction was included in the characterization (Fig 4.7). ATP exhibits an inhibitory effect at concentrations greater than 5 mM, which was not included in the rate equation as it is far above physiological concentrations. The data was fitted using an irreversible Michaelis-Menten equation (Eq. 4.8) which describes the kinetics well. The fitted parameters

values are displayed in Table 4.7. Although PGK does catalyse a reversible reaction, due to limitations in the coupled enzyme assays it was not possible to perform reversible kinetics for this characterisation. However, a reversible rate equation (Eq. 4.20) is used for model construction using an equilibium constant and binding constants from literature (see Table 4.13 and 4.14).

$$vPGK = -\frac{V_{r_{PGK}} \cdot \frac{3pg}{K_{3pg}} \cdot \frac{ATP}{K_{ATP}}}{(1 + \frac{ATP}{K_{ATP}} + \frac{ADP}{K_{ADP}}) \cdot (1 + \frac{3pg}{K_{3pg}})} \tag{4.8}$$

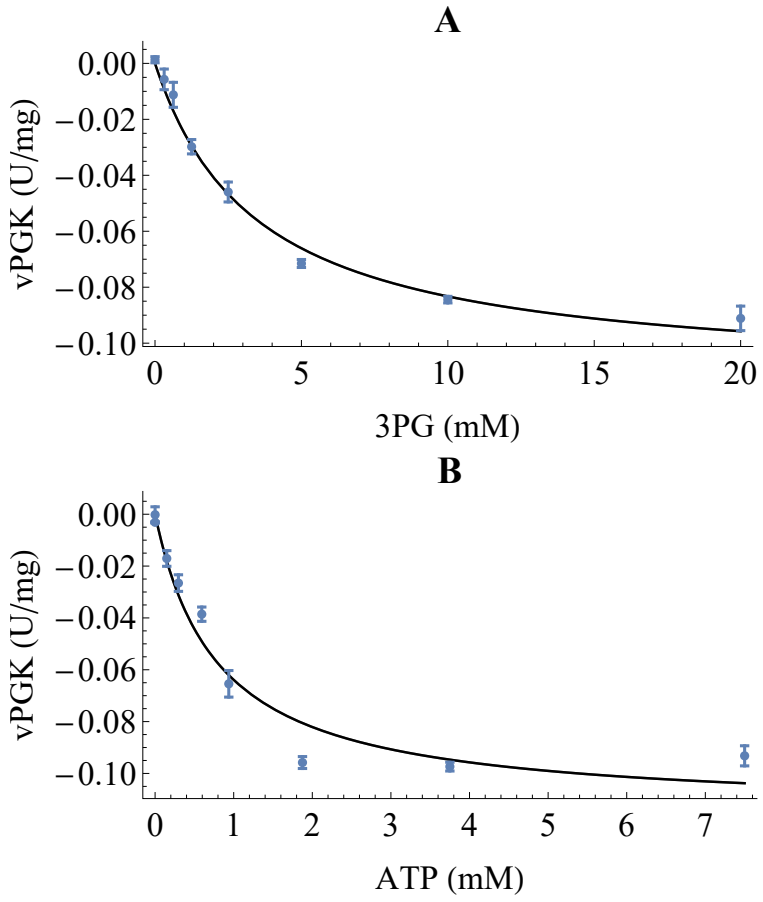

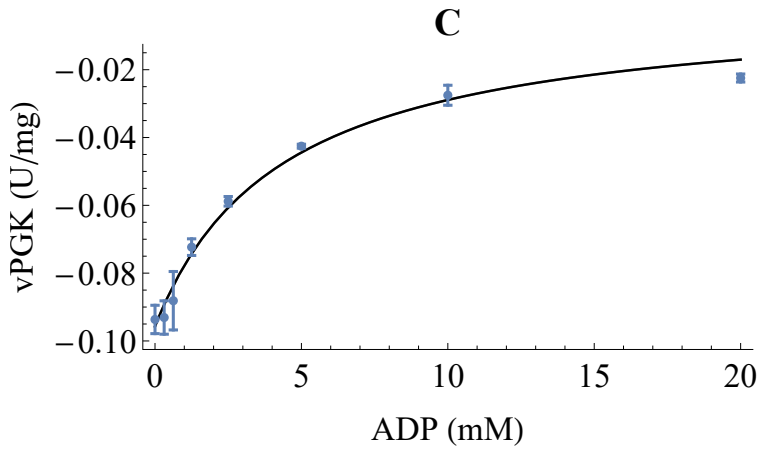

Figure 4.7: Characterization of 3T3-L1 adipocyte PGK. PGK converts 1,3BPG and ADP to 3PG and ATP. PGK saturation curves using 3PG (A) and ATP (B) are shown as well as the inhibition of the reverse reaction by ADP (C). High concentrations of ATP have a clear inhibitory effect on the reverse reaction of PGK as well. The points represent experimental data while the fitted lines represent the result of fitting equation 4.8 to the entire dataset. This fitting provides the parameter values presented in Table 4.7. The error bars represent standard deviation with each data point measured in three technical repeats.

Table 4.7: Kinetic parameters for 3T3-L1 adipocyte PGK. Kinetic data for the reverse reaction of PGK was fitted using equation 4.8. The fitted parameters (± standard error) include maximal specific activity for the reverse reaction as well as binding constants of PGK for ATP and 3PG.

Parameter	Fitted Value	Literature Value	Reference
$V_{r_{PGK}}$ (μmol.min^{-1}.mg^{-1})	0.13 ± 0.0074	-	-
K_{3pg} (mM)	3.5 ± 0.60	1.37	114
K_{ATP} (mM)	0.80 ± 0.13	0.42	114
K_{ADP} (mM)	0.72 ± 0.13	0.05	124

4.1.8 Phosphoglycerate mutase

Phosphoglycerate mutase catalyses the conversion of 3PG to 2-phosphoglyceric acid (2PG). 3T3-L1 adipocyte PGM could not be characterised as a reliable data set could not be obtained. This is because the activity of PGM was so low (or non-existent) that no distinguishable change in absorbance at 340 nm could be detected. It is assumed the reaction is in equilibrium in the model.

4.1.9 Enolase

Enolase catalyses the conversion of 2PG to PEP. 3T3-L1 adipocyte enolase was characterised in the forward direction using 2PG as substrate (Fig 4.8). 2PG exhibits an inhibitory effect at concentrations greater than 1.00 mM. The mechanism underlying this inhibition is not known so a non-competitive mechanism is assumed with one 2PG molecule being able to bind to enolase allosterically. The data was fitted using an irreversible Michaelis-Menten equation (Eq. 4.9) which describes the kinetics quite well. The fitted parameters values are displayed in Table 4.8. Although enolase does catalyse a reversible reaction, due to limitations in the coupled enzyme assays it was not possible to perform reversible kinetics for this characterisation. However, a reversible rate equation (Eq. 4.22) is used for model construction using an equilibium constant and binding constants from literature (see Table 4.13 and 4.14).

$$vENO = \frac{V_{f_{ENO}} \cdot \frac{2pg}{K_{2pg}}}{(1 + \frac{2pg}{K_{2pg}}) \cdot (1 + \frac{2pg}{K_{i_{2pg}}})} \tag{4.9}$$

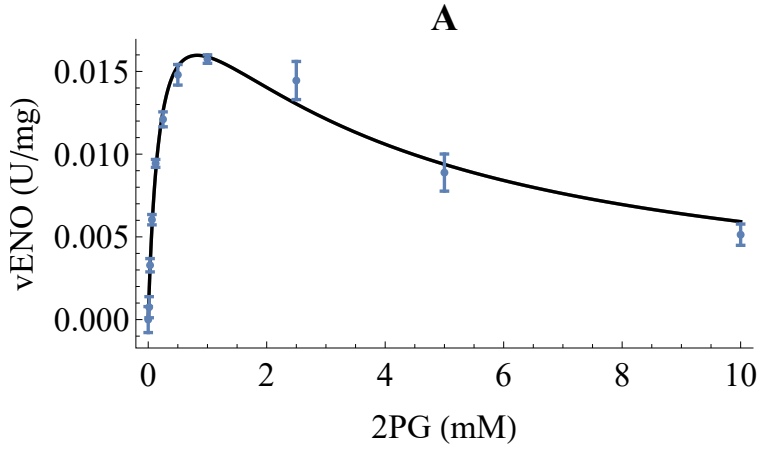

Figure 4.8: Characterization of 3T3-L1 adipocyte enolase. Enolase converts 2PG to PEP. An enolase saturation curve using 2PG (A) is shown with high concentrations 2PG having a clear inhibitory effect on the forward reaction of enolase. The points represent experimental data while the fitted lines represent the result of fitting equation 4.9 to the entire dataset. This fitting provides the parameter values presented in Table 4.8. The error bars represent standard deviation with each data point measured in three technical repeats.

Table 4.8: Kinetic parameters for 3T3-L1 adipocyte enolase. Kinetic data for the forward reaction of enolase was fitted using equation 4.9. The fitted parameters (± standard error) include maximal specific activity for the forward reaction as well as binding constants of enolase for 2PG.

Parameter	Fitted Value	Literature Value	Reference
$V_{f_{ENO}}$ (μmol.min^{-1}.mg^{-1})	0.26 ± 0.0029	-	-
K_{2pg} (mM)	0.22 ± 0.048	0.12	115
$K_{i_{2pg}}$ (mM)	3.1 ± 0.69	-	-

4.1.10 Pyruvate kinase

Pyruvate kinase catalyses the conversion of PEP and ADP to pyruvate and ATP. 3T3-L1 adipocyte PK was characterised in the forward direction using PEP and ADP as substrates (Fig 4.9). The inhibitory effect of ATP on the forward reaction was included in the characterization (Fig 4.9). The data was fitted using an irreversible Michaelis-Menten equation (Eq. 4.10). When the PK rate eqaution was fitted to the experimental data, an accurate estimate for the binding constant of PEP could not be obtained. This is because sufficiently low PEP concentrations were not included in the assay range. Due to time constraints, the experiment could not be repeated. A literature value is used for this parameter. The fitted parameters values are displayed in Table 4.9.

$$vPK = \frac{V_{f_{PK}} \cdot \frac{pep}{K_{pep}} \cdot \frac{ADP}{K_{ADP}}}{(1 + \frac{ADP}{K_{ADP}} + \frac{ATP}{K_{ATP}}) \cdot (1 + \frac{pep}{K_{pep}})} \tag{4.10}$$

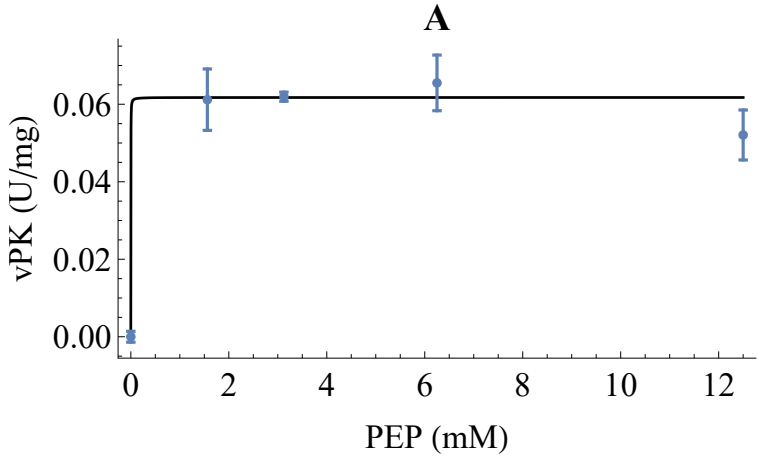

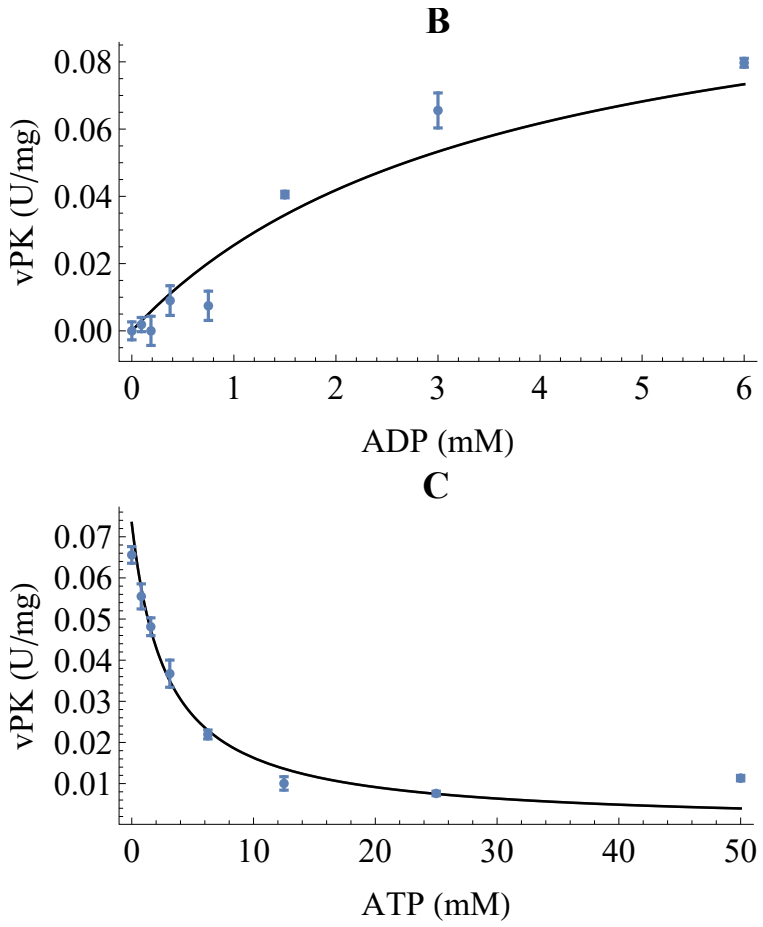

Figure 4.9: Characterization of 3T3-L1 adipocyte PK. PK converts PEP and ADP to pyruvate and ATP. PK saturation curves using PEP (A) and ADP (B) are shown as well as the inhibition of the forward reaction by ATP (C). High concentrations of PEP have a clear inhibitory effect on the forward reaction of PK as well. The points represent experimental data while the fitted lines represent the result of fitting equation 4.10 to the entire dataset. This fitting provides the parameter values presented in Table 4.9. The error bars represent standard deviation with each data point measured in three technical repeats.

Table 4.9: Kinetic parameters for 3T3-L1 adipocyte PK. Kinetic data for the forward reaction of PK was fitted using equation 4.10. The fitted parameters (± standard error) include maximal specific activity for the forward reaction as well as binding constants of PK for ADP, ATP, and PEP.

Parameter	Fitted Value	Literature Value	Reference
$V_{f_{PK}}$ (μmol.min^{-1}.mg^{-1})	0.12 ± 0.021	-	-
K_{pep} (mM)	0.00053 ± 0.16	0.08	116
K_{ADP} (mM)	3.6 ± 1.4	0.3	116
K_{ATP} (mM)	1.1 ± 0.30	1.5	126

4.1.11 Lactate dehydrogenase

Lactate dehydrogenase catalyses the conversion of pyruvate and NADH to lactate and NAD$^+$. 3T3-L1 adipocyte LDH was characterised in the forward direction using pyruvate and NADH as substrates as well as in the reverse direction using lactate and NAD$^+$ as substrates (Fig 4.10). The data was fitted using a reversible Michaelis-Menten equation (Eq. 4.11) which describes the kinetics well. The fitted parameters values are displayed in Table 4.10.

$$vLDH = \frac{V_{f_{LDH}} \cdot \frac{pyr}{K_{pyr}} \cdot \frac{nadh}{K_{NADH}} - V_{r_{LDH}} \cdot \frac{lac}{K_{lac}} \cdot \frac{nad}{K_{NAD}}}{(1 + \frac{lac}{K_{lac}} + \frac{pyr}{K_{pyr}}) \cdot (1 + \frac{nadh}{K_{NADH}} + \frac{nad}{K_{NAD}})} \tag{4.11}$$

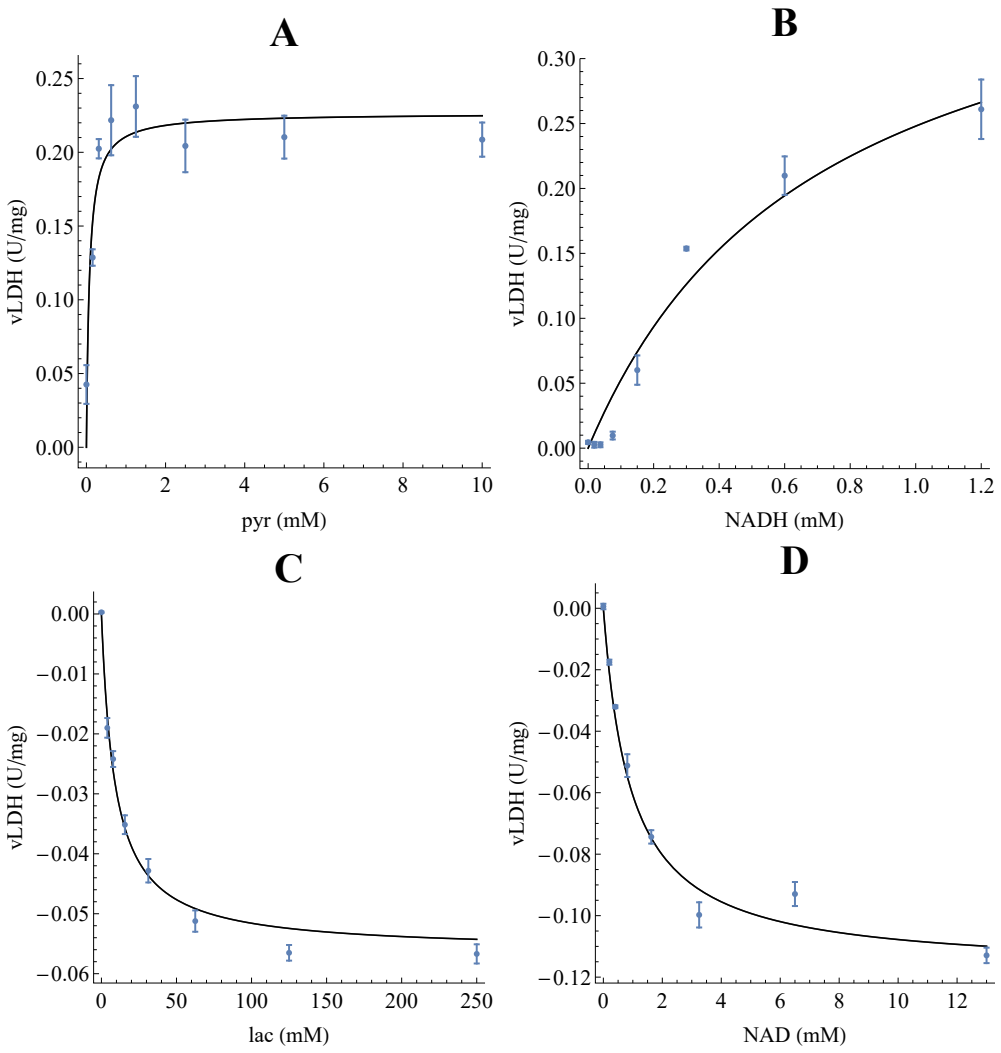

Figure 4.10: Characterization of 3T3-L1 adipocyte LDH. LDH converts pyruvate and NADH to lactate and NAD^+. LDH saturation curves using pyruvate (A) and NADH (B) for the forward reaction and lactate (C) and NAD^+ (D) for the reverse reaction are shown. The points represent experimental data while the fitted lines represent the result of fitting equation 4.11 to the entire dataset. This fitting provides the parameter values presented in Table 4.10. The error bars represent standard deviation with each data point measured in three technical repeats.

Using the Haldane equation (Eq. 4.3), an equilibrium constant for LDH was calculated to be 577. This is comparable with the literature value range of 227-7194.[139,140]

Table 4.10: Kinetic parameters for 3T3-L1 adipocyte LDH. Kinetic data for the forward and reverse reaction of LDH was fitted using equation 4.11. The fitted parameters (± standard error) include maximal specific activity for the forward and reverse reaction as well as binding constants of LDH for pyruvate, NAD^+, lactate and NADH.

Parameter	Fitted Value	Literature Value	Reference
$V_{f_{LDH}}$ (μmol.min^{-1}.mg^{-1})	0.43 ± 0.063	-	-
$V_{r_{LDH}}$ (μmol.min^{-1}.mg^{-1})	0.12 ± 0.015	-	-
K_{pyr} (mM)	0.075 ± 0.023	0.1 - 0.35	117
K_{NAD} (mM)	0.94 ± 0.35	0.253	118
K_{lac} (mM)	9.0 ± 7.3	9.34 - 23.0	117
K_{NADH} (mM)	0.70 ± 0.22	0.008	119

It can be seen that the fitted value for K_{NADH} differs greatly from that of its literature value. The effect of this discrepancy is described in chapter 5. The literature value was sourced from guinea-pig skeletal muscle lactate dehydrogenase utilizing the 4M isozyme.[119] All five LDH isozymes, including 4M, are expressed in adipose tissue.[72] The difference in expression of the 4M isozyme in 3T3-L1 adipocytes and guinea-pig skeletal muscle in unknown at this time. The guinea-pig skeletal muscle study utilized a 50 mM, pH 7.0 phosphate buffer while a 5 mM, pH 7.0 phosphate buffer was utilized in the characterisation of 3T3-L1 adipocyte LDH. The former study carried out assays at 30°C while our assays were carried out at 37°C. These experimental differences cannot account for the 2 orders of magnitude difference between experimental and literature values. The cause is more likely due to the problem that arises in the GAPDH and G3PDH assays as well. NADH at low concentrations cannot produce a quantifiable change in absorbance when converted to NAD^+. A repeat of the LDH assays would be required, including more concentrations of NADH, in order to increase the accuracy of the K_{NADH} estimation.

4.1.12 Glycerol-3-Phosphate Dehydrogenase

Glycerol 3-phosphate dehydrogenase catalyses the conversion of DHAP and NADH to G3P and NAD^+. 3T3-L1 adipocyte G3PDH was characterised in the forward direction using DHAP as substrate with two different NADH concentrations (Fig 4.11). A reliable data set using NADH as the varying substrate could not be obtained. This is because the majority of the NADH concentrations used in the attempted saturation curve were too low to produce a change in absorbance at 340 nm upon conversion to NAD^+. The data was fitted using a irreversible Michaelis-Menten equation (Eq. 4.12) which describes the

kinetics well. The fitted parameters values are displayed in Table 4.11. Although G3PDH does catalyse a reversible reaction, due to limitations in the coupled enzyme assays it was not possible to perform reversible kinetics for this characterisation. However, a reversible rate equation (Eq. 4.25) is used for model construction using an equilibium constant and binding constants from literature (see Table 4.13 and 4.14).

$$vG3PDH = \frac{V_{f_{G3PDH}} \cdot \frac{dhap}{K_{dhap}}}{1 + \frac{dhap}{K_{dhap}}} \tag{4.12}$$

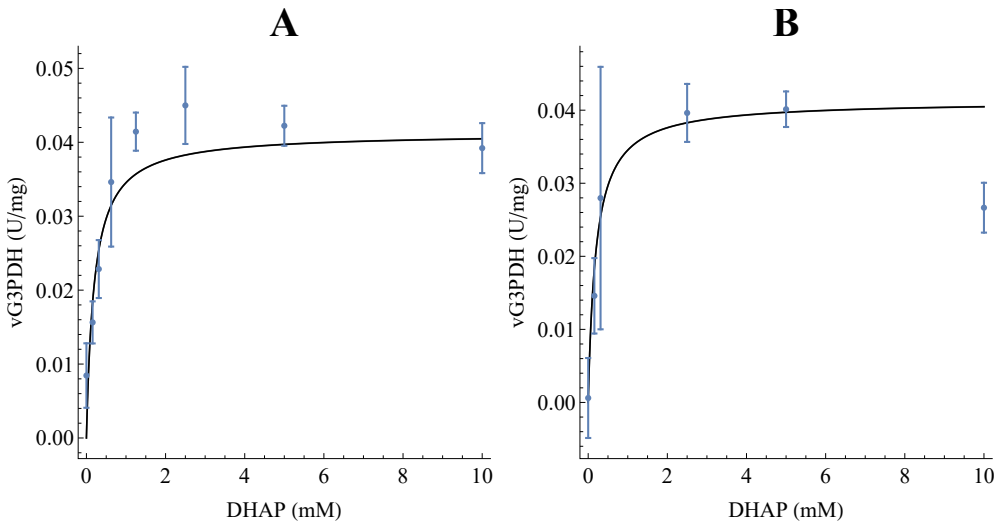

Figure 4.11: Characterization of 3T3-L1 adipocyte G3PDH. G3PDH converts DHAP and NADH to G3P and NAD^+. G3PDH saturation curves using DHAP as substrate with a NADH concentration of 0.8 mM (A) and 0.4 mM (B) are shown. The points represent experimental data while the fitted lines represent the result of fitting equation 4.12 to the entire dataset. While NADH is not included in equaton 4.12, NADH is included in the NonlinearModelFit performed for the fitting. In this way, the fit can account for the two different NADH concentrations used. This fitting provides the parameter values presented in Table 4.11. The error bars represent standard deviation with each data point measured in three technical repeats.

Table 4.11: Kinetic parameters for 3T3-L1 adipocyte G3PDH. Kinetic data for the forward reaction of G3PDH was fitted using equation 4.12. The fitted parameters (± standard error) include maximal specific activity for the forward reaction as well as binding constants of G3PDH for DHAP.

Parameter	Fitted Value	Literature Value	Reference
$V_{f_{G3PDH}}$ (μmol.min^{-1}.mg^{-1})	0.041 ± 0.0026	-	-
K_{dhap} (mM)	0.19 ± 0.065	0.27	93

4.1.13 Adenylate Kinase

Adenylate kinase catalyses the conversion of two ADP molecules to one ATP and one AMP molecule. 3T3-L1 adipocyte AK was characterised in the forward direction using ADP substrate. In the reverse direction, AMP and ATP was used as substrates (Fig 4.12). The data was fitted using a reversible equation (Eq. 4.13) describing a spatio-temporal bi-bi mechanism taken from an in-house thesis.[145] This equation describes the kinetics of both forward and reverse reactions very well. The fitted parameters values are displayed in Table 4.12.

$$vAK = \frac{ADP^2 \cdot V_{f_{AK}} \cdot (1 - \frac{AMP \cdot ATP}{Keq \cdot ADP^2})}{K_{ADP}{}^2 \cdot (1 + \frac{ADP}{K_{ADP}}(2 + \frac{ADP}{K_{ADP}} + \frac{2AMP}{K_{AMP}}) + \frac{AMP}{K_{AMP}}(2 + \frac{AMP}{K_{AMP}} + \frac{ATP}{K_{ATP}}) + \frac{ATP}{K_{ATP}})} \tag{4.13}$$

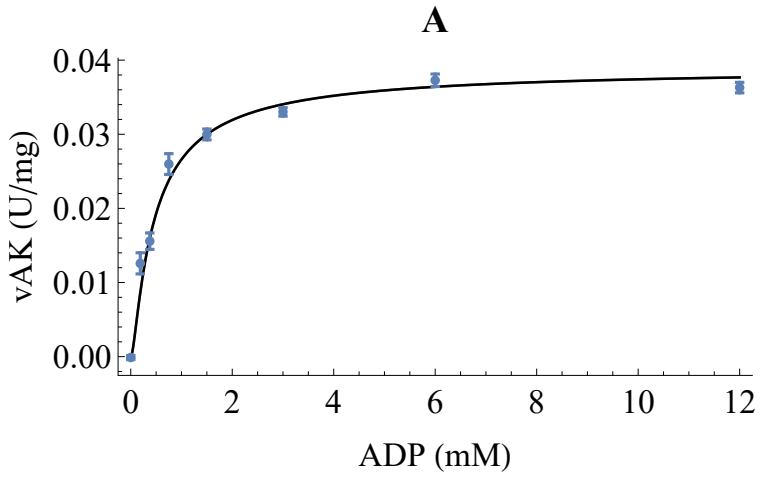

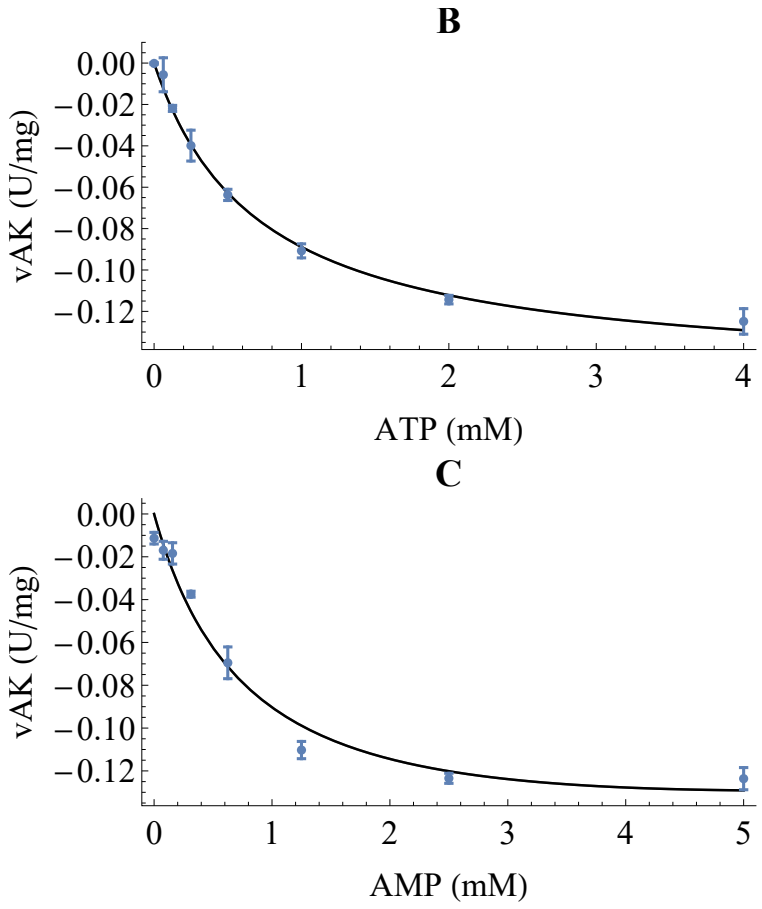

Figure 4.12: Characterization of 3T3-L1 adipocyte AK. AK converts two ADP molecules to one ATP and one AMP molecule. AK saturation curves using ADP (A) for the forward reaction and ATP (B) and AMP (C) for the reverse reaction are shown. The points represent experimental data while the fitted lines represent the result of fitting equation 4.13 to the entire dataset. This fitting provides the parameter values presented in Table 4.12. The error bars represent standard deviation with each data point measured in three technical repeats.

Table 4.12: Kinetic parameters for 3T3-L1 adipocyte AK. Kinetic data for the forward and reverse reaction of AK was fitted using equation 4.13. The fitted parameters (± standard error) include maximal specific activity for the forward reaction as well as binding constants of AK for ADP, ATP and AMP.

Parameter	Fitted Value	Literature Value	Reference
$V_{f_{AK}}$ (μmol.min^{-1}.mg^{-1})	0.039 ± 0.0030	-	-
K_{ATP} (mM)	0.11 ± 0.019	0.27	120
K_{ADP} (mM)	0.21 ± 0.028	0.35	120
K_{AMP} (mM)	0.87 ± 0.098	0.32	120

4.2 Model construction

The kinetic model comprises of five elements: Variables, initial conditions, rate equations, parameter values and ordinary differential equations. Variables represent each species within the model. Initial conditions are the concentrations at which each variable starts. Rate equations calculate the rate of each enzyme as a function of the species (variable) and parameter values. Parameter values are the kinetic parameters obtained from the enzyme characterisation. The ordinary differential equations calculate the change in each species as a function of time using the rate equations.

1. **Variables, initial conditions and rate equations**

   With glucose as substrate and lactate and glycerol (G3P) as end products, all glycolytic intermediates were included as variables in the model as well as the co-factors AMP, ADP, ATP, NAD^+ and NADH. The initial value of all intermediates was set to 0 with the exception of glucose, which was set to the concentration of glucose at the beginning of the corresponding time course (see model validation). Similarly, the initial values for co-factors were set to an experimentally determined value at the beginning of the time course. The model consists of fourteen reaction steps, which consist of the glycolytic reactions as well as glycerol-3-phosphate dehydrogenase, ATPase, and adenylate kinase. Each reaction step has a corresponding kinetic rate equation (Eq. 4.14 - 4.27). These rate equations are reversible. To achieve reversibility unlike equations 4.5 - 4.9, and 4.12, equilibirum constants and binding constants were used from literature (Table 4.13 and 4.14).

$$vHK = \frac{V_{f_{HK}} \cdot \frac{ATP[t]}{K_{ATP}} \cdot \frac{glc[t]}{K_{glc}} \cdot (1 - \frac{ADP[t] \cdot g6p[t]}{ATP[t] \cdot glc[t] \cdot Keq})}{(1 + \frac{ATP[t]}{K_{ATP}} + \frac{ADP[t]}{K_{ADP}}) \cdot (1 + \frac{g6p[t]}{K_{g6p}} + \frac{glc[t]}{K_{glc}}) \cdot (1 + \frac{AMP[t]}{K_{i_{AMP}}})} \tag{4.14}$$

$$vPGI = \frac{\frac{V_{f_{PGI}} \cdot g6p[t]}{K_{g6p}} - \frac{V_{r_{PGI}} \cdot f6p[t]}{K_{f6p}}}{1 + \frac{f6p[t]}{K_{f6p}} + \frac{g6p[t]}{K_{g6p}}} \tag{4.15}$$

$$vPFK = \frac{V_{f_{PFK}} \cdot \frac{ATP[t]}{K_{ATP}} \cdot \frac{f6p[t]}{K_{f6p}}}{(1 + \frac{ATP[t]^2}{K_{ATP}{}^2}) \cdot (1 + \frac{f6p[t]}{K_{f6p}})} \tag{4.16}$$

$$vALD = \frac{V_{f_{ALD}} \cdot \frac{f16bp[t]}{K_{f16bp}} \cdot (1 - \frac{dhap[t] \cdot gap[t]}{f16bp[t] \cdot Keq})}{(1 + \frac{dhap[t]}{K_{dhap}} + \frac{f16bp[t]}{K_{f16bp}} + \frac{gap[t]}{K_{gap}} + \frac{dhap[t] \cdot gap[t]}{K_{dhap} \cdot K_{gap}})} \tag{4.17}$$

$$vTPI = -\frac{V_{r_{TPI}} \cdot \frac{gap[t]}{K_{gap}} \cdot (-1 + \frac{dhap[t] \cdot Keq}{gap[t]})}{(1 + \frac{dhap[t]}{K_{dhap}} + \frac{gap[t]}{K_{gap}})} \tag{4.18}$$

$$vGAPDH = -\frac{V_{r_{GAPDH}} \cdot \frac{1,3bpg[t]}{K_{1,3bpg}} \cdot \frac{nadh[t]}{K_{NADH}} \cdot (-1 + \frac{gap[t] \cdot nad[t] \cdot Keq}{1,3bpg[t] \cdot nadh[t]})}{(1 + \frac{1,3bpg[t]}{K_{1,3bpg}} + \frac{gap[t]}{K_{gap}}) \cdot (1 + \frac{nad[t]}{K_{NAD}} + \frac{nadh[t]}{K_{NADH}})} \tag{4.19}$$

$$vPGK = -\frac{V_{r_{PGK}} \cdot \frac{ATP[t]}{K_{ATP}} \cdot \frac{3pg[t]}{K_{3pg}} \cdot (-1 + \frac{1,3bpg[t] \cdot ADP[t] \cdot Keq}{ATP[t] \cdot 3pg[t]})}{(1 + \frac{ATP[t]}{K_{ATP}} + \frac{ADP[t]}{K_{ADP}}) \cdot (1 + \frac{3pg[t]}{K_{3pg}} + \frac{1,3bpg[t]}{K_{1,3bpg}})} \tag{4.20}$$

$$vPGM = \frac{\frac{V_{f_{PGM}} \cdot 3pg[t]}{K_{3pg}} - \frac{V_{r_{PGM}} \cdot 2pg[t]}{K_{2pg}}}{1 + \frac{2pg[t]}{K_{2pg}} + \frac{3pg[t]}{K_{3pg}}} \tag{4.21}$$

$$vENO = \frac{V_{f_{ENO}} \cdot \frac{2pg[t]}{K_{2pg}} \cdot (1 - \frac{pep[t]}{2pg[t] \cdot Keq})}{(1 + \frac{2pg[t]}{K_{2pg}} + \frac{pep[t]}{K_{pep}}) \cdot (1 + \frac{2pg[t]}{K_{i_{2pg}}})} \tag{4.22}$$

$$vPK = \frac{V_{f_{PK}} \cdot \frac{ADP[t]}{K_{ADP}} \cdot \frac{pep[t]}{K_{pep}} \cdot (1 - \frac{ATP[t] \cdot pyr[t]}{ADP[t] \cdot pep[t] \cdot Keq})}{(1 + \frac{ATP[t]}{K_{ATP}} + \frac{ADP[t]}{K_{ADP}}) \cdot (1 + \frac{pep[t]}{K_{pep}} + \frac{pyr[t]}{K_{pyr}})} \tag{4.23}$$

$$vLDH = -\frac{\frac{V_{r_{LDH}} \cdot lac[t] \cdot nad[t]}{K_{lac} \cdot K_{NAD}} + \frac{V_{f_{LDH}} \cdot pyr[t] \cdot nadh[t]}{K_{pyr} \cdot K_{NADH}}}{(1 + \frac{lac[t]}{K_{lac}} + \frac{pyr[t]}{K_{pyr}}) \cdot (1 + \frac{nad[t]}{K_{NAD}} + \frac{nadh[t]}{K_{NADH}})} \tag{4.24}$$

$$vG3PDH = \frac{V_{f_{G3PDH}} \cdot \frac{dhap[t]}{K_{dhap}} \cdot \frac{nadh[t]}{K_{NADH}} \cdot (1 - \frac{g3p[t] \cdot nad[t]}{dhap[t] \cdot nadh[t] \cdot Keq})}{(1 + \frac{nad[t]}{K_{NAD}} + \frac{nadh[t]}{K_{NADH}}) \cdot (1 + \frac{dhap[t]}{K_{dhap}} + \frac{g3p[t]}{K_{g3p}})} \tag{4.25}$$

$$vAK = \frac{ADP^2 \cdot V_{f_{AK}} \cdot (1 - \frac{AMP \cdot ATP}{Keq \cdot ADP^2})}{{K_{ADP}}^2 \cdot (1 + \frac{ADP}{K_{ADP}}(2 + \frac{ADP}{K_{ADP}} + \frac{2AMP}{K_{AMP}}) + \frac{AMP}{K_{AMP}}(2 + \frac{AMP}{K_{AMP}} + \frac{ATP}{K_{ATP}}) + \frac{ATP}{K_{ATP}})} \tag{4.26}$$

$$vATPase = V_{f_{ATPase}} \cdot ATP[t] \tag{4.27}$$

2. Parameter values and ordinary differential equations

Parameters values for each enzyme are obtained from the kinetic enzyme assays (see Table 4.1-4.12). With the exception of PGI, LDH and AK, each glycolytic enzyme has only been investigated in either its forward or reverse direction. The fully reversible rate equations (Eq. 4.14 - 4.27) utilized parameters values and equilibrium constants obtained from literature for enzymes that were only characterised in one direction.

Table 4.13: The Michaelis constant values for all glycolytic enzymes as well as adenylate kinase used in model construction. The majority is experimentally determined while the remaining were sourced from literature.

Enzyme	Parameter	Experimental (mM)	Literature (mM)	Parameter	Experimental (mM)	Literature (mM)
HK	K_{glc}	0.25	0.3^{107}	K_{g6p}	-	0.065^{121}
	K_{ATP}	0.20	0.7^{107}	K_{ADP}	-	1.9^{121}
	$K_{i_{AMP}}$	14	2.5^{108}			
PGI	K_{g6p}	4.7	0.48^{109}	K_{f6p}	0.59	0.031^{110}
PFK	K_{f6p}	0.43	0.18^{111}	K_{ATP}	1.3	0.08^{111}
	K_{ADP}	-	2.5^{108}			
ALD	K_{f16bp}	0.37	0.05^{105}	K_{dhap}	-	2.1^{122}
	K_{gap}	-	1.1^{122}			
TPI	K_{dhap}	-	0.61^{123}	K_{gap}	0.63	0.47^{112}
GAPDH	K_{gap}	-	0.21^{113}	$K_{1,3bpg}$	0.0013	0.0008^{113}
	K_{NAD}	-	11^{113}	K_{NADH}	0.25	0.0033^{113}
PGK	$K_{1,3bpg}$	-	0.0030^{114}	K_{3pg}	3.5	1.37^{114}
	K_{ADP}	0.72	0.05^{124}	K_{ATP}	0.80	0.42^{114}
PGM	K_{3pg}	-	0.050^{125}	K_{2pg}	-	0.1^{125}
ENO	K_{2pg}	0.22	0.12^{115}	K_{pep}	-	0.0050^{127}
	$K_{i_{2pg}}$	3.1	-			
PK	K_{pep}	-	0.08^{116}	K_{pyr}	-	21^{126}
	K_{ADP}	3.6	0.3^{116}	K_{ATP}	1.1	1.5^{126}
LDH	K_{lac}	9.0	$9.34 - 23.0^{117}$	K_{NAD}	0.94	0.253^{118}
	K_{pyr}	0.075	$0.1 - 0.35^{117}$	K_{NADH}	0.70	0.008^{119}
G3PDH	K_{dhap}	0.19	0.27^{93}	K_{g3p}	-	0.505^{93}
	K_{NADH}	-	0.0045^{93}	K_{NAD}	-	0.37^{93}
AK	K_{ATP}	0.11	0.27^{120}	K_{ADP}	0.21	0.35^{120}
	K_{AMP}	0.87	0.32^{120}			

Equilibrium constants for all enzymes not characterised in both the forward and reverse direction were included in the model as the rate equations used in the model represent reversible reactions (i.e. the Haldane relation was used for the V_{max} of the opposing direction).

Table 4.14: The equilibrium constants used for model construction. PGI and LDH K_{eqs} are not included as they were characterised in the forward and reverse direction.

Enzyme	K_{eq}	Reference
HK	1310	128
PFK	800	129
ALD	0.09	130
TPI	0.046	131
GAPDH	0.0056	132
PGK	3200	133
ENO	4.6	130
PK	6500	134
G3PDH	32600	135
AK	0.45	134

Maximal specific activity of each enzyme in the forward and/or reverse direction obtained from the enzyme assays is in μmol.min^{-1}.mg^{-1}. To model glycolysis in 3T3-L1 adipocyte cell extracts rather than just isolated glycolytic enzymes, the maximal activities will have to be multiplied by the protein concentration of the lysate in mg/ml used in the HPLC model validation, resulting in the maximal activity in the model being in mM/min. Below are the maximal activities as they were acquired from the enzyme assays.

Table 4.15: The maximal activities used in model construction.

Enzyme	$V_f(\mu\text{mol.min}^{-1}.\text{mg}^{-1})$	$V_r(\mu\text{mol.min}^{-1}.\text{mg}^{-1})$
HK	0.0079	-
PGI	0.23	0.056
PFK	0.023	-
ALD	0.032	-
TPI	-	0.10
GAPDH	-	0.038
PGK	-	0.13
PGM	0.43[136]	0.49[137]
ENO	0.026	-
PK	0.12	-
LDH	0.43	0.12
G3PDH	0.041	-
AK	0.039	-
ATPase	0.00067[145]	-

The model consists of eighteen ordinary differential equations (ODEs) for the thirteen glycolytic intermediates and five co-factors (equation 4.28-4.45). The ODEs consist of enzymes that produce and consume the corresponding intermediate and co-factor to give the change in their concentrations as a function of time.

$$Glucose'[t] = -1.0 \cdot vHK \tag{4.28}$$

$$G6P'[t] = 1.0 \cdot vHK - 1.0 \cdot vPGI \tag{4.29}$$

$$F6P'[t] = 1.0 \cdot vPGI - 1.0 \cdot vPFK \tag{4.30}$$

$$F16BP'[t] = 1.0 \cdot vPFK - 1.0 \cdot vALD \tag{4.31}$$

$$DHAP'[t] = 1.0 \cdot vALD - 1.0 \cdot vTPI - 1.0 \cdot vG3PDH \tag{4.32}$$

$$GAP'[t] = 1.0 \cdot vALD + 1.0 \cdot vTPI - 1.0 \cdot vGAPDH \tag{4.33}$$

$$1,3BPG'[t] = 1.0 \cdot vGAPDH - 1.0 \cdot vPGK \tag{4.34}$$

$$3PG'[t] = 1.0 \cdot vPGK - 1.0 \cdot vPGM \tag{4.35}$$

$$2PG'[t] = 1.0 \cdot vPGM - 1.0 \cdot vENO \tag{4.36}$$

$$PEP'[t] = 1.0 \cdot vENO - 1.0 \cdot vPK \tag{4.37}$$

$$Pyruvate'[t] = 1.0 \cdot vPK - 1.0 \cdot vLDH \tag{4.38}$$

$$Lactate'[t] = 1.0 \cdot vLDH \tag{4.39}$$

$$G3P'[t] = 1.0 \cdot vG3PDH \tag{4.40}$$

$$AMP'[t] = 1.0 \cdot vAK \tag{4.41}$$

$$NAD'[t] = -1.0 \cdot vGAPDH + 1.0 \cdot vLDH + 1.0 \cdot vG3PDH \tag{4.42}$$

$$NADH'[t] = 1.0 \cdot vGAPDH - 1.0 \cdot vLDH - 1.0 \cdot vG3PDH \tag{4.43}$$

$$ATP'[t] = -1.0 \cdot vHK - 1.0 \cdot vPFK + 1.0 \cdot vPGK + 1.0 \cdot vPK + 1.0 \cdot vAK - 1.0 \cdot vATPase \tag{4.44}$$

$$ADP'[t] = 1.0 \cdot vHK + 1.0 \cdot vPFK - 1.0 \cdot vPGK - 1.0 \cdot vPK - 2.0 \cdot vAK + 1.0 \cdot vATPase \tag{4.45}$$

4.3 Model validation

The cell-free extract model predicts concentration changes over time for all glycolytic intermediates and co-factors. The validation of this model comprised of data that was experimentally obtained via HPLC analysis of 3T3-L1 cell-free extracts. Eight time point samples were prepared and run through a reverse-phase HPLC column. Upon elution from the column, samples were run through two detectors: UV-VIS spectrophotometric for co-factors and radiolabelled for glycolytic intermediates. (See methods and materials)

1. **Glycolytic intermediate measurements**

   HPLC chromatograms obtained from the radiolabelled detector (Figure 4.13 shows three time points for illustration) show peaks for all intermediates, if present at sufficiently high concentrations. Typically, we observed

glucose, lactate, G6P, F6P, pyruvate, DHAP, 2PG and 3PG. Skewed normal distrubutions were fitted to the peaks and integrated using *Wolfram Mathematica 11.2*® to obtain areas of the peaks. Peak areas were converted to concentration using a response factor calculated as the total sum of peak areas within the sample. An "impurity" peak was always in the radiolabelled glucose and remained constant during the incubation. The impurity did not co-elute with any intermediate and was present if radiolabelled glucose alone is injected into the HPLC column. It is for these reasons that the impurity (i.e. its counts) was ignored in the HPLC model validation. Glucose was also seen to directly co-elute with an impurity. This impurity was ignored by subtracting the counts of the final time point "glucose" peak (Figure 4.13 C) from the glucose peak in all other time points.

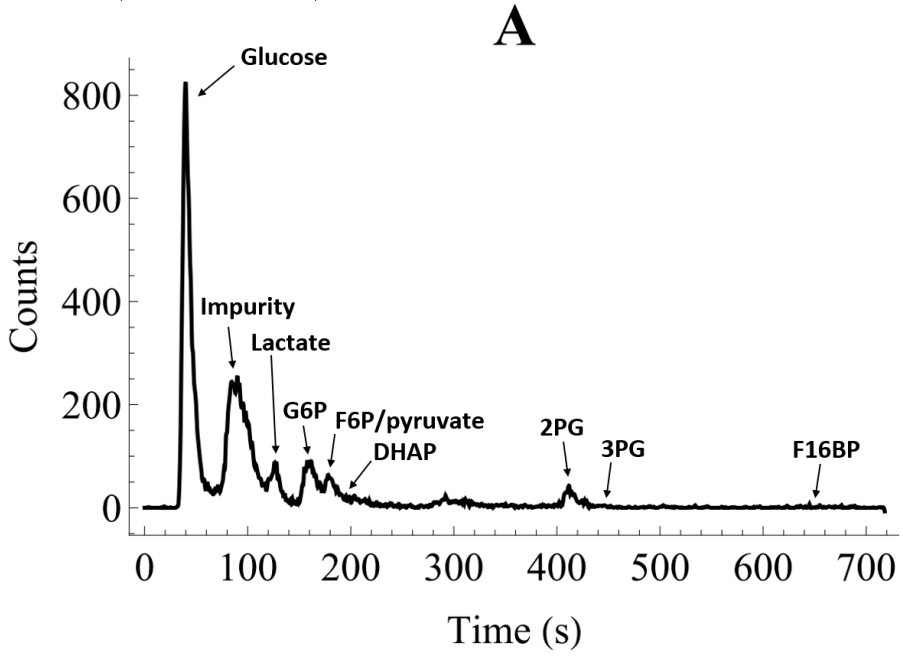

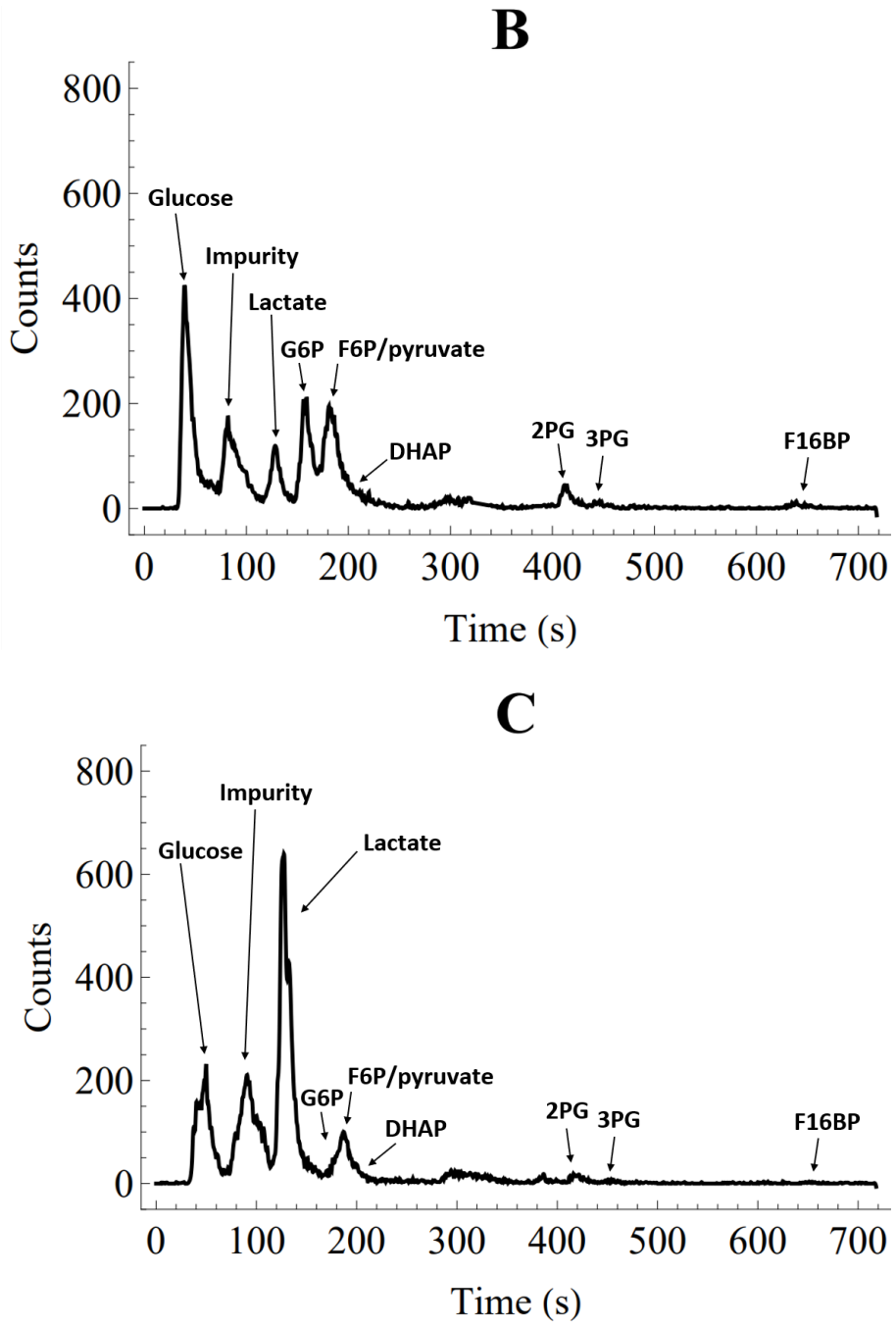

Figure 4.13: Cell-free extract HPLC chromatograms. Three of the total eight chromatograms are provided for time point 20 seconds (A), 5 minutes (B) and 120 minutes (C). The integration of peaks provides the concentration of the intermediate it represents. The change in concentration as a function of time can thus be seen from the changes in peak height and width.

The total counts of each time point sample remained constant but not all

the counts within each time point sample were accounted for in a combination of glucose, lactate and intermediates. This recovery of the label is crucial as any counts unaccounted for suggest an underestimation of any of the observed metabolites within glycolysis. Fortunately the percentage recovery of label was very high: 20 second (95%), 5 minute (95%), 10 minute (94%), 15 minute (96%), 20 minute (97%), 30 minute (100%), 40 minute (95%), 60 minute 94%), 90 minute (103%), 120 minute (95%). It can be seen from the 97% average recovery of label that only a small fraction of counts was unaccounted for within glycolysis. The percentages over 100% would suggest the area of one or more peaks is overestimated. However, the degree to which the integration was overestimated is too small to have an adverse effect on the validation of the model.

Due to overlapping of peaks for pyruvate and F6P, it was not possible to integrate each peak as is performed with the other peaks. The concentration of F6P was calculated using the concentration of G6P and the equilibrium constant of PGI. The concentration of pyruvate was calculated using the concentrations of lactate, NAD^+, and NADH and the equilibrium constant of LDH. The entire pyruvate and F6P peak was then integrated and compared to the sum of pyruvate and F6P calculated from equilibrium constants. The similarity in summation and integration indicate this was adequate in providing an accurate estimate for pyruvate and F6P validation data.

2. **Co-factor measurements**

   HPLC chromatograms obtained from the UV-VIS detector (data not shown) provided peaks for ATP, ADP, AMP, NAD^+ and NADH. Co-factor concentrations were calculated from integrating each peak and using calibration curves for each co-factor obtained from the same HPLC method.

3. **Overlaying model and validation data**

   Before model time courses were generated, initial values for ATP, ADP, AMP, NAD^+ and NADH were set to their concentrations obtained from the first time point sample. Glucose was set to 1 mM, the concentration of radiolabelled glucose incubated with the cell lysate. After time course data was generated for every co-factor and glycolytic intermediate in the model, it was overlaid with HPLC validation data (Figure 4.14). Only glycolytic intermediates and co-factors visible using the HPLC method were included in the model validation. For the purpose of discussion, the model time course of G3P and F1,6BP were included without experimental data. The model time course data of those not included can be

found in the supplementary data section (Fig 5.1 and 5.2).

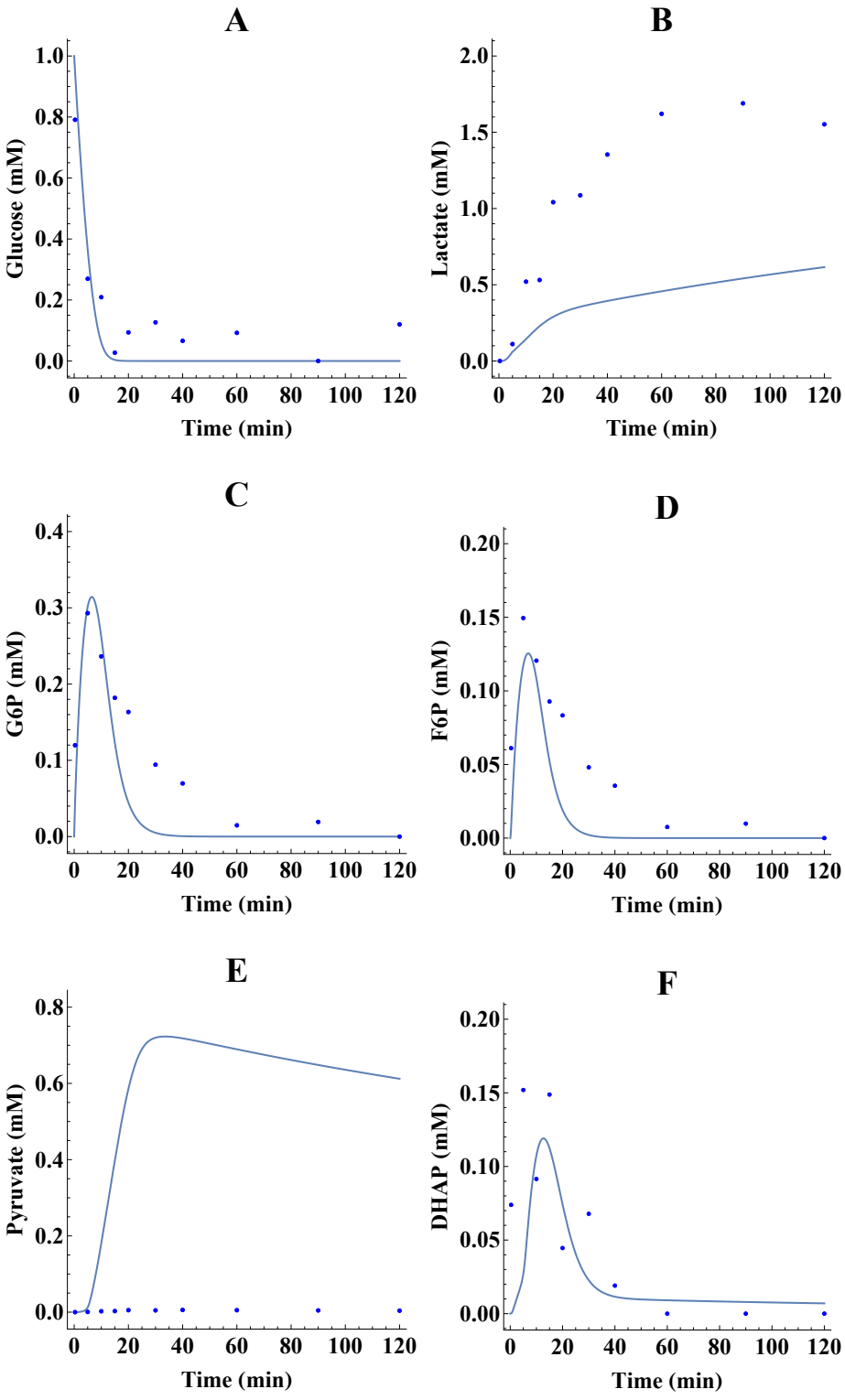

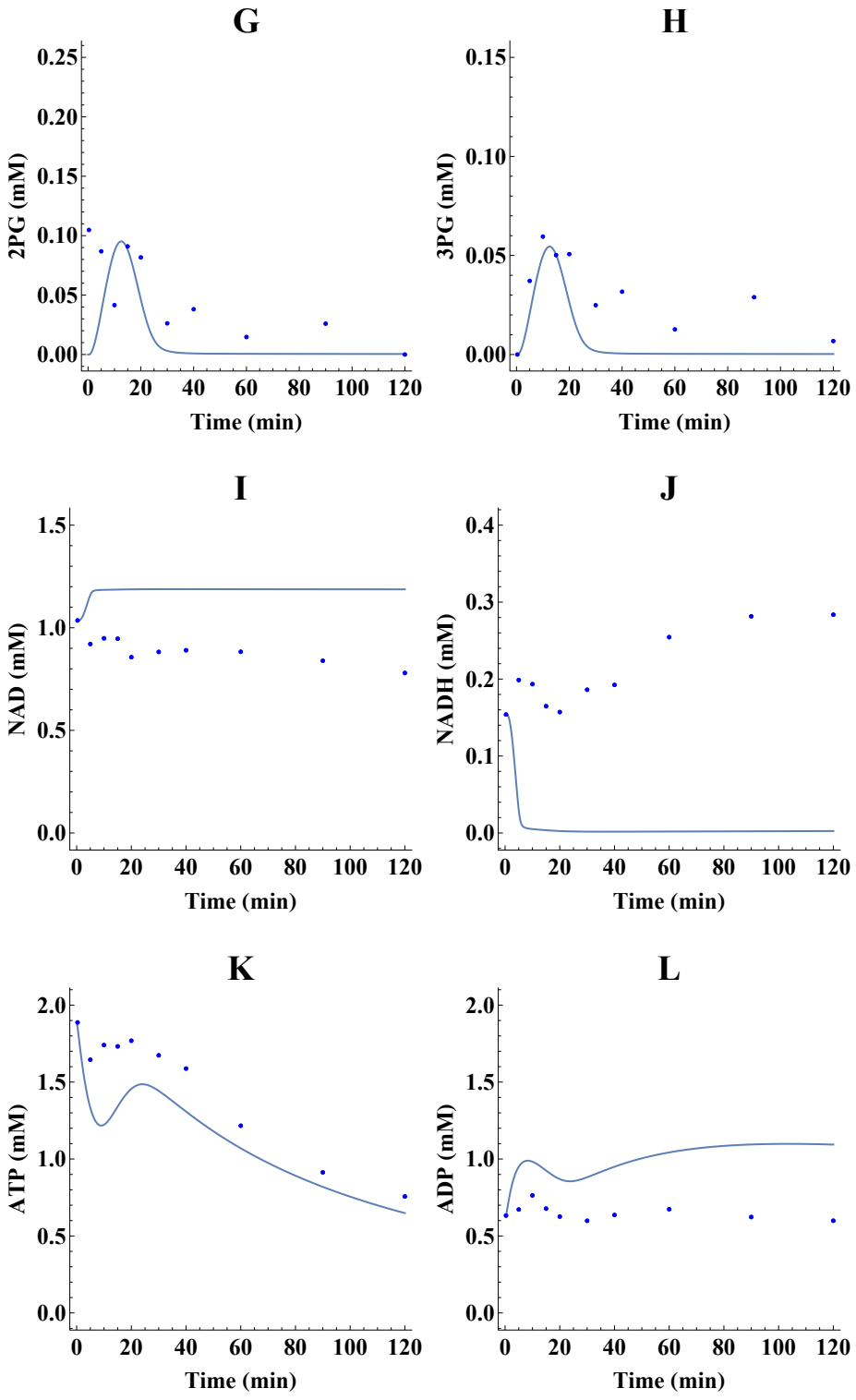

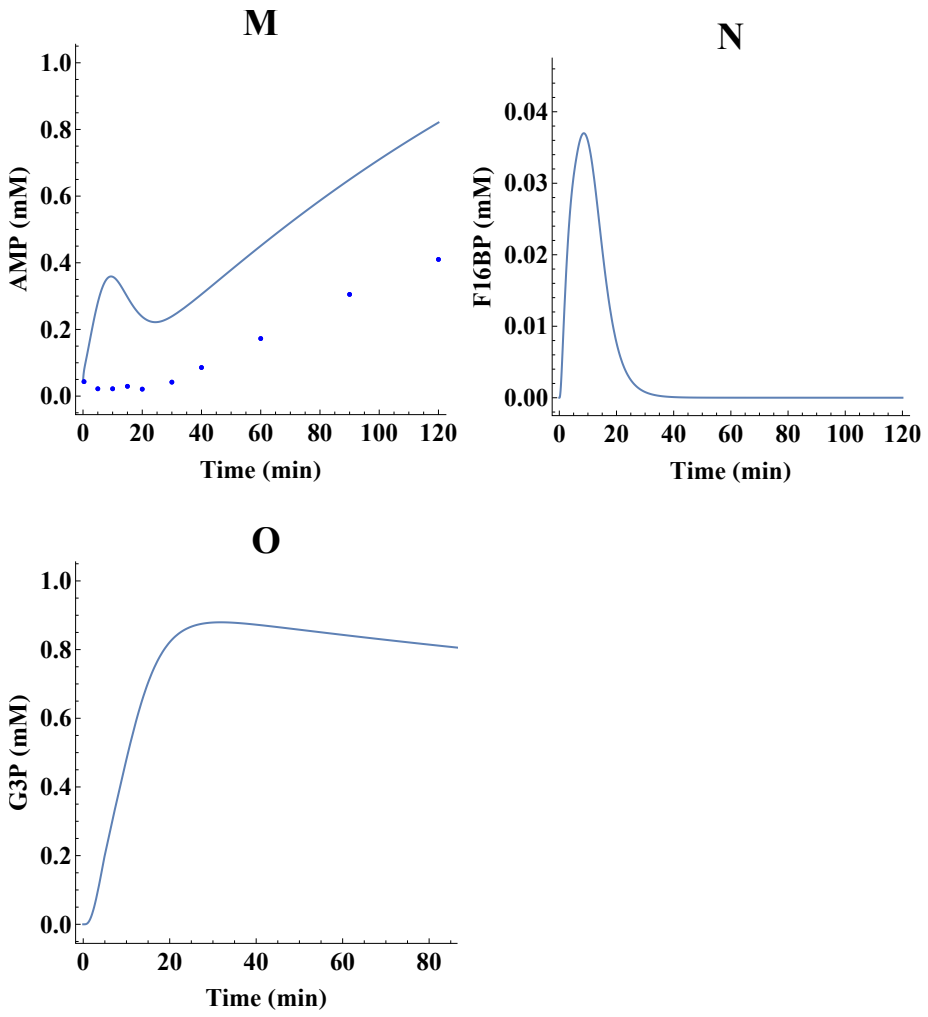

Figure 4.14: Validation data plotted together with model time courses. The overlays are of glucose (A), lactate (B), G6P (C), F6P (D), pyruvate (E), DHAP (F), 2PG (G), 3PG (H), NAD^+ (I), NADH (J), ATP (K), ADP (L), AMP (M). The experimental data is represented by the data points while the model prediction is represented by the solid curves. F16BP (N) and G3P (O) model predictions are also provided but without experimental data.

Although not all intermediates could be resolved, due to too low concentrations and due to some overlap in elution peaks, the time evolution of the abundant metabolites could be evaluated. As such, the quantification of glucose, lactate, six glycolytic intermediates, and five co-factors provided a fair level of detail for the model validation. With the result obtained in Figure 4.14, it can be seen that the relatively crude model was, in part, accurate in representing 3T3-L1 adipocyte cell extract glycolysis. The model prediction for most of the intermediates was quite accurate, particularly for the more abundant species in upper glycolysis.

The model is inaccurate in its prediction of G3P, pyruvate and lactate. The model predicted a high flux to G3P which was not observed experimentally, where most glucose was converted to lactate. This leaded to an underestimation of lactate and an overprediction of G3P and pyruvate.

The model prediction for pyruvate (Figure 4.14 - E) was inaccurate. This is indicative of the larger problem with the model: the high activity of G3PDH. NADH (Figure 4.14 - J) in the model was quickly utilised by G3PDH in order to create G3P in large quantities (Figure 4.14 - O). It appears as if the G3PDH activity in the model was overestimated. G3PDH and LDH typically compete for NADH produced by GAPDH. However, the high activity of G3PDH resulted in the depletion of NADH and the stalling of glycolysis. This is why pyruvate accumulated, while in the validation data it did not. As mentioned previously, pyruvate could not be quantified by integrating its peak as F6P co-eluted with pyruvate, but estimates based on equilibrium calculations for LDH were low.

We tested the model performance when G3PDH was removed from the model (Figure 4.15). Lactate is produced to levels in agreement with the model validation data. However, this resulted in an overprediction of F16BP (Figure 4.15 - n) and DHAP (Figure 4.15 - f) at 40 minutes after incubation with glucose but the pyruvate is predicted more accurately. It can be seen that F16BP was greatly overpredicted as the signal for F16BP on the HPLC chromatograms at an elution time of 650 seconds was so low it was not even quantifiable.

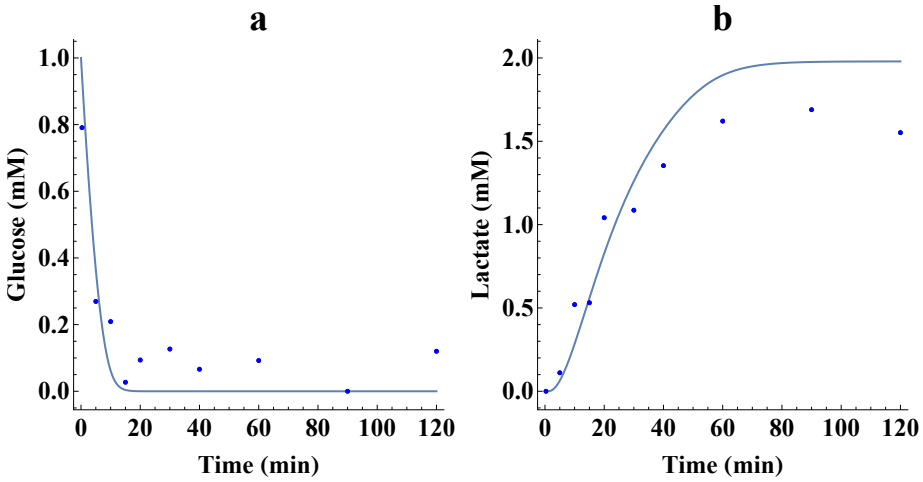

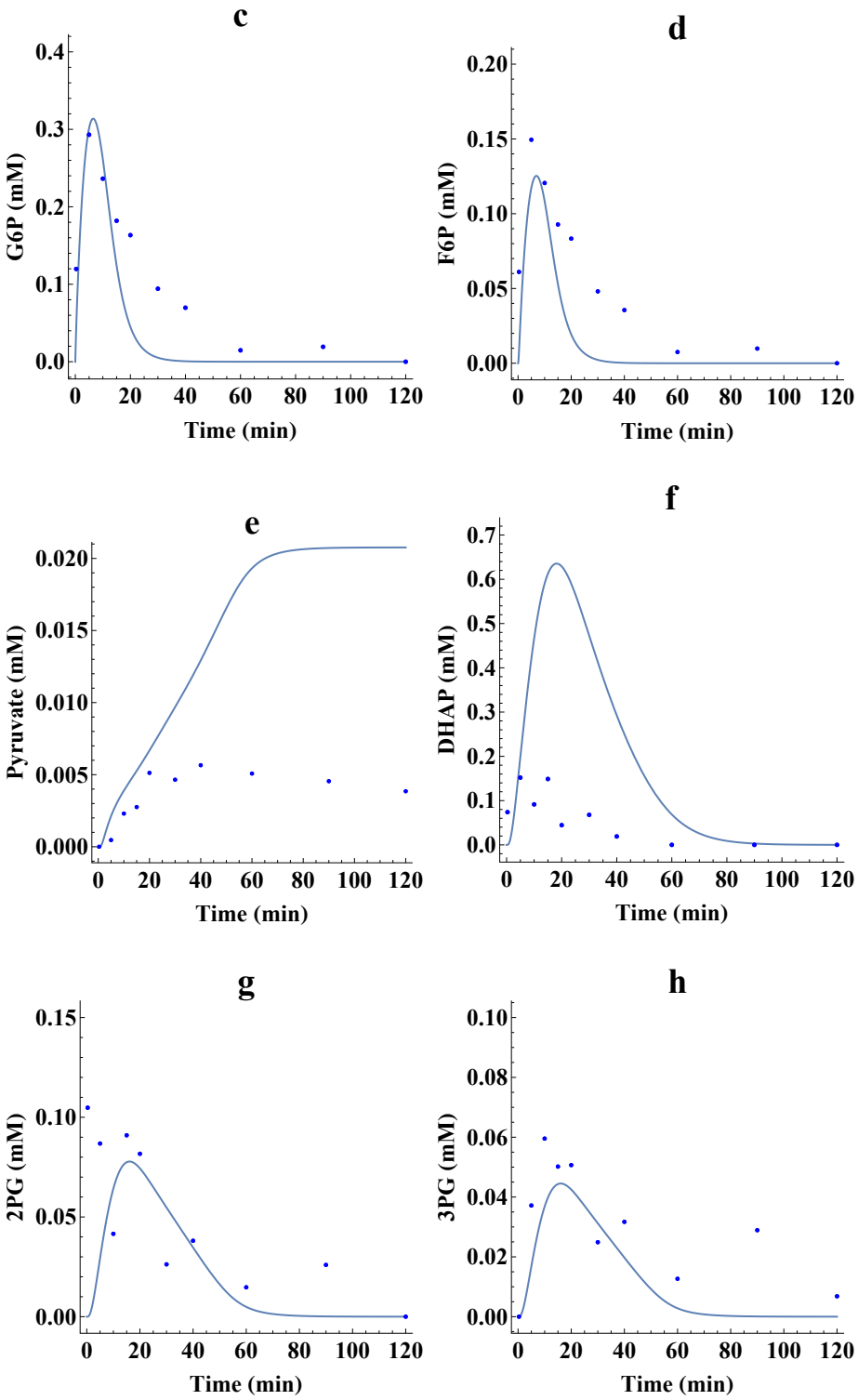

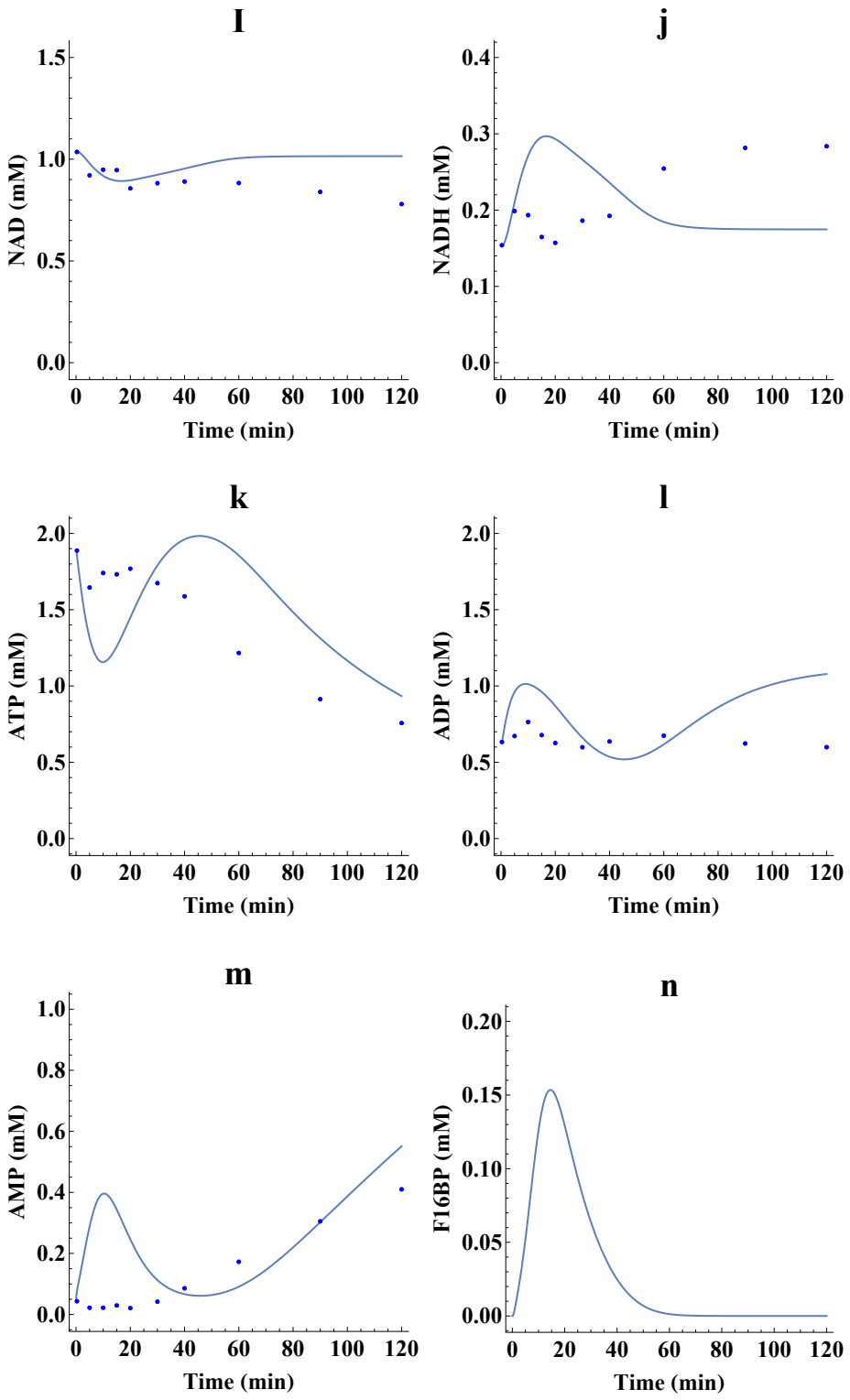

Figure 4.15: Validation data overlaid with model time courses (no G3PDH included). The overlays are of glucose (a), lactate (b), G6P (c), F6P (d), pyruvate (e), DHAP (f), 2PG (g), 3PG (h), NAD^+ (i), NADH

(j), ATP (k), ADP (l), AMP (m). The experimental data is represented by the data points while the model prediction is represented by the solid line. The model prediction for F16BP (n) is also provided but without experimental data.

It would appear as if removing G3PDH completely reduced the NADH capacity to such an extent that NADH accumulated up to 40 minutes after incubation with glucose, leading to the potential inhibition of GAPDH activity thereby causing an overprediction of DHAP and F16BP. On the other hand, including the measured G3PDH activity in the model leaded to an overestimated flux to G3P, resulting in the underprediction of LDH activity.

Ultimately, the construction of a detailed kinetic model for glycolysis in 3T3-L1 adipocytes on the basis of in vitro enzyme kinetics gave satisfactory results. The model was fairly good in predicting glucose metabolism in the cell extracts despite the problems that arised from the introduction of the initial step of the lipogenic pathway. The high activity of G3PDH needs to be addressed in a follow up study.

Chapter 5

Discussion and Conclusions

The aim of this project was threefold: Culture 3T3-L1 adipocytes for the characterisation of glycolytic enzymes, construct a kinetic model for glycolysis in 3T3-L1 using the parameters from the characterisation, and validate this model using a novel in-house HPLC method. These aims were designed to answer the question: Can glycolysis in 3T3-L1 adipocytes be described on the basis of individual glycolytic enzyme kinetics?

3T3-L1 preadipocytes were successfully cultured and differentiated into mature adipocytes with reliable reproducibility. Following the lysis of the harvested cells, cell-free extracts were created. The produced lysate served as a stable solution in which all glycolytic enzymes were present. Well-established enzyme-linked assays could be performed using these lysates. In the assays, individual enzyme rates were measured in the presence of varying substrates and co-factors. Rate equations were derived for each glycolytic enzyme as well as adenylate kinase and G3PDH. This was completed for each glycolytic enzyme to acquire data sets that were then fitted with NonlinearModelfit functions in *Wolfram Mathematica 11.2*®. The quality of these fits, while differing from enzyme to enzyme, was of a high standard. Binding constants and specific activities were acquired from these fits which formed the basis of the kinetic model for glycolysis in 3T3-L1 adipocyte cell-free extracts.

Ordinary differential equations were set up using the derived rate equations to describe the change in concentration of glycolytic intermediates and co-factors as a function of time. The model result is a time course for each intermediate and co-factor within glycolysis as well as the start of the lipogenesis pathway. The model simulations showed the complete consumption of glucose while producing approximately 0.6 moles of lactate, 0.6 moles of pyruvate, and 0.8 moles of glycerol-3-phosphate per mole of glucose consumed.

An HPLC in-house method was used to quantify eight intermediates (glucose, lactate, G6P, F6P, DHAP, pyruvate, 2PG and 3PG) and five co-factors (AMP, ADP, ATP, NAD^+, NADH) in the 3T3-L1 adipocyte cell-free extract. From

this, a time course for each intermediate and co-factor was obtained showing an almost complete conversion of glucose to lactate. These time courses served as the validation for the model. The largest problem in the model seems to be the incorporation of G3PDH. Because of the high specific activity of G3PDH, the flux to glycerol-3-phosphate was too high. For all other enzymes, it would appear that, the bottom-up approach of systems biology modelling and sourcing kinetic parameters from the characterisation of individual enzymes in glycolysis to describe glycolysis as a whole was not only possible, but that good results could be achieved with a relatively simple model.

This is the first kinetic model for glycolysis in 3T3-L1 adipocyte cell-free extracts that includes the characterisation of all glycolytic enzymes. The inclusion of the entire glycolytic pathway from glucose to lactate is not seen in any adipocyte model created to date. Interestingly, the inclusion of just the first reaction of the lipogenic pathway was seen to have a tremendous effect on the flow of carbon through glycolysis. The measured high activity of G3PDH and the subsequent accumulation of glycerol-3-phosphate is in agreement with what is seen in whole cell adipocyte cultures flux experiments where 50% of glucose is converted to lactate, with visible fat accumulation accounting for the other 50% consumed glucose (data not shown). In cell extracts this is not observed, where 90% of glucose is converted into lactate. There is no clear indication as to why G3PDH is less active in cell extracts even though the measurement of G3PDH activity used in the model takes place in cell extracts. The contradictory measured and apparent G3PDH activities in 3T3-L1 adipocyte cell extracts could potentially be dependent on how active the entire glycolytic pathway is during any given experiment. G3PDH activity is measured in enzyme-linked assays in the presence of DHAP, NADH, and cell extract. The lack of other glycolytic intermediates and co-factors is to ensure other glycolytic enzymes are not active. In the case of the HPLC time course incubation, glucose is injected into cell extract with the appropriate concentrations of co-factors. As the time course spans a 2-hour period, seeing a conversion of glucose to lactate, it is apparent that all glycolytic enzymes are active. The root cause for the difference in G3PDH activity may be a regulatory mechanism that elicits its effect when the entire glycolytic pathway is active.

The measured high activity of G3PDH is comparable to literature values from a variety of cell types, even being lower than some. Compared to the 3T3-L1 adipocyte cell extract G3PDH activity of 0.064 μmol.min^{-1}.mg^{-1}, black-tailed prairie dog (*Cynomys ludivicianus*) skeletal muscle and liver have a G3PDH activity of 0.282 μmol.min^{-1}.mg^{-1} and 0.257 μmol.min^{-1}.mg^{-1} respectively.[141] Another species of prairie dog, jerboa, has a muscle G3PDH activity of 0.0536 μmol.min^{-1}.mg^{-1}.[142] *Plasmodium falciparum* G3PDH has an activity of 0.06 μmol.min^{-1}.mg^{-1} [143] and human white adipose tissue G3PDH has an activity

of 0.25 μmol.min^{-1}.mg^{-1}.[93] All substrate affinities are comparable with any differences having little effect on the outcome of the model. It is interesting to note that *Plasmodium falciparum* G3PDH activity and affinities are remarkably similar to those of 3T3-L1 adipocyte cell extract G3PDH with a K_{dhap} of 0.34 mM and 0.37 mM respectively as well as a K_{NADH} of 0.09 mM and 0.11 mM respectively. If all glycolytic enzymes are compared between 3T3-L1 adipocyte cell extracts and *Plasmodium falciparum*, it can be seen that 3T3-L1 adipocyte cell extract enzymes have a considerably lower maximal activity with G3PDH activity being almost exactly the same. This, in combination with the G3PDH activities from muscle, liver, and human adipose tissue, further suggest that the measured activity of 3T3-L1 adipocyte cell extract G3PDH is not inaccurate but is not representative within a cell extract mixture wherein all glycolytic enzymes are active for a prolonged period of time.

The literature value comparison leads to questions about the feasibility of using HPLC analysis to validate the constructed model. While it can be seen that the model has definitely been at least partially validated, the overestimation of G3P production points to a difference in flux in an isolated system of single active enzymes versus an entire active pathway. As a cell extract model is the first step to the goal of constructing whole cell models for 3T3-L1 adipocyte glycolysis to understand glucose metabolism in adipose tissue, it is fortunate that the high activity of G3PDH will affect the predictive capabilities of a cell extract model far more than a whole cell model. The high activity of G3PDH and its resulting effect on time course simulations much closer resemble whole cell 3T3-L1 adipocyte cultures than they do cell extracts. An interesting follow up experiment would be to use permeabilized cells as an intermediate between whole cells and cell extracts. It could be that lipid production in whole cells is dependent on intracellular structures that are ruptured upon cell lysis. This could cause the marked difference between whole cell and cell extract metabolism in regards to lipid production.

Provided in table 4.13 are affinity literature values for each glycolytic enzyme as well as adenylate kinase and G3PDH. Only affinity values that could not be obtained experimentally were used from literature in the model. Two questions arise from this that may give solutions to the problems presented in the models: firstly, what would result if only experimental values were used in the model construction and secondly, what would result if only literature values were used? The first question cannot be answered due to experimental limitations but one can assume that the model would increase in accuracy due to all parameters taking the same experimental conditions (pH, temp, etc.) into account. The second question can be answered by creating a model with only literature values as they are available in table 4.13. If all affinity values used in model construction are taken from literature, the glucose to lactate conversion is slightly more accurately represented while all intermediate overlays see

the opposite effect. This is a common modelling approach but its use in this model construction specifically does not seem to present an obvious advantage. However, due to the large discrepancy in experimental and literature values of specific affinities for PGI, GAPDH, PGK, PK, and LDH, it was tested to what extent exchanging these single experimental values for their corresponding literature values had on the model outcome. Literature values of K_{g6p} and K_{f6p} for PGI have a minimal effect on the model outcome as does K_{NAD} for GAPDH, K_{ADP} for PGK, and K_{ADP} for PK. The literature value of K_{ATP} for PFK has a negative effect on the accuracy of the model. The literature value of K_{NADH} for LDH has a positive outcome on the model, resulting in a better representation of lactate production while decreasing the accumulation of pyruvate but not solving the problem completely. This, in combination with the high measured activity of G3PDH, may explain why LDH is not able to compete effectively with G3PDH for available NADH.

The ultimate goal of our research program on type II diabetes is to understand the molecular basis of reduced insulin sensitivity in type II diabetes patients. Ultimately modelling intact cell glucose metabolism will require whole cell models that would need to take cell volume and glucose influx rates into account. The insulin signal transduction pathway needs to be included as glucose transport is directly dependent upon it. Insulin sensitivity studies need to be conducted to fully understand the extent to which insulin affects glucose transport. These models then need to be replicated with diabetic adipocytes to begin to understand the kinetics behind the diabetic state of adipose tissue. This would have to be achieved in 3T3-L1 adipocytes and only then would it be replicated in human adipocytes. From this point, perturbations to the system would then be introduced to find potential drug targets that have control over carbon metabolism in adipose tissue, leading to the control of triacylglycerol formation. If this is achieved, significant progress would have been made in understanding and combatting diabetic mellitus in humans. The model constructed in this study is a first step in that direction.

List of References

1. Cho, N., Shaw, J., Karuranga, S., Huang, Y., da Rocha Fernandes, J., Ohlrogge, A. and Malanda, B., IDF Diabetes Atlas: Global estimates of diabetes prevalence for 2017 and projections for 2045., *Diabetes Research and Clinical Practice*, 138: 271-281, 2018.

2. Vos, T., Allen, C., Arora, M., Barber, R., Bhutta, Z., Global, regional, and national incidence, prevalence, and years lived with disability for 310 diseases and injuries, 1990-2015: a systematic analysis for the Global Burden of Disease Study 2015., *The Lancet*, 388: 1545-1602, 2016.

3. Kolb, H. and Martin, S., Environmental/lifestyle factors in the pathogenesis and prevention of type 2 diabetes., *BMC Medicine*, 15(1), 2017.

4. *Diabetes Care*, Report of the Expert Committee on the Diagnosis and Classification of Diabetes Mellitus. 20(7): 1183-1197, 1997.

5. Rosen, E. and Spiegelman, B., Adipocytes as regulators of energy balance and glucose homeostasis., *Nature*, 444(7121): 847-853, 2006.

6. Huang S, Czech MP. The GLUT4 glucose transporter., *Cell Metabolism*, 5(4):237-52, 2007.

7. Sears, B. and Perry, M., The role of fatty acids in insulin resistance., *Lipids in Health and Disease*, 14(1), 2015.

8. Pang, C., Gao, Z., Yin, J., Zhang, J., Jia, W. and Ye, J., Macrophage infiltration into adipose tissue may promote angiogenesis for adipose tissue remodeling in obesity., *American Journal of Physiology-Endocrinology and Metabolism*, 295(2): 313-322, 2008.

9. Zajac, J., Shrestha, A. and Poretsky, L., The Main Events in the History of Diabetes Mellitus., *Principles of Diabetes Mellitus*, 19-37, 2004.

10. Caprio, S., Obesity and Type 2 Diabetes: The Twin Epidemic: Preface., *Diabetes Spectrum*, 16(4): 230-230, 2003.

11. Wilcox G., Insulin and insulin resistance., *Clin. Biochem. Rev.*, 26: 19-39, 2005.

12. Funaki, M., Randhawa, P. and Janmey, P., Separation of Insulin Signaling into Distinct GLUT4 Translocation and Activation Steps., *Molecular and Cellular Biology*, 24(17): 7567-7577, 2004.

13. James, D., Brown, R., Navarro, J. and Pilch, P., Insulin-regulatable tissues express a unique insulin-sensitive glucose transport protein., *Nature*, 333(6169): 183-185, 1988.

14. Ho-Palma, A., Toro, P., Rotondo, F., Romero, M., Alemany, M., Remesar, X. and Fernandez-Lopez, J., Insulin Controls Triacylglycerol Synthesis through Control of Glycerol Metabolism and Despite Increased Lipogenesis., *Nutrients*, 11(3): 513, 2019.

15. Berg JM, Tymoczko JL, Stryer L. Biochemistry., Food Intake and Starvation Induce Metabolic Changes., *Biochemistry*,5: Section 30.3, 2002.

16. Kaisanlahti, A. and Glumoff, T., Browning of white fat: agents and implications for beige adipose tissue to type 2 diabetes., *Journal of Physiology and Biochemistry*, 75(1): 1-10, 2018.

17. van Marken Lichtenbelt, W. and Schrauwen, P., Implications of nonshivering thermogenesis for energy balance regulation in humans., *American Journal of Physiology-Regulatory, Integrative and Comparative Physiology*, 301(2): 285-296, 2011.

18. Guilherme, A., Virbasius, J., Puri, V. and Czech, M., Adipocyte dysfunctions linking obesity to insulin resistance and type 2 diabetes., *Nature Reviews Molecular Cell Biology*, 9(5): 367-377, 2008.

19. Mogilevskaya, E., Demin, O. and Goryanin, I., Kinetic Model of Mitochondrial Krebs Cycle: Unraveling the Mechanism of Salicylate Hepatotoxic Effects., *Journal of Biological Physics*, 32(3-4): 245-271, 2006.

20. Philp, A., Lactate - a signal coordinating cell and systemic function., *Journal of Experimental Biology*, 208(24): 4561-4575, 2005.

21. Hao, Q. and Yadav, R., Transcriptome profiling of brown adipose tissue during cold exposure reveals extensive regulation of glucose metabolism., *American Journal of Physiology-Endocrinology and Metabolism*, 308(5): 380-392, 2015.

22. Basse, A., Isidor, M. and Winther, S., Regulation of glycolysis in brown adipocytes by HIF-1α., *Scientific Reports*, 7(1), 2017.

23. Sabater, D., Arriaran, S., Romero, M., Agnelli, S., Remesar, X., Fernandez-Lopez, J. and Alemany, M., Cultured 3T3L1 adipocytes dispose of excess medium glucose as lactate under abundant oxygen availability., *Scientific Reports*, 4(1), 2014.

24. Cordeiro, A., Godoi, P., Silva, C., Garratt, R., Oliva, G. and Thiemann, O., Crystal structure of human phosphoglucose isomerase and analysis of the initial catalytic steps., *Biochimica et Biophysica Acta (BBA) - Proteins and Proteomics*, 1645(2): 117-122, 2003.

25. Somarowthu, S., Brodkin, H., D'Aquino, J., Ringe, D., Ondrechen, M. and Beuning, P., A Tale of Two Isomerases: Compact versus Extended Active Sites in Ketosteroid Isomerase and Phosphoglucose Isomerase., *Biochemistry*, 50(43): 9283-9295, 2011.

26. Gurney, M., Heinrich, S., Lee, M. and Yin, H., Molecular cloning and expression of neuroleukin, a neurotrophic factor for spinal and sensory neurons., *Science*, 234(4776): 566-574, 1986.

27. Haga, A., Niinaka, Y. and Raz, A., Phosphohexose isomerase/autocrine motility factor/neuroleukin/maturation factor is a multifunctional phosphoprotein., *Biochimica et Biophysica Acta (BBA) - Protein Structure and Molecular Enzymology*, 1480(1-2): 235-244, 2000.

28. Gallardo-Perez, J., Rivero-Segura, N., Marin-Hernandez, A., Moreno-Sanchez, R. and Rodriguez-Enriquez, S., GPI/AMF inhibition blocks the development of the metastatic phenotype of mature multi-cellular tumor spheroids., *Biochimica et Biophysica Acta (BBA) - Molecular Cell Research*, 1843(6): 1043-1053, 2014.

29. Dunaway, G., Kasten, T., Sebo, T. and Trapp, R., Analysis of the phosphofructokinase subunits and isoenzymes in human tissues., *Biochemical Journal*, 251(3): 677-683, 1988.

30. Sale, E. and Denton, R., Adipose-tissue phosphofructokinase. Rapid purification and regulation by phosphorylation in vitro., *Biochemical Journal*, 232(3): 897-904, 1985.

31. Du, S., Guan, Z., Hao, L., Song, Y., Wang, L., Gong, L., Liu, L., Qi, X., Hou, Z. and Shao, S., Fructose-Bisphosphate Aldolase A Is a Potential Metastasis-Associated Marker of Lung Squamous Cell Carcinoma and Promotes Lung Cell Tumorigenesis and Migration., *PLoS ONE*, 9(1), p.e85804, 2014.

32. Sekar, Y., Moon, T., Slupsky, C. and Befus, A., Protein Tyrosine Nitration of Aldolase in Mast Cells: A Plausible Pathway in Nitric Oxide-Mediated Regulation of Mast Cell Function., *The Journal of Immunology*, 185(1): 578-587, 2010.

33. Mamczur, P., Gamian, A., Kolodziej, J., Dziegiel, P. and Rakus, D., Nuclear localization of aldolase A correlates with cell proliferation., *Biochimica et Biophysica Acta (BBA) - Molecular Cell Research*, 1833(12): 2812-2822, 2013.

34. Merkulova, M., Hurtado-Lorenzo, A., Hosokawa, H., Zhuang, Z., Brown, D., Ausiello, D. and Marshansky, V., Aldolase directly interacts with ARNO and modulates cell morphology and acidic vesicle distribution., *American Journal of Physiology-Cell Physiology*, 300(6): 1442-1455, 2011.

35. Dalby, A., Tolan, D. and Littlechild, J., The structure of human liver fructose-1,6-bisphosphate aldolase., *Acta Crystallographica Section D Biological Crystallography*, 57(11): 1526-1533, 2001.

36. Langellotti, S., Romano, M., Guarnaccia, C., Granata, V., Orru, S., Zagari, A., Baralle, F. and Salvatore, F., A novel anti-aldolase C antibody specifically interacts with residues 85-102 of the protein., *mAbs*, 6(3): 707-716, 2014.

37. Liu, J., Desai, K., Wang, R. and Wu, L., Up-regulation of aldolase A and methylglyoxal production in adipocytes., *British Journal of Pharmacology*, 168(7): 1639-1646, 2013.

38. Liu, J., Wang, R., Desai, K. and Wu, L., Upregulation of aldolase B and overproduction of methylglyoxal in vascular tissues from rats with metabolic syndrome., *Cardiovascular Research*, 92(3): 494-503, 2011.

39. Harris, T., Cole, R., Comer, F. and Mildvan, A., Proton Transfer in the Mechanism of Triosephosphate Isomerase., *Biochemistry*, 37(47): 16828-16838, 1998.

40. Dang Y, Wang Z, Guo Y, Yang J, Xing Z, Mu L, Zhang X, Ding Z., Overexpression of triosephosphate isomerase inhibits proliferation of chicken embryonal fibroblast cells., *Asian Pac J Cancer Prev*, 12(12): 3479-82, 2011.

41. Pancholi, V. and Chhatwal, G., Housekeeping enzymes as virulence factors for pathogens., *International Journal of Medical Microbiology*, 293(6): 391-401, 2003.

42. Chuang, J., Su, S., Chiang, B., Lee, H. and Chow, L., Proteome mining for novel IgE-binding proteins from the German cockroach (Blattella germanica) and allergen profiling of patients., *PROTEOMICS - Clinical Applications*, 5(3-4): 202-202, 2011.

43. Roland, B., Zeccola, A., Larsen, S., Amrich, C. and Talsma, A., Structural and Genetic Studies Demonstrate Neurologic Dysfunction in Triosephosphate Isomerase Deficiency Is Associated with Impaired Synaptic Vesicle Dynamics., *PLOS Genetics*, 12(3), p.e1005941, 2016.

44. Edwards, Y., Clark, P. and Harris, H., Isozymes of glyceraldehyde-3-phosphate dehydrogenase in man and other mammals., *Annals of Human Genetics*, 40(1): 67-77, 1976.

45. Sirover, M., New nuclear functions of the glycolytic protein, glyceraldehyde-3-phosphate dehydrogenase, in mammalian cells., *Journal of Cellular Biochemistry*, 95(1): 45-52, 2005.

46. Harris, J. I. & Waters, M., *Enzymes* 3rd Ed. 13, 1-49, 1976.

47. Dugail, I., Quignard-Boulange, A., Bazin, R., Le Liepvre, X. and Lavau, M., Adipose-tissue-specific increase in glyceraldehyde-3-phosphate dehydrogenase activity and mRNA amounts in suckling pre-obese Zucker rats. Effect of weaning., *Biochemical Journal*, 254(2): 483-487, 1988.

48. Willard, H., Goss, S., Holmes, M. and Munroe, D., Regional localization of the phosphoglycerate kinase gene and pseudogene on the human X chromosome and assignment of a related DNA sequence to chromosome 19., *Human Genetics*, 71(2), 1985.

49. Boer, P., Adra, C., Lau, Y. and McBurney, M., The testis-specific phosphoglycerate kinase gene pgk-2 is a recruited retroposon., *Molecular and Cellular Biology*, 7(9): 3107-3112, 1987.

50. Popanda, O., Fox, G. and Thielmann, H., Modulation of DNA polymerases α, δ and ϵ by lactate dehydrogenase and 3-phosphoglycerate kinase., *Biochimica et Biophysica Acta (BBA) - Gene Structure and Expression*, 1397(1): 102-117, 1998.

51. Danshina, P., Geyer, C., Dai, Q., Goulding, E., Willis, W., Kitto, G., McCarrey, J., Eddy, E. and O'Brien, D., Phosphoglycerate Kinase 2 (PGK2) Is Essential for Sperm Function and Male Fertility in Mice1., *Biology of Reproduction*, 82(1): 136-145, 2010.

52. Stenkula, K. and Erlanson-Albertsson, C., Adipose cell size: importance in health and disease., *American Journal of Physiology-Regulatory, Integrative and Comparative Physiology*, 315(2): 284-295, 2018.

53. Jedrzejas, M., Structure, function, and evolution of phosphoglycerate mutases: comparison with fructose-2,6-bisphosphatase, acid phosphatase, and alkaline phosphatase., *Progress in Biophysics and Molecular Biology*, 73(2-4): 263-287, 2000.

54. Omenn, G., Cheung, S., Phosphoglycerate mutase isozyme marker for tissue differentiation in man., *Am J Hum Genet.*, 26(3): 393-399, 1974.

55. Mikawa, T., Maruyama, T., Okamoto, K., Nakagama, H., Lleonart, M., Tsusaka, T., Hori, K., Murakami, I., Izumi, T., Takaori-Kondo, A., Yokode, M., Peters, G., Beach, D. and Kondoh, H., Senescence-inducing stress promotes proteolysis of phosphoglycerate mutase via ubiquitin ligase Mdm2., *Journal of Cell Biology*, 204(5): 729-745, 2014.

56. Shinozaki, S., Chiba, T., Kokame, K. and Miyata, T., Site-specific Effect of Estradiol on Gene Expression in the Adipose Tissue of ob/ob Mice., *Hormone and Metabolic Research*, 39(3): 192-196, 2007.

57. Fernandez-Trasancos, A., Fandino-Vaquero, R., Agra, R., Fernandez, A., Vinuela, J., Gonzalez-Juanatey, J. and Eiras, S., Impaired Adipogenesis and Insulin Resistance in Epicardial Fat-Mesenchymal Cells From Patients With Cardiovascular Disease., *Journal of Cellular Physiology*, 229(11): 1722-1730, 2014.

58. Marangos, P., Zis, A., Clark, R. and Goodwin, F., Neuronal, non-neuronal and hybrid forms of enolase in brain: Structural, immunological and functional comparisons., *Brain Research*, 150(1): 117-133, 1978.

59. Kato, K., Ishiguro, Y., Suzuki, F., Ito, A. and Semba, R., Distribution of nervous system-specific forms of enolase in peripheral tissues., *Brain Research*, 237(2): 441-448, 1982.

60. Fletcher, L., Rider, C. and Taylor, C., Enolase isoenzymes., *Biochimica et Biophysica Acta (BBA) - Enzymology*, 452(1): 245-252, 1976.

61. Schmechel, D., Brightman, M. and Marangos, P., Neurons switch from non-neuronal enolase to neuron-specific enolase during differentiation., *Brain Research*, 190(1): 195-214, 1980.

62. Rider, C. and Taylor, C., Enolase isoenzymes., *Biochimica et Biophysica Acta (BBA) - Protein Structure*, 405(1): 175-187, 1975.

63. Perez-Perez, R., Lopez, J., Garcia-Santos, E. and Camafeita, E., Uncovering Suitable Reference Proteins for Expression Studies in Human Adipose Tissue with Relevance to Obesity., *PLoS ONE*, 7(1), p.e30326, 2012.

64. Mukherjee, R., Choi, J., Choi, D., Oh, T., Liu, H. and Yun, J., Gender-dependent Protein Expression in White Adipose Tissues of Lean and Obese Rats Fed a High Fat Diet., *Cellular Physiology and Biochemistry*, 29(3-4): 617-634, 2012.

65. Hall, E. and Larry Cottam, G., Isozymes of pyruvate kinase in vertebrates: their physical, chemical, kinetic and immunological properties., *International Journal of Biochemistry*, 9(11): 785-794, 1978.

66. Eigenbrodt, E., Mazurek, S. and Friis, R., Double role of pyruvate kinase type M2 in the regulation of phosphometabolite pools., *Cell Growth and Oncogenesis*, 15-30, 1998.

67. Prakasam, G., Iqbal, M., Bamezai, R. and Mazurek, S., Posttranslational Modifications of Pyruvate Kinase M2: Tweaks that Benefit Cancer., *Frontiers in Oncology*, 8, 2018.

68. Iqbal, M., Siddiqui, F., Gupta, V. and Chattopadhyay, S., Insulin enhances metabolic capacities of cancer cells by dual regulation of glycolytic enzyme pyruvate kinase M2., *Molecular Cancer*, 12(1): 72, 2013.

69. Rajala, A., Soni, K. and Rajala, R., Metabolic and Non-metabolic Roles of Pyruvate Kinase M2 Isoform in Diabetic Retinopathy., *Scientific Reports*, 10(1), 2020.

70. R R Traxinger 1, S Marshall, Insulin regulation of pyruvate kinase activity in isolated adipocytes. Crucial role of glucose and the hexosamine biosynthesis pathway in the expression of insulin action., *J Biol Chem*, 15;267(14): 9718-23, 1992.

71. Van Eerd J., Kreutzer E., *Klinisc he Chemie voor Analisten deel*, 2: 138-139, 1996.

72. Chang, A. and Rothrock, D., The effect of diabetes and insulin on adipose lactate dehydrogenase isozymes., *Canadian Journal of Biochemistry*, 55(1): 113-116, 1977.

73. Kalhan, S., Mahajan, S., Burkett, E., Reshef, L. and Hanson, R., Glyceroneogenesis and the Source of Glycerol for Hepatic Triacylglycerol Synthesis in Humans., *Journal of Biological Chemistry*, 276(16): 12928-12931, 2001.

74. Jenkins, C., Mancuso, D., Yan, W., Sims, H., Gibson, B. and Gross, R., Identification, Cloning, Expression, and Purification of Three Novel Human Calcium-independent Phospholipase A2Family Members Possessing Triacylglycerol Lipase and Acylglycerol Transacylase Activities., *Journal of Biological Chemistry*, 279(47): 48968-48975, 2004.

75. Fredrikson, G., Tornqvist, H. and Belfrage, P., Hormone-sensitive lipase and monoacylglycerol lipase are both required for complete degradation of adipocyte triacylglycerol., *Biochimica et Biophysica Acta (BBA) - Lipids and Lipid Metabolism*, 876(2): 288-293, 1986.

76. Holm, C., Molecular mechanisms regulating hormone-sensitive lipase and lipolysis., *Biochemical Society Transactions*, 31(6): 1120-1124, 2003.

77. Rotondo, F., Ho-Palma, A., Remesar, X., Fernandez-Lopez, J., Romero, M. and Alemany, M., Glycerol is synthesized and secreted by adipocytes to dispose of excess glucose, via glycerogenesis and increased acyl-glycerol turnover., *Scientific Reports*, 7(1), 2017.

78. Sul, H. and Smith, S., *Biochemistry Of Lipids, Lipoproteins And Membranes*, 5th ed. Elsevier: 155-190, 2008.

79. Ke, J., Behal, R., Back, S., Nikolau, B., Wurtele, E. and Oliver, D., The Role of Pyruvate Dehydrogenase and Acetyl-Coenzyme A Synthetase in Fatty Acid Synthesis in Developing Arabidopsis Seeds., *Plant Physiology*, 123(2): 497-508, 2000.

80. Wiegand, G. and Remington, S., Citrate Synthase: Structure, Control, and Mechanism., *Annual Review of Biophysics and Biophysical Chemistry*, 15(1): 97-117, 1986.

81. Mycielska, M., Patel, A., Rizaner, N., Mazurek, M., Keun, H., Patel, A., Ganapathy, V. and Djamgoz, M., Citrate transport and metabolism in mammalian cells., *BioEssays*, 31(1): 10-20, 2009.

82. Salati, L. and Goodridge, A., *New Comprehensive Biochemistry*, Elsevier, 101-127, 1996.

83. Tehlivets, O., Scheuringer, K. and Kohlwein, S., Fatty acid synthesis and elongation in yeast., *Biochimica et Biophysica Acta (BBA) - Molecular and Cell Biology of Lipids*, 1771(3): 255-270, 2007.

84. Heil, C., Wehrheim, S., Paithankar, K. and Grininger, M., Fatty Acid Biosynthesis: Chain-Length Regulation and Control., *ChemBioChem*, 20(18): 2298-2321, 2019.

85. Holmes, R., VandeBerg, J. and Cox, L., Comparative studies of vertebrate lipoprotein lipase: A key enzyme of very low density lipoprotein metabolism., *Comparative Biochemistry and Physiology Part D: Genomics and Proteomics*, 6(2): 224-234, 2011.

86. Schwenk, R., Holloway, G., Luiken, J., Bonen, A. and Glatz, J., Fatty acid transport across the cell membrane: Regulation by fatty acid transporters., *Prostaglandins, Leukotrienes and Essential Fatty Acids (PLEFA)*, 82(4-6): 149-154, 2010.

87. van der Vusse, G., Albumin as Fatty Acid Transporter., *Drug Metabolism and Pharmacokinetics*, 24(4): 300-307, 2009.

88. Dircks, L. and Sul, H., Acyltransferases of de novo glycerophospholipid biosynthesis., *Progress in Lipid Research*, 38(5-6): 461-479, 1999.

89. Carman, G. and Han, G., Roles of phosphatidate phosphatase enzymes in lipid metabolism., *Trends in Biochemical Sciences*, 31(12): 694-699, 2006.

90. Coleman, R., Enzymes of triacylglycerol synthesis and their regulation., *Progress in Lipid Research*, 43(2): 134-176, 2004.

91. Guindalini, C., Lee, K., Andersen, M., Santos-Silva, R., Bittencourt, L. and Tufik, S., The influence of obstructive sleep apnea on the expression ofglycerol-3-phosphate dehydrogenase1gene., *Experimental Biology and Medicine*, 235(1): 52-56, 2010.

92. Kota, V., Dhople, V. and Shivaji, S., Tyrosine phosphoproteome of hamster spermatozoa: Role of glycerol-3-phosphate dehydrogenase 2 in sperm capacitation., *PROTEOMICS*, 9(7): 1809-1826, 2009.

93. Koekemoer, T., Litthauer, D. and Oelofsen, W., Isolation and characterization of adipose tissue glycerol-3-phosphate dehydrogenase., *The International Journal of Biochemistry & Cell Biology*, 27(6): 625-632, 1995.

94. Swierczynski, J., Zabrocka, L., Goyke, E., Raczynska, S., Adamonis, W. and Sledzinski, Z., *Molecular and Cellular Biochemistry*, 254(1/2): 55-59, 2003.

95. Sledzinski, T., Korczynska, J., Goyke, E., Stefaniak, T., Proczko-Markuszewska, M., Kaska, L. and Swierczynski, J., Association Between Cytosolic Glycerol 3-Phosphate Dehydrogenase Gene Expression in Human Subcutaneous Adipose Tissue and BMI., *Cellular Physiology and Biochemistry*, 32(2): 300-309, 2013.

96. Honka, M., Latva-Rasku, A., Bucci, M., Virtanen, K., Hannukainen, J., Kalliokoski, K. and Nuutila, P., Insulin-stimulated glucose uptake in skeletal muscle, adipose tissue and liver: a positron emission tomography study., *European Journal of Endocrinology*, 178(5): 523-531, 2018.

97. Surmi, B. and Hasty, A., Macrophage infiltration into adipose tissue: initiation, propagation and remodeling., *Future Lipidology*, 3(5): 545-556, 2008.

98. Longo, M., Zatterale, F., Naderi, J., Parrillo, L., Formisano, P., Raciti, G., Beguinot, F. and Miele, C., Adipose Tissue Dysfunction as Determinant of Obesity-Associated Metabolic Complications., *International Journal of Molecular Sciences*, 20(9): 2358, 2019.

99. Dash, R., DiBella, J. and Cabrera, M., A computational model of skeletal muscle metabolism linking cellular adaptations induced by altered loading states to metabolic responses during exercise., *BioMedical Engineering OnLine*, 6(1), 2007.

100. Park, H. (2018). HUMAN BRAIN, MUSCLE AND ADIPOSE TISSUES MATHEMATICAL MODELING FOR NORMAL AND DISEASED STATE

STUDIES. M. Sc. Eng. Thesis. Johns Hopkins University . Available at https://jscholarship.library.jhu.edu/handle/1774.2/59292 (Accessed: 18 May 2020).

101. Jensen, J., Rustad, P., Kolnes, A. and Lai, Y., The Role of Skeletal Muscle Glycogen Breakdown for Regulation of Insulin Sensitivity by Exercise., *Frontiers in Physiology*, 2, 2011.

102. Sarvari, A., Doan-Xuan, Q., Bacso, Z., Csomos, I., Balajthy, Z. and Fesus, L., Interaction of differentiated human adipocytes with macrophages leads to trogocytosis and selective IL-6 secretion., *Cell Death & Disease*, 6(1): 1613-1613, 2015.

103. Sallam, R., Adipokines in obesity and metabolic disease., *QJM: An International Journal of Medicine*, 111(suppl_1), 2018.

104. Boden, G., Fatty acid-induced inflammation and insulin resistance in skeletal muscle and liver., *Current Diabetes Reports*, 6(3): 177-181, 2006.

105. Lambeth, M. and Kushmerick, M., A Computational Model for Glycogenolysis in Skeletal Muscle., *Annals of Biomedical Engineering*, 30(6): 808-827, 2002.

106. Kim, J., Saidel, G. and Kalhan, S., A computational model of adipose tissue metabolism: Evidence for intracellular compartmentation and differential activation of lipases., *Journal of Theoretical Biology*, 251(3): 523-540, 2008.

107. Wilson, J., Isozymes of mammalian hexokinase: structure, subcellular localization and metabolic function., *Journal of Experimental Biology*, 206(12): 2049-2057, 2003.

108. Bachelard, H., Clark, A. and Thompson, M., Cerebral-cortex hexokinases. Elucidation of reaction mechanisms by substrate and dead-end inhibitor kinetic analysis., *Biochemical Journal*, 123(5): 707-715, 1971.

109. Puigjaner, J., Rais, B., Burgos, M., Comin, B., Ovadi, J. and Cascante, M., Comparison of control analysis data using different approaches: modelling and experiments with muscle extract., *FEBS Letters*, 418(1-2): 47-52, 1997.

110. Kahana, S., Lowry, O., Schulz, D., Passoneau J. and Crawford E., The kinetics of phosphoglucoisomerase., *J. Biol. Chem*, 235: 2178-2184, 1960.

111. Nagata, K., Suzuki, K. and Imahori, K., Analysis of the Allosteric Properties of Rabbit Muscle Phosphofructokinase by Means of Affinity Labeling with a Reactive ATP Analog1., *The Journal of Biochemistry*, 86(5): 1179-1189, 1979.

112. Putman, S., Coulson, A., Farley, I., Riddleston, B. and Knowles, J., Specificity and kinetics of triose phosphate isomerase from chicken muscle., *Biochemical Journal*, 129(2): 301-310, 1972.

113. Velick, S., Furfine, C., Glyceraldehyde 3-phosphate dehydrogenase. In: The Enzymes, 7, edited by P. D. Boyer, H. Lardy, and K. Myrback. New York: Academic, 1963, Vol. 7, Chap. 12.

114. Krietsch W., Bucher T., 3-phosphoglycerate kinase from rabbit sceletal muscle and yeast., *Eur. J. Biochem.*, 17: 568-580, 1970.

115. Rider, C., Taylor, C., Enolase isoenzymes in rat tissues. Electrophoretic, chromatographic, immunological, and kinetic properties., *Biochim. Biophys. Acta*, 365: 285-300, 1974.

116. Imamura, K., Tanaka, T., Pyruvate kinase isozymes from rat., *Methods Enzymol.*, 90: 150-165, 1982.

117. Stambaugh. R., Post, D., Substrate and product inhibition of rabbit muscle lactic dehydrogenase heart (H4) and Muscle (M4) isozymes., *J. Biol. Chem.*, 241: 1462-1467, 1966.

118. Zewe, V., Fromm H., Kinetic studies of rabbit muscle lactate dehydrogenase., *J. Biol. Chem.*, 237: 1668-1675, 1962.

119. Sempere, S., Cortes, A., Bozal, J., Kinetic mechanism of guinea-pig skeletal muscle lactate dehydrogenase (M4) with oxaloacetate-NADH and pyruvate-NADH as substrates., *Int. J. Biochem.*, 13: 727-731, 1981.

120. Thuma E, Schirmer RH and Schirmer I., Preparation and characterization of a crystalline human ATP: AMP phosphotransferase., *Biochim. Biophys. Acta*, 268: 81-91, 1972.

121. Rees, B., Ropson, I., Hand, S., Kinetic Properties of Hexokinase under Near-physiological Conditions., *J. Biol. Chem*, 264: 15410-15417, 1989.

122. Penhoet, E., Kochman, M., Rutter, W., Isolation of fructose diphosphate aldolases A, B, and C., *Biochemistry*, 8:4391-4395, 1969.

123. Dabrowska, A., Kamrowska, I., Baranowski, T., Purification, crystallization, and properties of triosephosphate isomerase from human skeletal muscle., *Acta Biochim. Pol.*, 25: 247-256, 1978.

124. Molnar, M., Vas, M., Mg2+ affects the binding of ADP but not ATP to 3-phosphoglycerate kinase. Correlation between equilibrium dialysis binding and enzyme kinetic data., *Biochem. J.*, 293:595-599, 1993.

125. Rose, Z., Dube, S., Phosphoglycerate mutase. Kinetics and effects of salts on the mutase and bisphosphoglycerate phosphatase activities of the enzyme from chicken breast muscle., *J. Biol. Chem.*, 253: 8583-8592, 1978.

126. Dyson, R., Cardenas, J., Barsotti, R., The reversibility of skeletal muscle pyruvate kinase and an assessment of its capacity to support glyconeogenesis., *J. Biol. Chem.*, 250: 3316-3321, 1975.

127. Rider, C., Taylor, C., Enolase isoenzymes in rat tissues. Electrophoretic, chromatographic, immunological, and kinetic properties., *Biochim. Biophys. Acta*, 365: 285-300, 1974.

128. Boyer, P., Robbins, E., Determination of theequilibrium of the hexokinase reaction and the free energy of hydrolysis of adenosine triphosphate. *J BiolChem*, 224: 121-135, 1957.

129. Hofmann, E., Kopperschlaeger, G., Phosphofructokinase from yeast., *Methods Enzymol.*, 90: 49-60, 1982.

130. Lowry, O., Passonneau, J., The relationship between substrates and enzymes of glycolysis in brain. *J Biol Chem*, 239: 31-42, 1964.

131. Blacklow, S., Raines, R., Lim, W., Zamore, P., Knowles, JR., Triosephosphate isomerase catalysis is diffusion controlled. appendix: analysis of triose phosphate equilibria in aqueous solution by31PNMR. *Biochemistry*, 31: 1158-1167, 1988.

132. Byers, L., She H., Alayoff, A., Interaction of phosphate analogues with glyceraldehyde-3-phosphate dehydrogenase., *Biochemistry*, 18: 2471-2480, 1979.

133. Teusink, B., Passarge, J., Reijenga, CA., Esgalhado, E., van der Weijden, CC., Schepper, M., Walsh, MC., Bakker, BM., van Dam, K., Westerhoff, HV., Snoep, JL., Can yeast glycolysis be understood in terms of in vitro kinetics of the constituent enzymes? Testing biochemistry., *Eur. J. Biochem.*, 267: 5313-5329, 2000.

134. Bergmeyer, H., Methods of Enzymatic Analysis., *Verlag Chemie*, Weinheim, Germany, 1974.

135. Young, H., Pace, N., Some physical and chemical properties of crystalline alphaglycerophosphate dehydrogenase. *Arch Biochem. Biophys.*, 75: 125-141, 1958.

136. Riol-Cimas, J., Melendez-Hevia, E., Distribution of metabolic fluxes towards glycerol phosphate and L-lactate from fructose-1,6-bisphosphate

in vitro: effect of glycerol phosphate dehydrogenase., *Int. J. Biochem. Cell Biol.*, 18: 853-856, 1986.

137. Johnson, MJ., Enzyme equilibria and thermodynamics. In: The Enzymes, 4, edited by H. Lardy, P. D. Boyer and K. Myrback., New York: Academic, 1959, 407-441.

138. Staples, J., Suarez, R., Honeybee flight muscle phosphoglucose isomerase: matching enzyme capacities to flux requirements at a near-equilibrium reaction. *J. Exp. Biol.*, 200(Pt 8): 1247-1254, 1997.

139. Dawkins, P., Dickens, F., The oxidation of d- and l-glycerate by rat liver. *Biochem. J.*, 94: 353-367, 1965.

140. Racker, E., Crystalline alcohol dehydrogenase from baker's yeast. *J. Biol. Chem.*, 184(1): 313-319, 1950.

141. Roche, M., Tessier, S., Storey, K., Structural and Functional Properties of Glycerol-3-Phosphate Dehydrogenase from a Mammalian Hibernator. *The Protein Journal*, 31(2): 109-119, 2011.

142. Berrada, W., Naya, A., Iddar, A., Bourhim, N., *Molecular and Cellular Biochemistry*, 231(1/2): 117-127, 2002.

143. Penkler, G., du Toit, F., Adams, W., Rautenbach, M., Palm, D., van Niekerk, D., Snoep, J., Construction and validation of a detailed kinetic model of glycolysis in *Plasmodium falciparum*. *FEBS Journal*, 282(8): 1481-1511, 2015.

144. Russo, J., Manuli, M., Ismail-Beigi, F., Sweadner, K., Edelman, I., Na(+)-K(+)-ATPase in adipocyte differentiation in culture. *American Journal of Physiology-Cell Physiology*, 259(6): 968 - 977, 1990.

145. van Wyk, M. (2019). The effect of adenylate kinase on the glycolytic oscillations of *Saccharomyces cerevisiae*. M. Sc. Biochemistry. Thesis. University of Stellenbosch. Available at https://scholar.sun.ac.za/handle/10019.1/105593 (Accessed: 20 August 2019).

146. Bakker, B., Michels, P., Opperdoes, F., Westerhoff, H., Glycolysis in bloodstream form *Trypanosoma brucei* can be understood in terms of the kinetics of the glycolytic enzymes. *Journal of Biological Chemistry*, 272(6): 3207 - 3215, 1997.

147. Tsouka, S., Hatzimanikatis, V., redLips: a comprehensive mechanistic model of the lipid metabolic network of yeast. *FEMS Yeast Research*, 20(2), 2020.

148. Schutzhold, V., Hahn, J., Tummler, K., Klipp, E., Computational Modeling of Lipid Metabolism in Yeast. *Frontiers in Molecular Biosciences*, 3, 2016.

149. Micheloni, A., Orsi, G., De Maria, C., Vozzi, G., ADMET: ADipocyte METabolism mathematical model. *Computer Methods in Biomechanics and Biomedical Engineering*, 18(13): 1386 - 1391, 2014.

150. van Eunen, K., Volker-Touw, C., Gerding, A., Bleeker, A., Wolters, J., van Rijt, W., Martines, A., Niezen-Koning, K., Heiner, R., Permentier, H., Groen, A., Reijngoud, D., Derks, T., Bakker, B., Living on the edge: substrate competition explains loss of robustness in mitochondrial fatty-acid oxidation disorders. *BMC Biology*, 14(1), 2016.

151. van Eunen, K., Simons, S., Gerding, A., Bleeker, A., den Besten, G., Touw, C., Houten, S., Groen, B., Krab, K., Reijngoud, D., Bakker, B., Biochemical Competition Makes Fatty-Acid β-Oxidation Vulnerable to Substrate Overload. *PLoS Computational Biology*, 9(8), 2013.

152. Martines, A., van Eunen, K., Reijngoud, D., Bakker, B., The promiscuous enzyme medium-chain 3-keto-acyl-CoA thiolase triggers a vicious cycle in fatty-acid beta-oxidation. *PLOS Computational Biology*, 13(4), 2017.

153. Edwards, L., Thiele, I., Applying systems biology methods to the study of human physiology in extreme environments. *Extreme Physiology & Medicine*, 2(1), 2013.

Appendix

Model simulations

All model simulations are provided with experimental data if applicable. This includes simulations for GAP, 1,3BPG, and PEP which were not included in Figure 4.14 or 4.15.

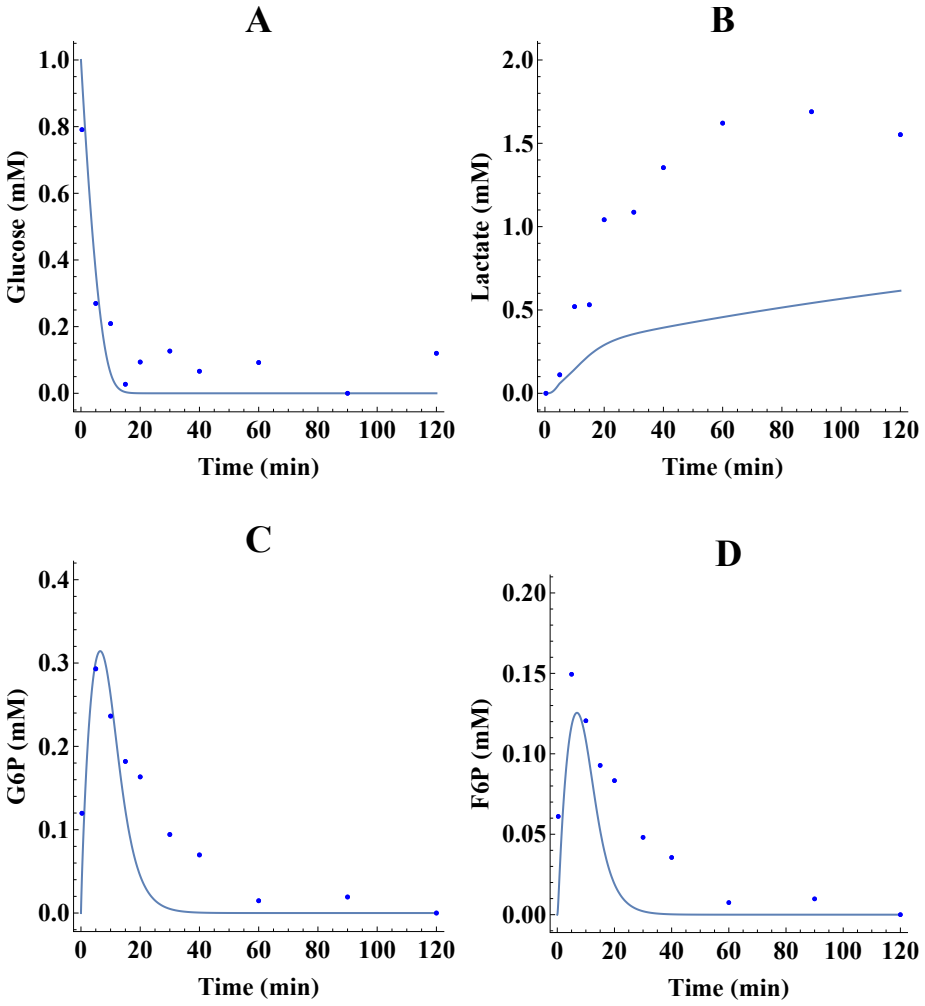

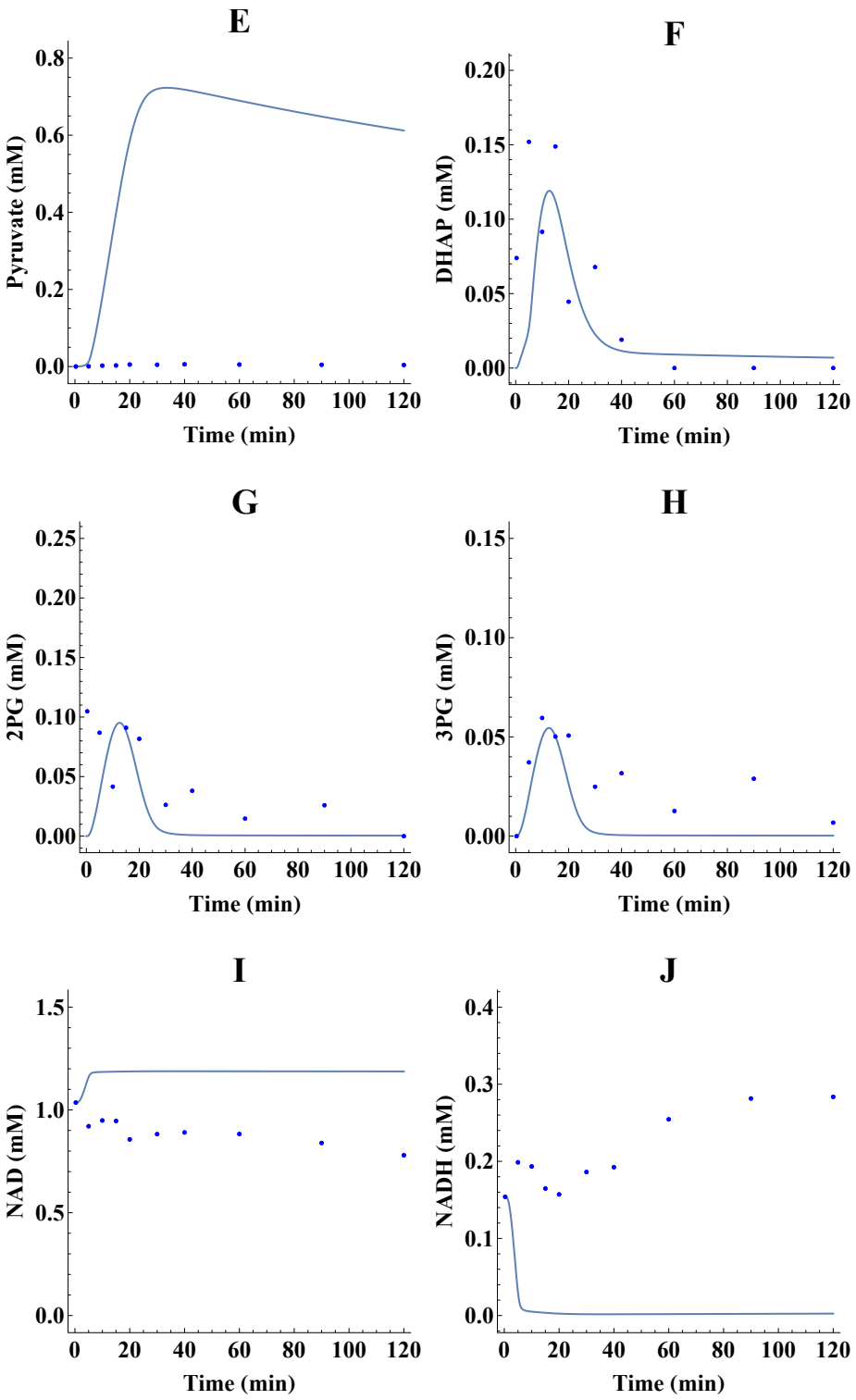

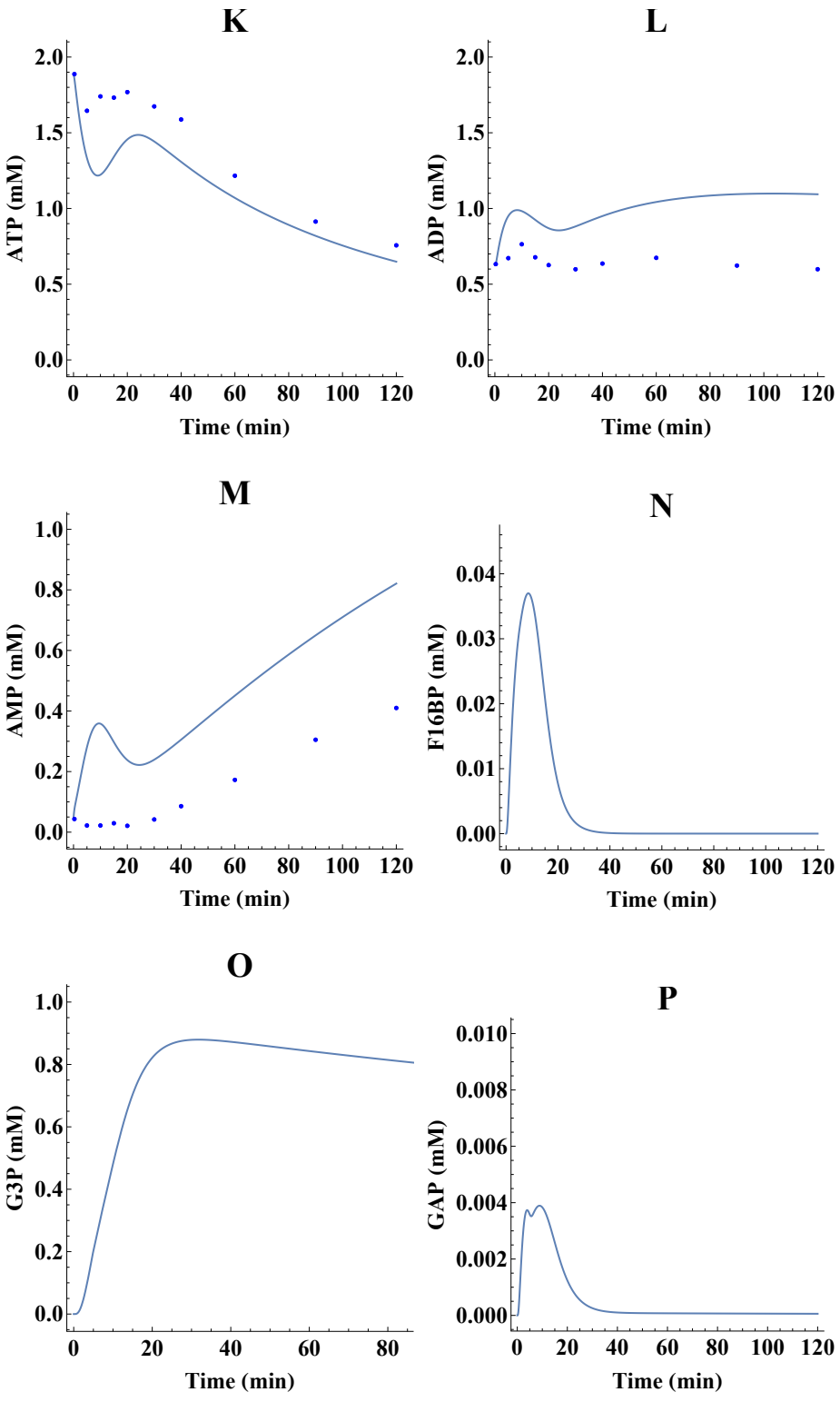

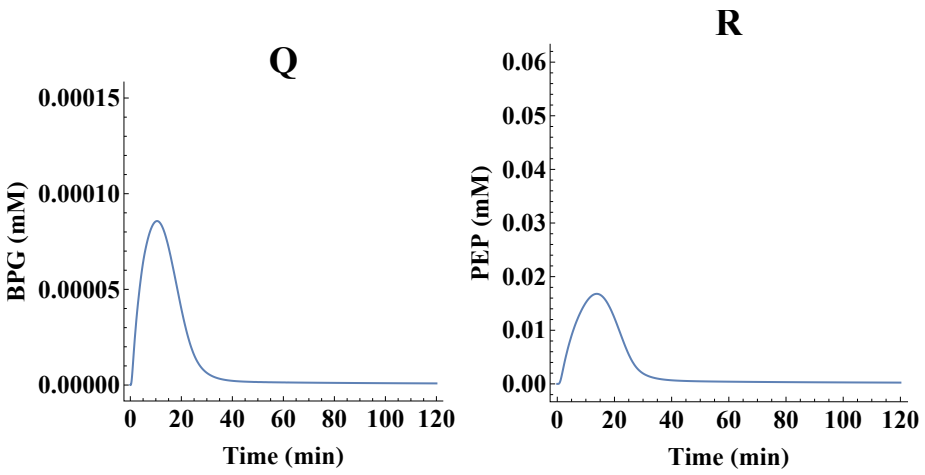

Figure 5.1: Validation data plotted together with model time courses. The overlays are of glucose (A), lactate (B), G6P (C), F6P (D), pyruvate (E), DHAP (F), 2PG (G), 3PG (H), NAD+ (I), NADH (J), ATP (K), ADP (L), AMP (M). The experimental data is represented by the data points while the model prediction is represented by the solid curve. F16BP (N), G3P (O), GAP (P), BPG (Q), and PEP (R) model predictions are also provided but without experimental data.

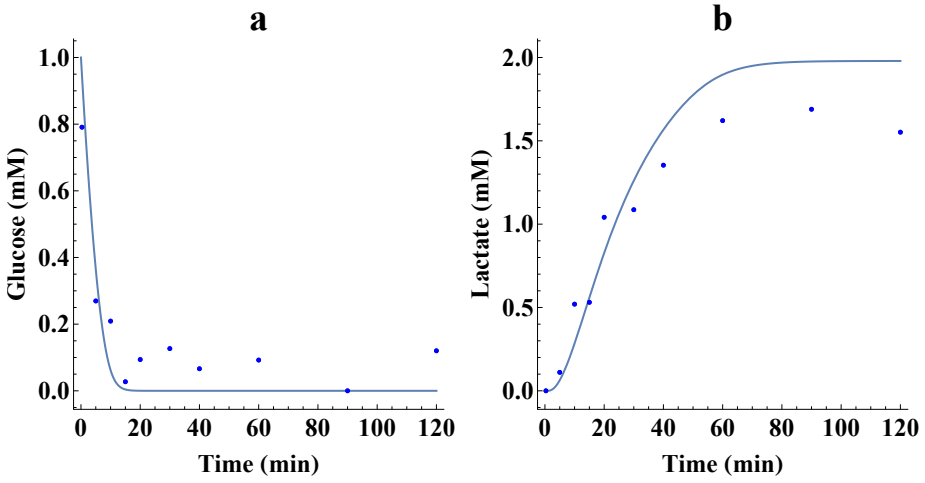

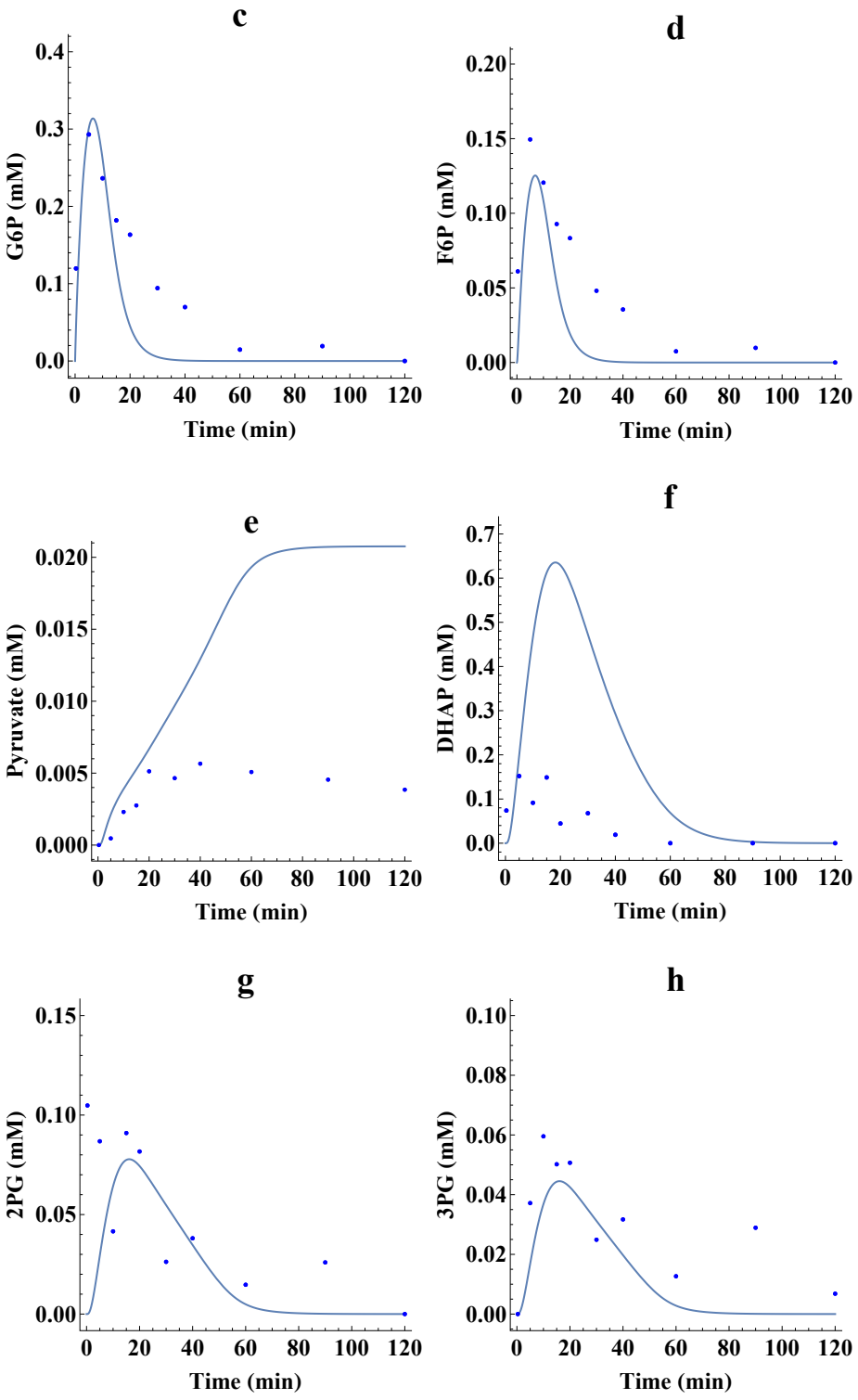

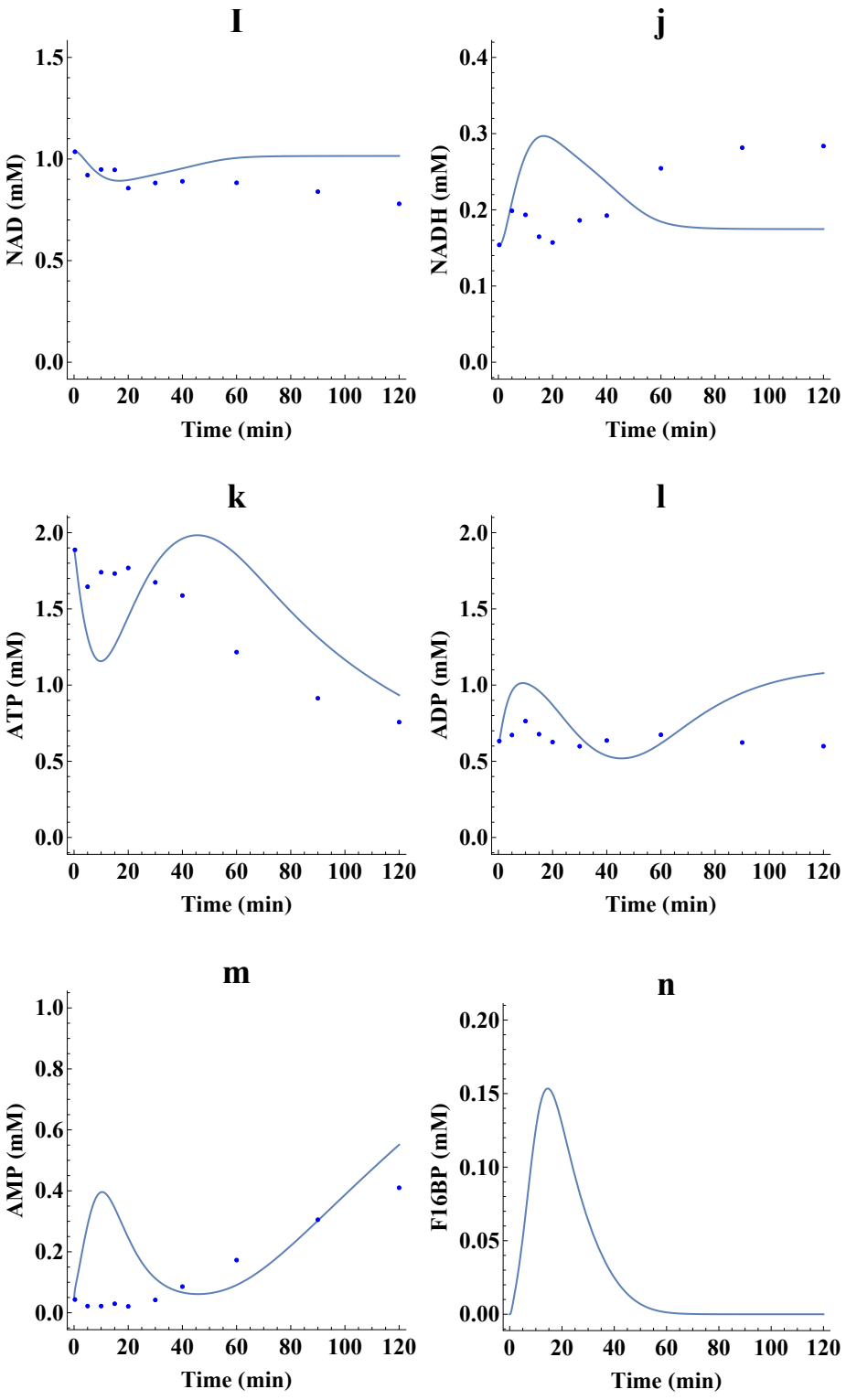

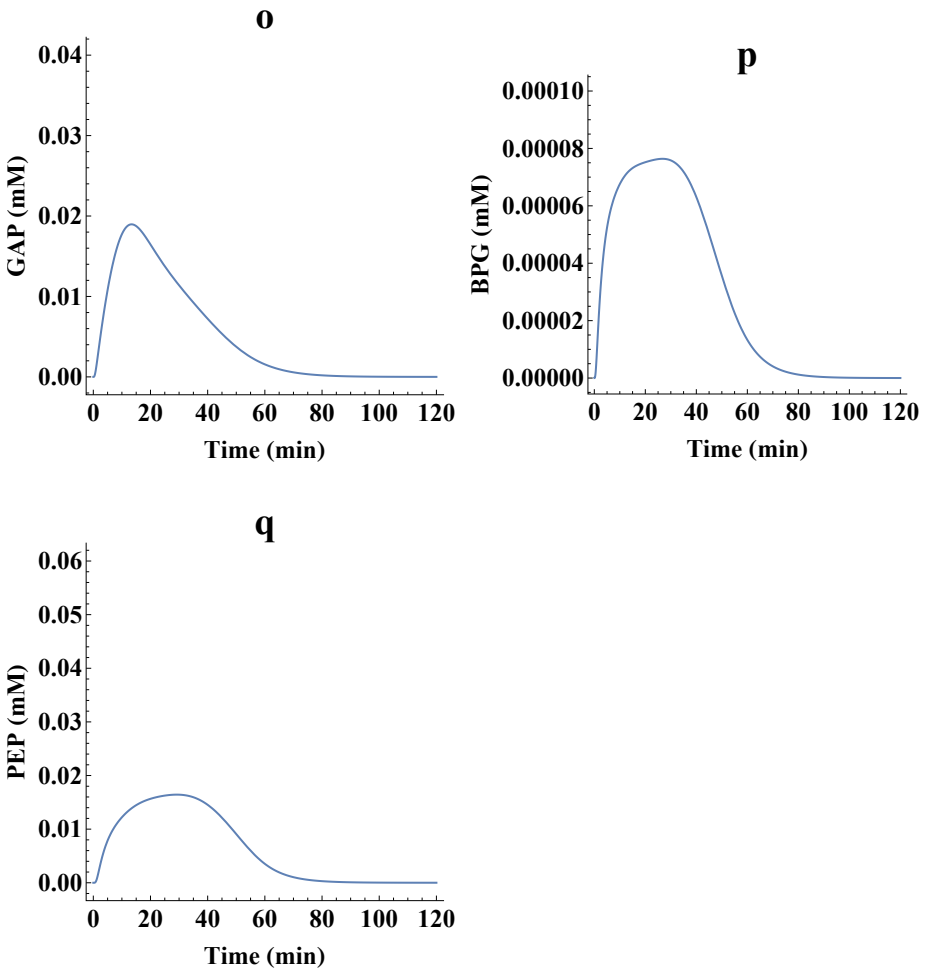

Figure 5.2: Validation data overlaid with model time courses (no G3PDH included). The overlays are of glucose (a), lactate (b), G6P (c), F6P (d), pyruvate (e), DHAP (f), 2PG (g), 3PG (h), NAD+ (i), NADH (j), ATP (k), ADP (l), AMP (m). The experimental data is represented by the data points while the model prediction is represented by the solid curve. The model prediction for F16BP (n), GAP (o), BPG (p), and PEP (q) is also provided but without experimental data.

HPLC chromatograms

HPLC chromatograms for all ten time point samples are provided below. This includes all chromatograms not included in Figure 4.13.

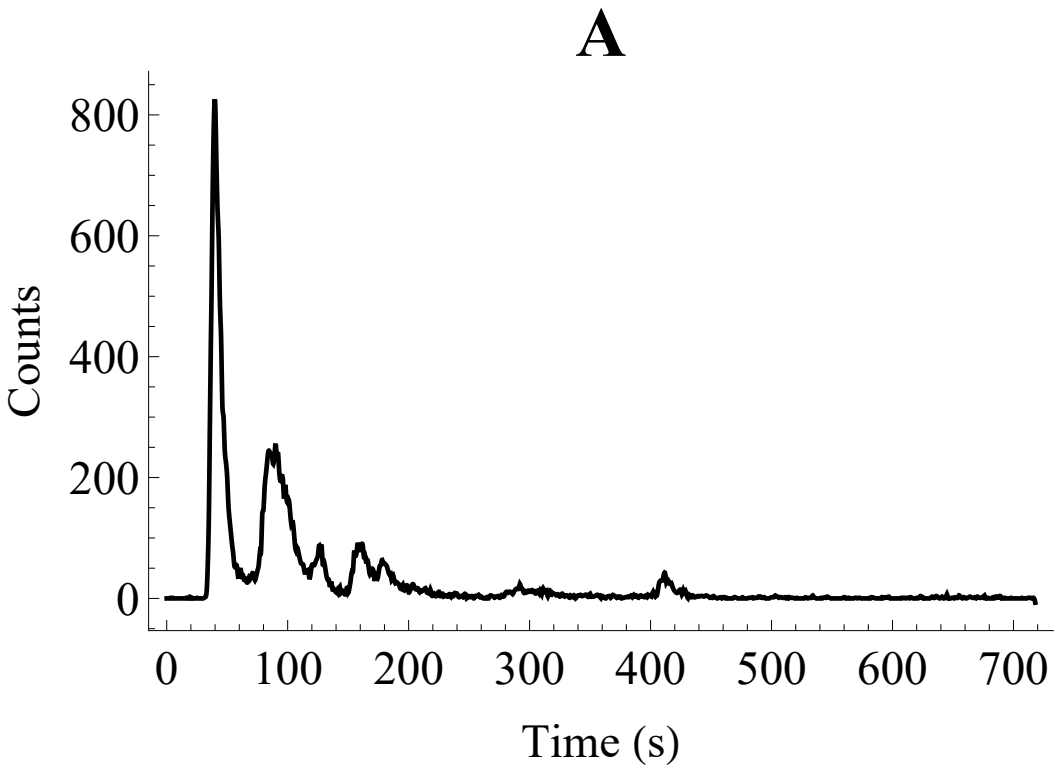

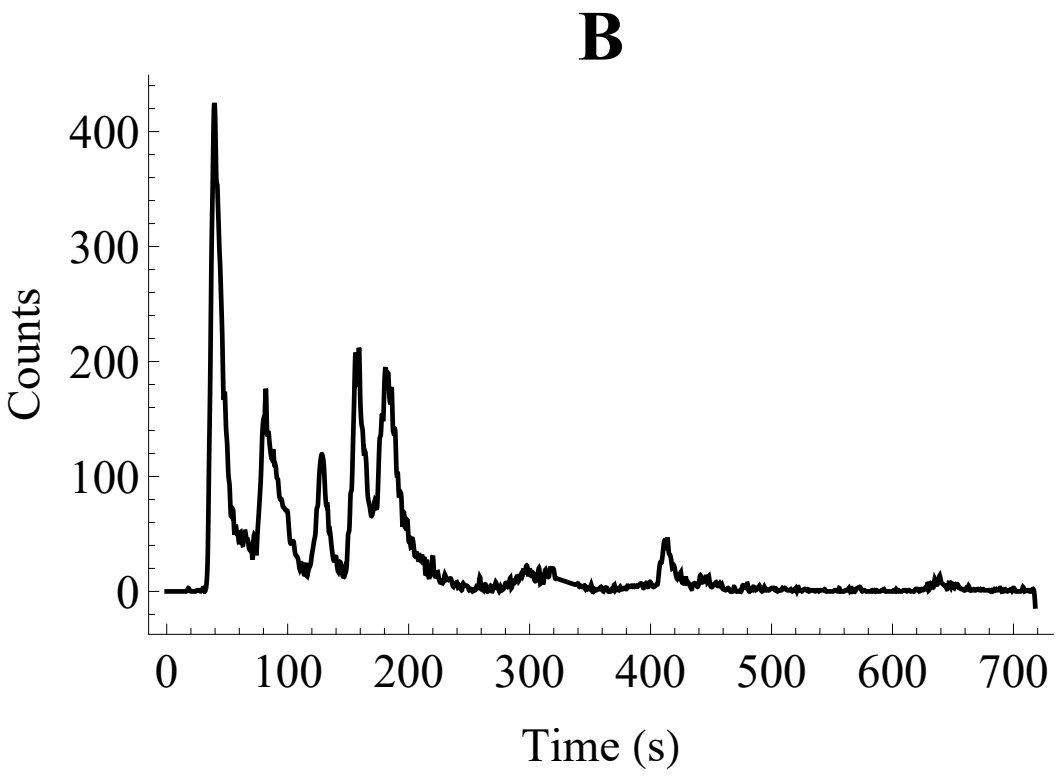

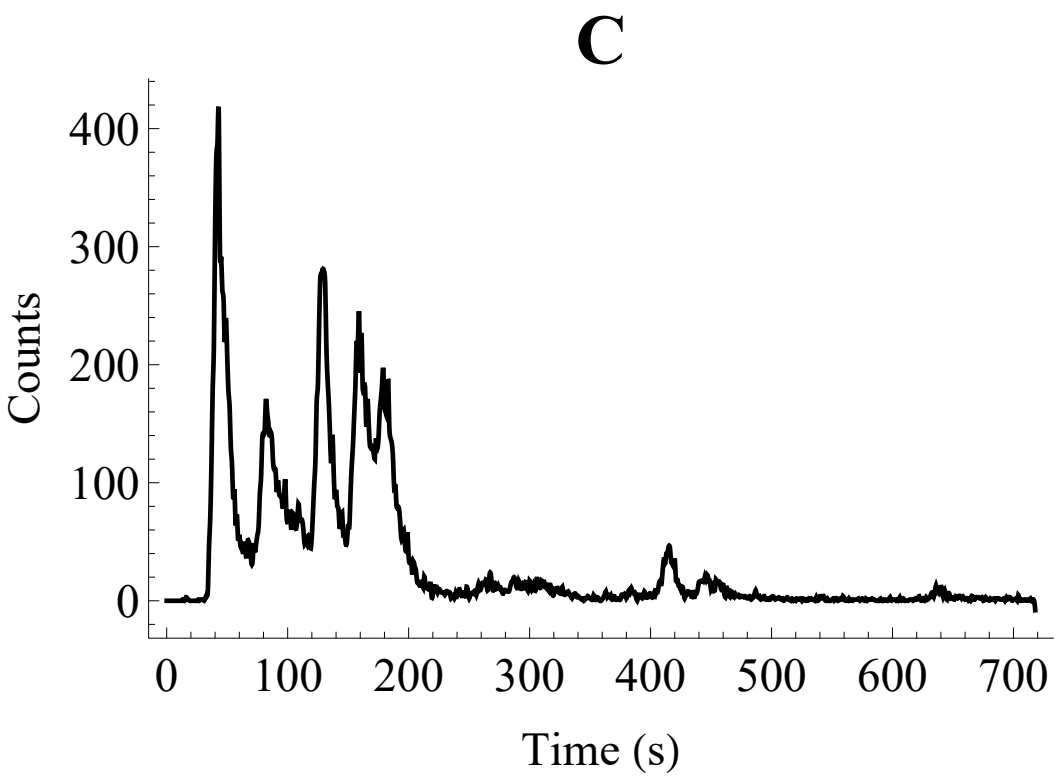

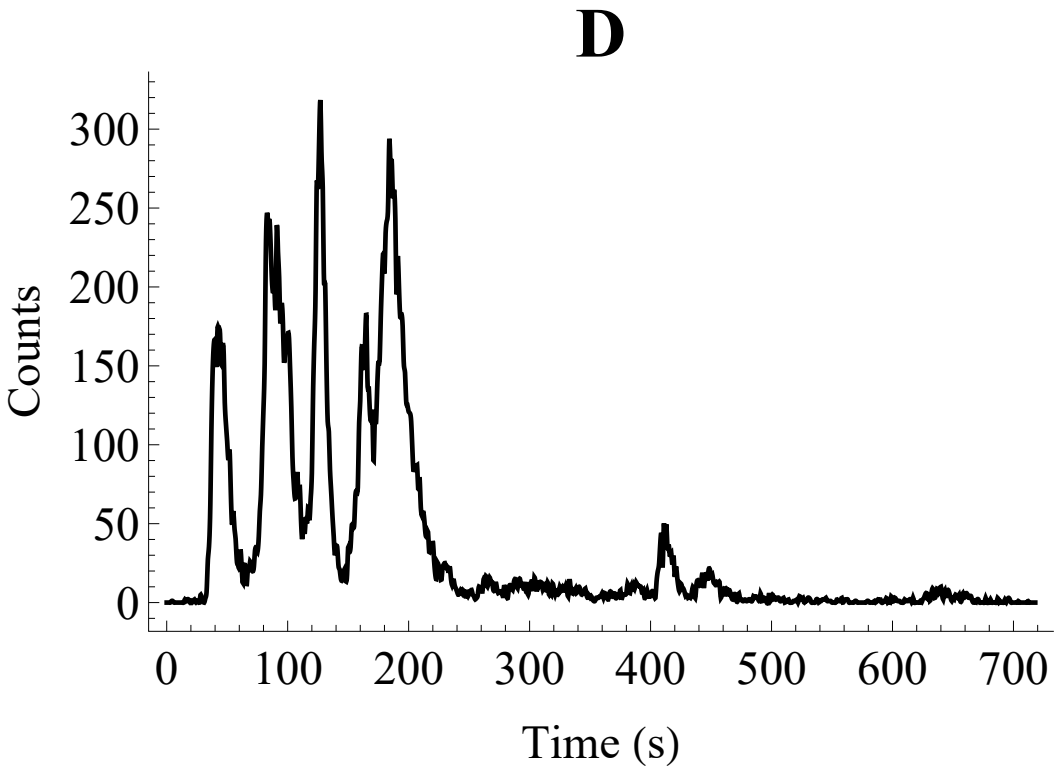

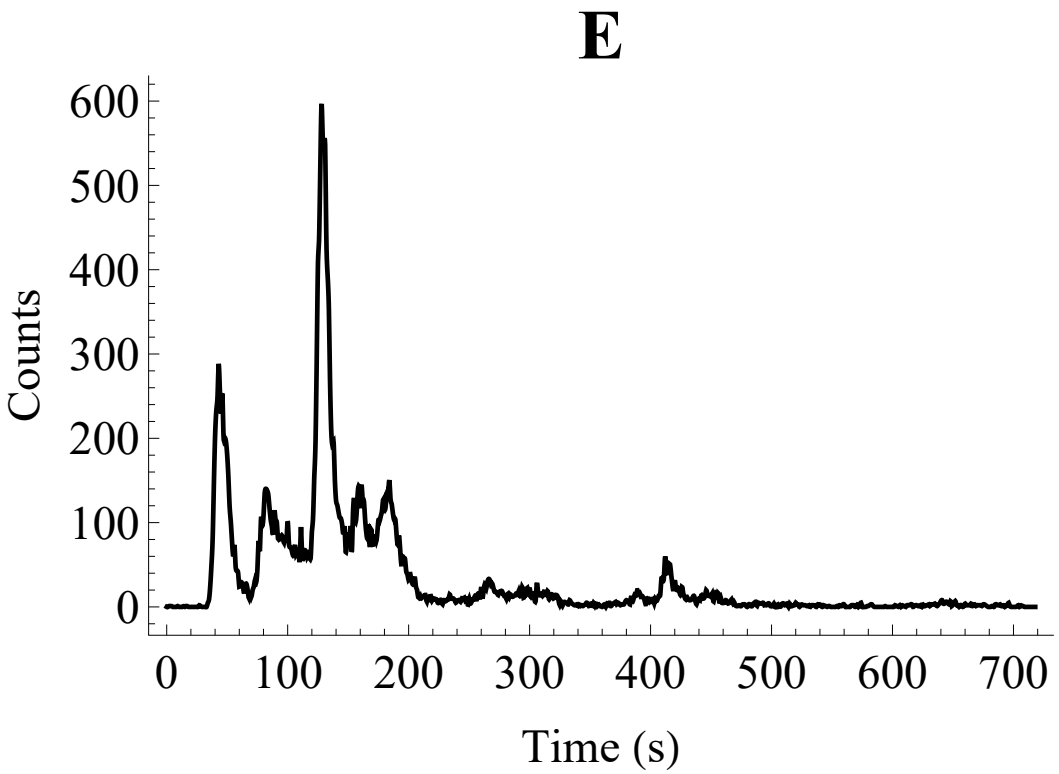

F

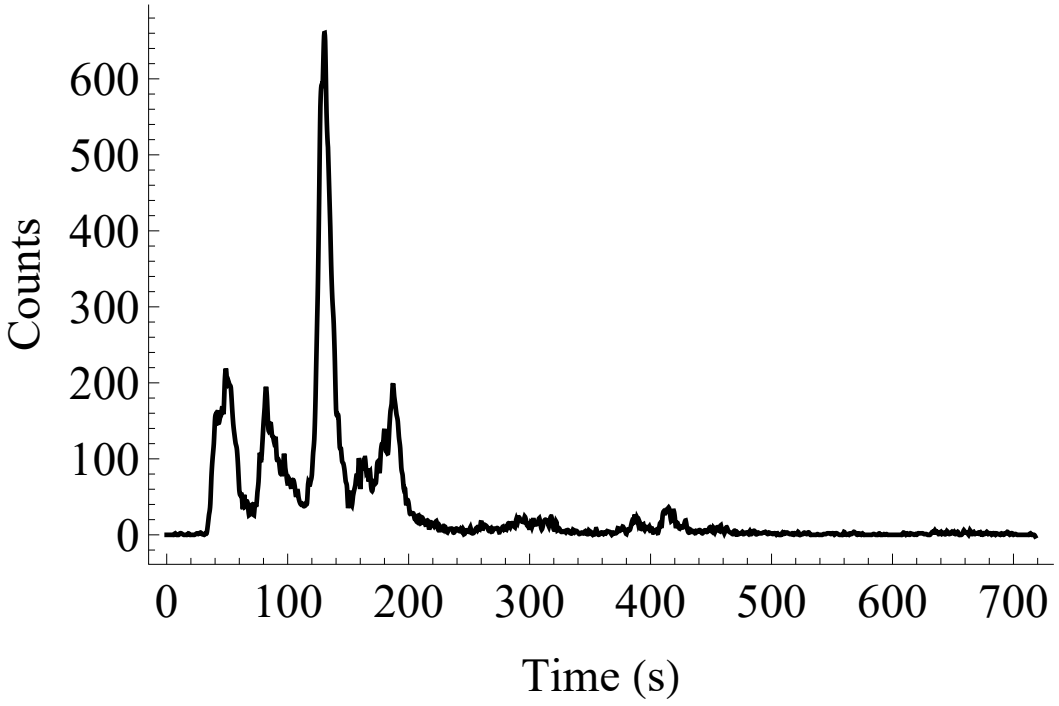

G

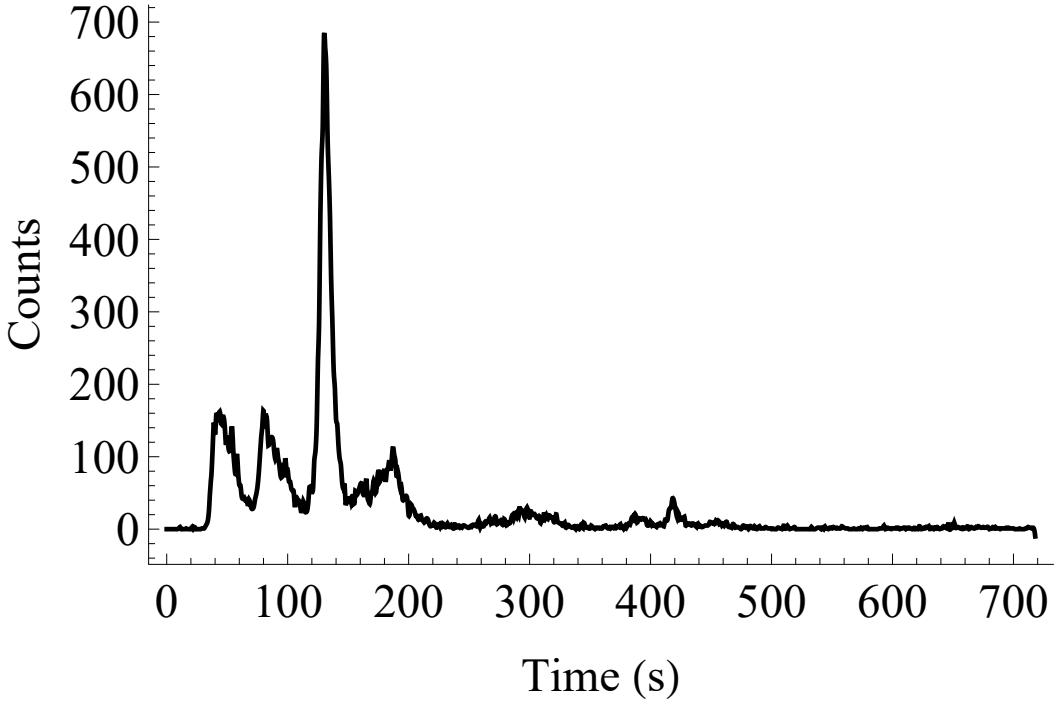

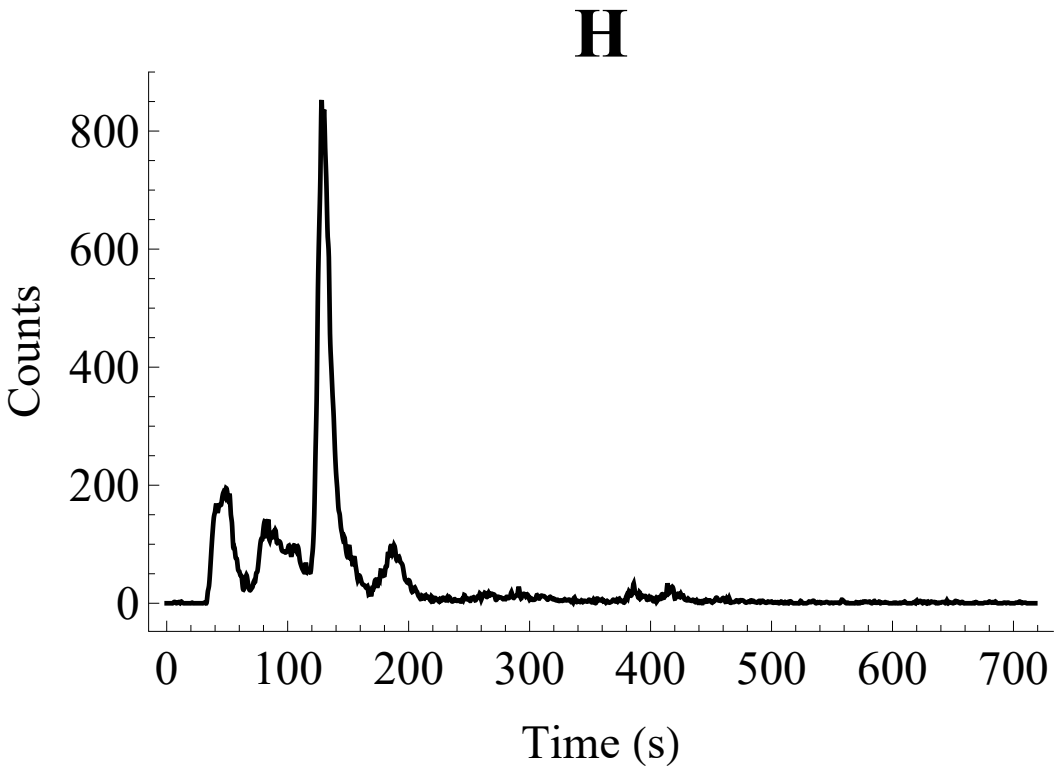

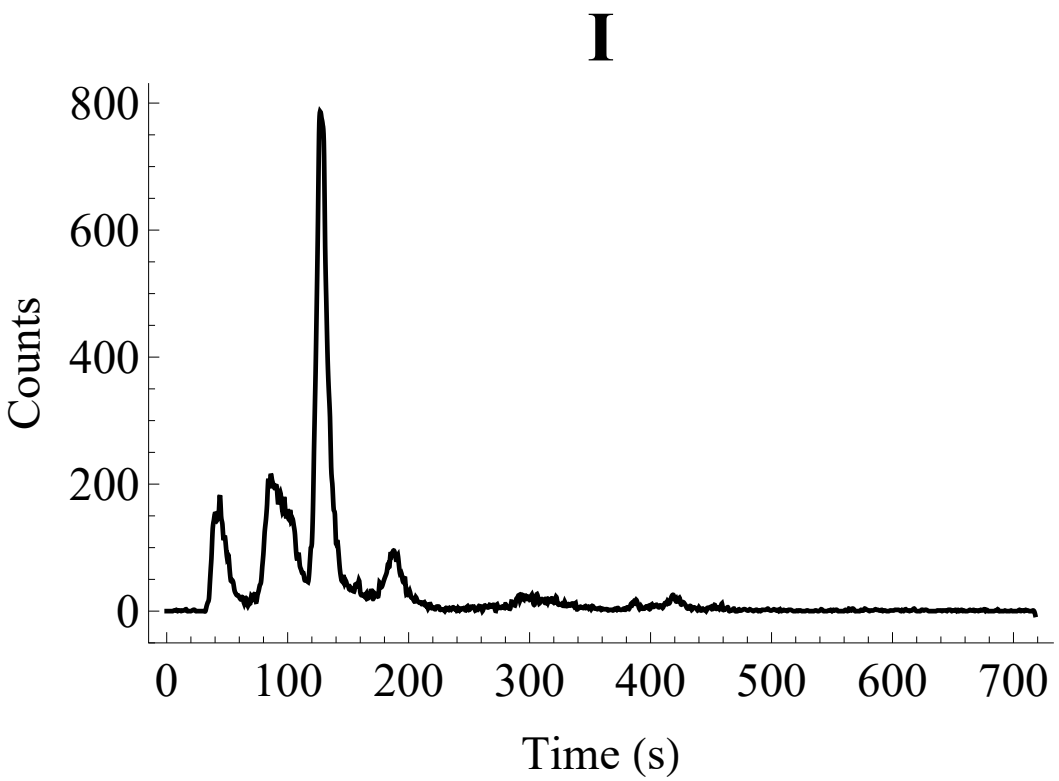

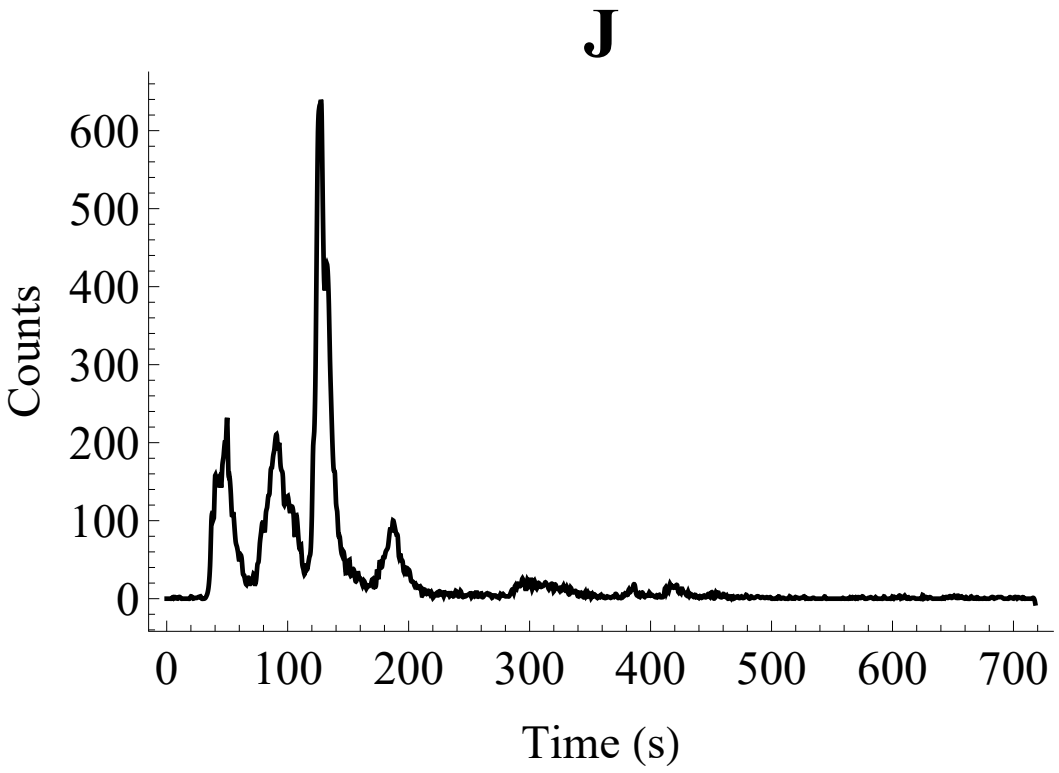

Figure 5.3: Cell-free extract HPLC chromatograms. All ten chromatograms are provided for time point 20 seconds (A), 5 minutes (B), 10 minutes (C), 15 minutes (D), 20 minutes (E), 30 minutes (F), 40 minutes (G), 60 minutes (H), 90 minutes (I), and 120 minutes (J). The integration of peaks provides the concentration of the intermediate it represents. The change in concentration as a function of time can thus be seen from the changes in peak height and width between subsequent chromatograms.